

การพัฒนาเกราะกันกระสุนสมรรถนะสูงจากพอลิเบนซอกซาซีนคอมพอลิธ
ที่เสริมแรงด้วยเส้นใยชนิดต่างๆ



บทคัดย่อและแฟ้มข้อมูลฉบับเต็มของวิทยานิพนธ์ตั้งแต่ปีการศึกษา 2554 ที่ให้บริการในคลังปัญญาจุฬาฯ (CUIR)
เป็นแฟ้มข้อมูลของนิสิตเจ้าของวิทยานิพนธ์ ที่ส่งผ่านทางบัณฑิตวิทยาลัย

The abstract and full text of theses from the academic year 2011 in Chulalongkorn University Intellectual Repository (CUIR)
are the thesis authors' files submitted through the University Graduate School.

วิทยานิพนธ์นี้เป็นส่วนหนึ่งของการศึกษาตามหลักสูตรปริญญาวิศวกรรมศาสตรดุษฎีบัณฑิต
สาขาวิชาวิศวกรรมเคมี ภาควิชาวิศวกรรมเคมี
คณะวิศวกรรมศาสตร์ จุฬาลงกรณ์มหาวิทยาลัย
ปีการศึกษา 2560
ลิขสิทธิ์ของจุฬาลงกรณ์มหาวิทยาลัย

Development of High Performance Ballistic Armor from Varied Fiber Reinforced
Polybenzoxazine Composites



A Dissertation Submitted in Partial Fulfillment of the Requirements
for the Degree of Doctor of Engineering Program in Chemical Engineering

Department of Chemical Engineering

Faculty of Engineering

Chulalongkorn University

Academic Year 2017

Copyright of Chulalongkorn University

Thesis Title	Development of High Performance Ballistic Armor from Varied Fiber Reinforced Polybenzoxazine Composites
By	Miss Manunya Okhawilai
Field of Study	Chemical Engineering
Thesis Advisor	Professor Sarawut Rimdusit, Ph.D.
Thesis Co-Advisor	Professor Salim Hiziroglu, Ph.D.

Accepted by the Faculty of Engineering, Chulalongkorn University in Partial Fulfillment of the Requirements for the Doctoral Degree

..... Dean of the Faculty of Engineering
(Associate Professor Supot Teachavorasinskun, D.Eng.)

THESIS COMMITTEE

.....Chairman
(Professor Paisan Kittisupakorn, Ph.D.)

.....Thesis Advisor
(Professor Sarawut Rimdusit, Ph.D.)

.....Thesis Co-Advisor
(Professor Salim Hiziroglu, Ph.D.)

.....Examiner
(Dr. Pimporn Ponpesh, Ph.D.)

.....Examiner
(Assistant Professor Vichitra Chongvisal, Ph.D.)

.....External Examiner
(Associate Professor Chanchira Jubslip, D.Eng.)

.....External Examiner
(Assistant Professor Sunan Tiptipakorn, D.Eng.)



จุฬาลงกรณ์มหาวิทยาลัย
CHULALONGKORN UNIVERSITY

มนัญญา โอฆวิไล : การพัฒนาเกราะกันกระสุนสมรรถนะสูงจากพอลิเบนซอกซาซีนคอมพอสิตที่เสริมแรงด้วยเส้นใยชนิดต่างๆ (Development of High Performance Ballistic Armor from Varied Fiber Reinforced Polybenzoxazine Composites) อ.ที่ปรึกษาวิทยานิพนธ์หลัก: ศ. ดร. ศรารุช ริมดุสิต, อ.ที่ปรึกษาวิทยานิพนธ์ร่วม: ศ. ดร. สาลิม อิชิรอกุล, 132 หน้า.

งานวิจัยนี้มีเป้าหมายเพื่อพัฒนาเสื้อเกราะกันกระสุนสำหรับติดตัวบุคคลจากวัสดุพอลิเมอร์คอมพอสิต โดยใช้เส้นใยเสริมแรงสมรรถนะสูงในพอลิเบนซอกซาซีน/พอลิยูรีเทนคอมพอสิต ให้มีความสามารถในการป้องกันการเจาะทะลุจากกระสุนชนิด 7.62×51 มม ที่ความเร็ว 847±9.1 เมตร/วินาที ตามมาตรฐาน National Institute of Justice ระดับ III เกราะกันกระสุนประกอบด้วย 2 ส่วนที่สำคัญคือส่วนหน้าทำหน้าที่ทำลายหัวกระสุน ผลิตจากพอลิเบนซอกซาซีนคอมพอสิตที่เสริมแรงด้วยเส้นใยแก้ว และส่วนหลังทำหน้าที่ดูดซับพลังงานปะทะแบบซีปนะ ผลิตจากพอลิเบนซอกซาซีน/พอลิยูรีเทนคอมพอสิตที่เสริมแรงด้วยเส้นใยอะรามิด โดยพบว่าเส้นใยแก้วชนิด S มีความสามารถในการต้านทานการเจาะทะลุที่สูงกว่าเส้นใยแก้วชนิด E ในพอลิเบนซอกซาซีนคอมพอสิตเมื่อเปรียบเทียบที่จำนวนชั้นเท่ากัน และพบงานร่วมในความสามารถในการต้านทานแรงดึงและการดูดซับพลังงานปะทะแบบซีปนะที่ทดสอบด้วยกระสุนขนาด 9 มม ที่ระดับ II และ III-A ที่ปริมาณพอลิยูรีเทน 20 เปอร์เซ็นต์โดยน้ำหนัก ในพอลิเบนซอกซาซีน/พอลิยูรีเทนคอมพอสิตที่เสริมแรงด้วยเส้นใยอะรามิด จากการศึกษาการต้านทานการเจาะทะลุในระดับ III พบว่าเกราะกันกระสุนที่ผลิตจากพอลิเบนซอกซาซีนที่เสริมแรงด้วยเส้นใยแก้วชนิด S เป็นแผ่นหน้า และพอลิเบนซอกซาซีน/พอลิยูรีเทน ที่ปริมาณพอลิยูรีเทน 20 เปอร์เซ็นต์โดยน้ำหนักที่เสริมแรงด้วยเส้นใยอะรามิดเป็นแผ่นดูดซับพลังงาน สามารถต้านทานการเจาะทะลุจากกระสุนปืนชนิด 7.62×51 มม ได้สูงถึง 6 นัด โดยความเสียหายของวัสดุเกิดจากการฉีกขาดของเส้นใยเป็นหลัก ร่วมกับการแตกของพอลิเมอร์เมตริกซ์และการแยกชั้นของวัสดุ จากการศึกษาด้วยเทคนิคไฟไนต์อีลิเมนต์พบว่าแผ่นเกราะกันกระสุนที่พัฒนาได้สามารถต้านทานการเจาะทะลุจากกระสุนชนิด 7.62×51 มม ได้ที่ความเร็วขีดจำกัดสูงสุดถึง 930 เมตร/วินาที โดยเสื้อเกราะกันกระสุนที่ผลิตได้มีประสิทธิภาพสูง และมีน้ำหนักเบา สามารถนำไปประยุกต์ใช้เป็นเสื้อเกราะกันกระสุนสำหรับบุคคลได้

ภาควิชา	วิศวกรรมเคมี	ลายมือชื่อนิสิต
สาขาวิชา	วิศวกรรมเคมี	ลายมือชื่อ อ.ที่ปรึกษาหลัก
ปีการศึกษา	2560	ลายมือชื่อ อ.ที่ปรึกษาร่วม

5771420621 : MAJOR CHEMICAL ENGINEERING

KEYWORDS: BALLISTIC ARMOR / BALLISTIC IMPACT /
POLYBENZOXAZINE/POLYURETHANE COMPOSITE

MANUNYA OKHAWILAI: Development of High Performance Ballistic Armor from Varied Fiber Reinforced Polybenzoxazine Composites. ADVISOR: PROF. SARAWUT RIMDUSIT, Ph.D., CO-ADVISOR: PROF. SALIM HIZIROGLU, Ph.D., 132 pp.

In this research, a hard ballistic armor based on fiber reinforced polybenzoxazine/polyurethane (PBA/PU) composite as human body armor was developed to protect the 7.62x51 mm projectile at a velocity of 847 ± 9.1 m/s according to National Institute of Justice at test level III. The hard armor consisted of two main panels, i.e., strike panel to destroy the tip of projectile which was made from glass fiber reinforced PBA composite and absorption panel from aramid fiber reinforced PBA/PU composite to absorb impact energy. It was found that S glass composite exhibited a greater performance than E glass composite having the same number of plies. Synergistic behaviors in tensile properties and energy absorption at test level II and III-A were observed from aramid fiber reinforced PBA/PU having 20wt% of PU content. The hard ballistic armor using S glass fiber reinforced PBA composite backed by aramid fiber reinforced PBA/PU composite having 20wt% of PU content could resist the penetration from 7.62x51 mm for up to six shots. Moreover, the failure mechanisms in the composite were dominant by fiber failure, matrix cracking and delamination. From finite element technique, the ballistic limit of the developed hard ballistic armor against 7.62x51 m/s was as high as 930 m/s. Such high performance and light weight ballistic armor is a potential candidate to be applied as a human body armor

Department: Chemical Engineering Student's Signature

Field of Study: Chemical Engineering Advisor's Signature

Academic Year: 2017 Co-Advisor's Signature

ACKNOWLEDGEMENTS

The author would like to express her sincerest gratitude and deep appreciation to my advisor, Prof. Dr. Sarawut Rimdusit for his kindness invaluable supervision, guidance, advice and encouragement throughout the course of this study. I am also grateful to my co-advisor, Professor Dr. Salim Hiziroglu from Natural Resource Ecology and Management, Oklahoma State University. He guided me through every difficult situation in my thesis. I also give sincere thanks to Professor Dr. Paisan Kittisupakorn, Assistant Professor Dr. Vichitra Chongvisal, Dr. Pimporn Ponpesh, Associate Professor Dr. Chanchira Jubsilp, Assistant Professor Dr. Sunan Tiptipakorn, for their constructive and scientific advices as dissertation committees.

In addition, I would like to thank all members of Polymer Engineering Laboratory, Department of Chemical Engineering, Faculty of Engineering, Chulalongkorn University for their guidance, assistance, discussion and sincere encouragement in solving problems. Finally, my deepest regards to my family members who have always been the source of my unconditional love, understanding, and generous encouragement during my studies. Also every person who deserves thanks for encouragement and support that cannot be listed.

CHULALONGKORN UNIVERSITY

CONTENTS

	Page
THAI ABSTRACT	iv
ENGLISH ABSTRACT	v
ACKNOWLEDGEMENTS	vi
CONTENTS	vii
LIST OF TABLES	x
LIST OF FIGURES	xii
LIST OF SCHEMES	xvii
CHAPTER I INTRODUCTION	1
CHAPTER II THEORY	8
CHAPTER III LITERATURE REVIEWS	55
CHAPTER IV EXPERIMENTS	61
CHAPTER V RESULTS AND DISCUSSION	74
REFERENCES	114
VITA.....	132

LIST OF TABLES

Table 1: A currently implemented NIJ standard for ballistic resistance of body armor, NIJ standard-0101.06.	9
Table 2: Armor protection levels and threats comparison between NIJ standard- 0101.04 and NIJ standard-0101.06.	10
Table 3: Properties of high performance ballistic fibers.	14
Table 4: Systems of soft ballistic armor produced from varied high-performance fibers.	18
Table 5: Hard ballistic armors from ceramic and metallic composites.	23
Table 6: Various polymer composites and their achieved ballistic protection levels.	30
Table 7: Property comparison of major thermosetting resins used as ballistic composite matrices.	39
Table 8: Parameters and simulation results of various composite armor systems using ANSYS AUTODYN program.	47
Table 9: Initial and residual velocities of projectile for various plate arrangements.	57
Table 10: Properties of fabric used in this study.	63
Table 11: Material properties for 9 mm FMJ and 7.62 mm projectiles.	71
Table 12: Energy absorption abilities of aramid fiber reinforced PBA/PU composites at various PU mass concentrations according to the NIJ protection level II.	81

Table 13: Energy absorption abilities of aramid fiber reinforced PBA/PU composites at various PU mass concentrations according to the NIJ protection level IIIA.	82
Table 14: The tensile properties of the aramid fiber reinforced PBA/PU composites at various PU mass concentrations.	90
Table 15: Materials properties of the aramid fiber reinforced 80/20 PBA/PU composite.	91
Table 16: Materials properties of S glass fiber reinforced PBA composite used for simulation.	108
Table 17: Comparison of areal weight density of our fiber reinforced PBA/PU composite and others hard ballistic armors.	112



LIST OF FIGURES

	Page
Figure 1: Ballistic test set up according to the US National Institute of Justice standard (NIJ-0101.06).	11
Figure 2: General armor panel impact locations according to NIJ standard.	12
Figure 3: Performance of various types of ballistic fibers.	15
Figure 4: Wave propagation in a transversely impacted fiber.	16
Figure 5: Relative ballistic efficiency of various ceramics as a function of their densities.	20
Figure 6: Commercial hard ballistic armor for high protection level.	24
Figure 7: Failure modes of ceramic alumina; crater on top surface, cracks and conoid crater on bottom surface ceramic conoid.	25
Figure 8: Chemical repeating units of para-aramid, meta-aramid and polybenzoxazole.	27
Figure 9: Arrangement of various fabrics in polymer composite armor.	28
Figure 10: Composite armor and its arrangement.	29
Figure 11: Cone formation by projectile during an impact event.	31
Figure 12: Principal energy absorption mechanisms in polymer composite.	33
Figure 13: Ballistic failure modes of unidirectional UHMWPE composite.	34
Figure 14: Monofunctional benzoxazine monomer.	36

Figure 15: Bifunctional or multifunctional benzoxazine monomer where R^1 , R^2 and R^3 , are organic radicals.	36
Figure 16: bisphenol-A, aniline based benzoxazine monomer.	37
Figure 17: Deformation of .projectile after penetrated E-glass fiber reinforced PBA composite.	43
Figure 18: Failure mechanism of E-glass fiber reinforced PBA composite by matrix cracking.	43
Figure 19: Comparison of the damage in the composite target a) simulated and b) observed.	48
Figure 20: Ballistic limit for Kevlar fiber/epoxy in glass fiber/epoxy having thickness of 1.8 mm subjected to blunt and hemispherical projectiles.	56
Figure 21: Ballistic limit as a function of composite laminate thickness.	58
Figure 22: Time histories of energy absorption by the yarn.	59
Figure 23: Bisphenol A – based benzoxazine monomer.	62
Figure 24: TDI and polypropylene glycol –based urethane prepolymer.	62
Figure 25 Set up for interlaminar shear strength test.	64
Figure 26: Interfacial adhesion test set up and specimen dimension.	65
Figure 27: Ballistic test set up with two sets of chronograph to determine striking and residual velocity of projectile before the specimen is impacted and after it was penetrated.	66

- Figure 28: General armor panel impact locations for multi hits performance evaluation. 69
- Figure 29: The mesh formation of a copper jacket and a lead core of a 9 mm FMJ bullet. 72
- Figure 30: a) Dimension of 7.62x51 mm projectile b) Material of the projectile and c) Specimen geometry. 73
- Figure 31: Interlaminar shear strength (ILSS) and peel resistance of aramid fiber reinforced PBA/PU composites. 76
- Figure 32: V_{50} value and energy absorption of aramid fiber reinforced 80/20 PBA/PU composites as a function of the sample thickness. 84
- Figure 33: Depth of deformation on the back side of aramid fiber reinforced 80/20 PBA/PU composite compared to aramid fabric with vary thickness after subjected to .44 Magnum at a velocity of 427 m/s regarding to NIJ standard test level III-A. 87
- Figure 34: The comparison of the material deformations on the impact side of the 25-ply aramid fiber reinforced 80/20 PBA/PU composite panel from the theoretical simulation and the actual experimental measurement. 93
- Figure 35: Time-dependent evolutions of the stress distribution and the panel deformations after impacting the 9 mm FMJ projectile onto the 25-ply aramid fiber reinforced 80/20 PBA/PU composite. 93

Figure 36: The theoretical ballistic limit determination (a), the failure mechanisms (b) and the stress distribution (c) of the 25-ply aramid fiber-reinforced 80/20 PBA/PU composite after subjected to an impact by a 9 mm FMJ projectile having an impact velocity of 800 m/s. 95

Figure 37: Ballistic impact behavior of the composite panels consisted of the first two panels of type E glass fiber reinforced PBA composites and aramid fiber reinforced 80/20 PBA/PU composite showing an ability of the composite to resist the penetration of 7.62x51 mm projectile at a velocity of 847 ± 9.1 m/s based on test level III of NIJ standard. 97

Figure 38: Comparison on depth of deformation on the back side of 3rd panel of aramid fiber reinforced PBA/PU composite with 20wt% and 10wt% of PU content after ballistic impacted by 7.62x51 mm based on test level III of NIJ standard. 100

Figure 39: Equivalent damage diameter of hole at different depths along the thickness of aramid fiber reinforced PBA/PU composite:—●—80/20 PBA/PU and —■—90/10 PBA/PU composite. 101

Figure 40: Ballistic impact response of the composite specimens made from two panels of 25 plies each of S-glass fiber reinforced PBA and 25 plies of aramid fiber reinforced 80/20 PBA/PU after impacted by 7.62x51 mm projectile. 103

- Figure 41: Ballistic impact response of composite specimens made from: 35 plies of S-glass fiber reinforced PBA composite and 25 plies of aramid fiber reinforced 80/20 PBA/PU composite after impacted by 7.62×51 mm projectile. 106
- Figure 42: Macrograph of the composite specimens after impacted by 7.62×51 mm projectile a) impact side b) rear side of S glass fiber reinforced PBA composite c) impact side of aramid fiber reinforced 80/20 PBA/PU composite. 107
- Figure 43: Back face deformation on the aramid composite after impacted by 7.62×51 mm showing the similar impact response of experimental and simulation. 108
- Figure 44: Ballistic characteristic a) Ballistic limit b) Failure in the composite panel by 7.62×51 mm having velocity of 950 m/s higher than its ballistic limit. 109
- Figure 45: Impact response of the specimens impacted by 7.62×51 mm having velocity of 838 m/s at each time interval. 110
- Figure 46: Multi-shot resistance of S-glass fiber reinforced PBA composite backed by aramid fiber reinforced 80/20 PBA/PU composite: showing impact velocity and depth of penetration measured from backing clay material for each impact shot. 111

LIST OF SCHEMES

	Page
Scheme 1: Chemical reaction of NCO-terminated PU prepared from toluene diisocyanate and poly(propylene glycol).	40
Scheme 2: Polymerization reaction of PBA and PU.	41



CHAPTER I

INTRODUCTION

1.1 INTRODUCTION

Body armor is an essential equipment for protection of officers from any injury during performing their duties. Such high performance and low weight body armor have been intensively investigated and new products were developed from the results of many researchers for centuries [1-3]. In general, hard armor refers armor which could withstand the penetration from high powerful projectile, particularly 7.62x51 mm based on National Institute of Justice standard (NIJ) at level III. Typically, first strike face and latter ductile panels are designed for hard body armor. The function of strike panel is to destroy the tip of bullet into fragments so that the impact kinetic energy is effectively reduced. For that purpose, ceramic materials with high hardness such as boron carbide, silicon carbide as well as aluminum oxide are widely used. It is well known that such those ceramics have high density so that armor with heavy weight is a crucial drawback. Moreover, crack propagation of ceramic limits the use of panel to multi hit resistance. Ceramic tiles having high hardness produced into various shapes including rectangular, hexagon and pellet have been emerged to restrict the propagation of damage within impacted tile, however, large interfaces between each tile are the main disadvantage [4, 5]. Glass fiber is an alternative choice of material to solve such problems of

ceramic armor [6, 7]. Typical type of glass fiber, i.e., E and S glass fiber have high modulus and strength which are suitable to manufacture as ballistic impact panel. Glass fiber reinforced polymer composites were used as backing material after ceramic panel to stop and capture the fragmentation of the projectile [7, 8]. However, the backing laminated composites are more susceptible to damage in terms of delamination, so that it was usually fabricated from superior toughness reinforcing fibers, for example, aramid fiber and UHMWPE having high energy absorption [4, 5, 9, 10]. The application of low toughness glass fiber composite as the last panel in turn suppressed the delamination thus the sample can easily be perforated.

Energy absorption of materials is one of the main parameters for assessing and evaluating the armor's performance to withstand the penetration of projectile during the impact incident. Among high performance ballistic fibers e.g. ultra-high molecular weight polyethylene (UHMWPE) aramid fibers (KevlarTM and TwaronTM), and carbon fibers, aramid fibers provide relatively high specific energy absorptions thus they were commonly employed to manufacture ballistic panels in the body armor [11]. High energy absorption materials have to possess high tensile strengths and elongation at breaks. Materials having high tensile modulus values also promoted lower back face deformations [3].

Fiber reinforced polymer composites made of the high-strength fiber-embedded polymer matrixes have been increasingly employed in the light-weight armor manufacturing due to the overall high strength and the stiffness to weight

ratio. An incorporation of the polymer matrix offered two essential functions. During an impact event, the yarn's integrity remained intact due to the presence of the polymer matrix as observed by Lee *et al.* [12]. The polymer matrix also reduced the effect of the curvature of the projectile on the penetration in which the damage ability of the projectile to puncture the armor decreased [3]. However, the excessive interaction between the polymer matrix and embedded yarns might hinder the movement of yarns to dissipate the absorbed energy and overall ballistic performance of the composites reduced [13]. Gopinath *et al.* [3] also found that the strong interactions between the stiff matrix and yarns decreased the deflection of the armor, whereas the deformation area increased. Therefore, the polymer matrix with the appropriate degree of flexibility and the felicitous polymer matrix-yarn interactions are cardinal for enhancing the ballistic performances of fiber reinforced polymer composites.

Various polymer matrices such as epoxy [13, 14], polyester [15], vinyl ester [16, 17], and phenolics are generally employed for armor manufacturing. In this work, benzoxazine resin (BA-a) was exploited as the polymer matrix. Benzoxazine resin (BA-a) is a novel kind of thermosetting phenolic resins. BA-a exhibited a myriad of outstanding characteristics, e.g. straightforward monomer preparation with the solvent-less synthesis technique [16], thermal-triggered ring-opening polymerization without additional catalysts or curing agents required, no by-product release during polymerization, near-zero volumetric shrinkage upon thermal curing, high thermal

stability, excellent mechanical properties, low melt viscosity, and ability to alloy with various types of resins [18-21]. PBA composites reinforced with aramid fibers provided improved ballistic performance over the epoxy reinforced with aramid fibers with respect to a higher damage area [22]. However, PBA having polar functional groups could form substantial interactions to aramid fibers and the ballistic performance of the composites decreased [22, 23]. To alleviate this problem, polyurethane (PU) having a long nonpolar hydrocarbon chain was introduced. PU are the most important tough engineering polymers and can be tailored to offer a wide spectrum of properties. They also possess the excellent flexibility. The toughness of benzoxazine resins could be enhanced by alloying with PU and the copolymer of polybenzoxazine and polyurethane (PBA/PU) also showed the synergism in glass transition temperatures (T_g) (i.e. T_g of PBA/PU was higher than 200°C , whereas those of the parent polymers were 165°C for PBA and -71°C for PU [24]. The research about effect of urethane prepolymer based on various types of isocyanate also reported that toluene-diisocyanate (TDI) resulted in the highest T_g , flexural modulus, and flexural strength of the alloys. The PBA/PU based on TDI blended were used as matrices for reinforced carbon fiber at 80wt% in cross-ply orientation [20, 24, 25]. Fine-tuned mechanical properties can thus be obtained from the PBA/PU alloys to provide suitable structural integrity and energy absorption for a ballistic composite application with synergistic behavior in their thermal stability as mentioned above.

Therefore, the objective of this study is to measure ballistic impact performance of glass fiber reinforced PBA as striking panel backed by aramid fiber reinforced PBA/PU samples subjected to 7.62x51 mm projectile and developed to be used as human body armor having protection in the level of III based on NIJ standard. The effects of type of fiber glass, i.e., type E and S glass fiber on penetration resistance, damage area as well as cone deformation of the samples were evaluated. Another approach of this research is to develop energy absorption panel employing aramid fiber reinforced PBA/PU composite. The aramid fiber-matrix interactions in the composites were optimized through the PU mass concentrations from 0–40wt%. The tensile properties of the PBA/PU composites were also characterized. Aramid fiber reinforced PBA/PU composites were subjected to the ballistic impacts of 9 mm Full Metal Jacketed (FMJ) at a velocity of 367 ± 9.1 m/s and .44 Magnum Semi Jacketed Hollow Point (SJHP) bullets at a velocity of 436 ± 9.1 m/s. Energy absorptions under ballistic impacts, energy dissipation mechanisms, and failure modes of the composites were also theoretically investigated using a commercial hydrocode (ANSYS AUTODYN software) and compared with the experimental results. In addition, the ballistic limit of the samples was also theoretically estimated.

1.2. OBJECTIVES

1. To develop a high performance ballistic armor based on fiber reinforced PBA/PU composite.
2. To investigate effects of urethane content on mechanical properties of aramid fiber reinforced PBA/PU composite as absorption panel.
3. To evaluate type of glass fiber reinforced PBA composites as striking panel.
4. To study ballistic impact behavior of the obtained composites using computer simulation technique.

1.3. SCOPES OF THE STUDY

1. Synthesis of benzoxazine resin based on bisphenol-A and aniline by a solvent-less technology at 100°C for 40 minutes.
2. Synthesis of urethane prepolymer based on polypropylene polyol and toluene diisocyanate.
3. Preparation of resin mixture of benzoxazine/urethane at 0-40wt% of urethane content.
4. Preparation of fiber reinforced PBA composite:
 - Type E and S-glass fiber reinforced PBA samples as strike panel
 - Aramid fiber reinforced PBA/PU samples as absorption panel

5. Characterization on mechanical and adhesion properties of fiber reinforced

PBA/PU composites:

- Interlaminar shear strength
- Interfacial adhesion
- Energy absorption
- Damage pattern
- Damage area using ImageJ software

6. Evaluation of ballistic impact properties of fiber reinforced polybenzoxazine composites according to NIJ standard:

- Test level III-A using 9 mm FMJ at velocity of 436 ± 9 m/s
- Test level III using 7.62 x 51 mm at velocity of 847 ± 9 m/s

7. Evaluation of multi-shot resistance and depth of penetration of the obtained composite after impacted using 7.62 x 51 mm NATO.

8. Simulation of ballistic impact performance of fiber reinforced PBA/PU specimens according to NIJ level IIIA and III using ANSYS AUTODYN software.

- Failure mechanism of the composite
- Ballistic limit (Maximum impact velocity of projectile which no perforation on the composite is observed.)

CHAPTER II

THEORY

2.1 STANDARD TEST METHOD FOR BALLISTIC ARMOR

Ballistic armor can be classified into 6 categories according to the threat levels suggested by the National Institute of Justice (NIJ standard-0101.04) and reduced to 5 categories according to the newer NIJ standard-0101.06 as can be seen in Table 1 [26]. The differences of the two standards are listed in Table 2. The former is currently adopted and widely used in various countries whereas the newer one is already implemented mainly in the US and some countries. Thai Army also plans to implement the new NIJ standard in the year 2016. From Table 2, NIJ level I has already been excluded from the new standard as this class of threat is considered to be too low and impractical at present. The first three levels (IIA, II, IIIA) are typically soft armors to protect against short gun threats. The last two levels (III, IV) are generally hard armor designed to protect officers against rifle threats [27]. Table 2 shows major differences of armor level and threat between NIJ-0101.04 and the recent version of NIJ-0101.06 [27]. NIJ standard also suggests type of ammunition, bullet velocity, maximum back face signature (BFS) and number of shot per ballistic panel needed for ballistic tests. Figure 1 exhibits a typical ballistic test set up according to NIJ standard-0101.06 above.

Table 11: A currently implemented NIJ standard for ballistic resistance of body armor, NIJ standard-0101.06 [26].

Armor Type	Test Round	Test Ammunition	Bullet Mass	Conditioned armor test velocity	New armor test velocity	Hits per armor at 0° angle	Maximum BFS depth (mm)	Hits per armor at 30° angle	Shot per panel
II-A	1	9 mm FMJ RN	8.0 g 124 gr.	355 m/s (1165 ft/s)	373 m/s (1255 ft/s)	4	44 mm 1.73 in	2	6
	2	40 S&W FMJ	11.7 g 180 gr.	325 m/s (1065 ft/s)	352 m/s (1155 ft/s)	4	44 mm 1.73 in	2	6
II	1	9 mm FMJ RN	8.0 g 124 gr.	379 m/s (1245 ft/s)	398 m/s (1305 ft/s)	4	44 mm 1.73 in	2	6
	2	357 Mag JSP	10.2 g 158 gr.	408 m/s (1340 ft/s)	436 m/s (1430 ft/s)	4	44 mm 1.73 in	2	6
III-A	1	9 mm FMJ RN	8.1 g 125 gr.	430 m/s (1410 ft/s)	448 m/s (1470 ft/s)	4	44 mm 1.73 in	2	6
	2	44 Mag JHP	15.6 g 240 gr.	408 m/s (1340 ft/s)	436 m/s (1430 ft/s)	4	44 mm 1.73 in	2	6
III	1	7.62 mm NATO FMJ	9.6 g 147 gr.	847 m/s (2780 ft/s)	-	6	44 mm 1.73 in	0	6
IV	1	.30 caliber M2 AP	10.8 g 166 gr.	878 m/s (2880 ft/s)	-	1 to 6	44 mm 1.73 in	0	1 to 6

Table 2 :Armor protection levels and threats comparison between NIJ standard-0101.04 and NIJ standard-0101.06 [27].

Armor type	0101.04	0101.06	0101.04	0101.06	0101.06 (conditioned)
	Test bullet	Test bullet	Reference velocity (ft/s)	Reference velocity (ft/s)	Reference velocity (ft/s)
I	.22 caliber LR LRN	N/A	1080	N/A	N/A
	.380 ACP FMJ RN	N/A	1055	N/A	N/A
II-A	9 mm FMJ RN	9 mm FMJ RN	1120	1225	1165
	40 S&W FMJ	40 S&W FMJ	1055	1155	1065
II	9 mm FMJ RN	9 mm FMJ RN	1205	1305	1245
	.357 Mag JSP	.357 Mag JSP	1430	-	1340
III-A	9 mm FMJ RN	9 mm FMJ RN	1430	1470	1410
	.44 Mag JHP	.44 Mag JHP	1430	1430	1340
III	7.62 mm NATO FMJ (M80)	7.62 mm NATO FMJ (M80)	2780	-	2780
IV	.30 Caliber M2 AP	.30 Caliber M2 AP	2880	-	2880

The test set up mainly consists of:

Test barrel: The pretest rounds should be done to “warm” or stabilize the temperature of the barrel before further testing.

Velocity measurement equipment: Recommended types of equipment for velocity measurement are:

- Photo electric light screen
- Printed make circuit screen
- Printed break circuit screen
- Ballistic radar
- Armor panel

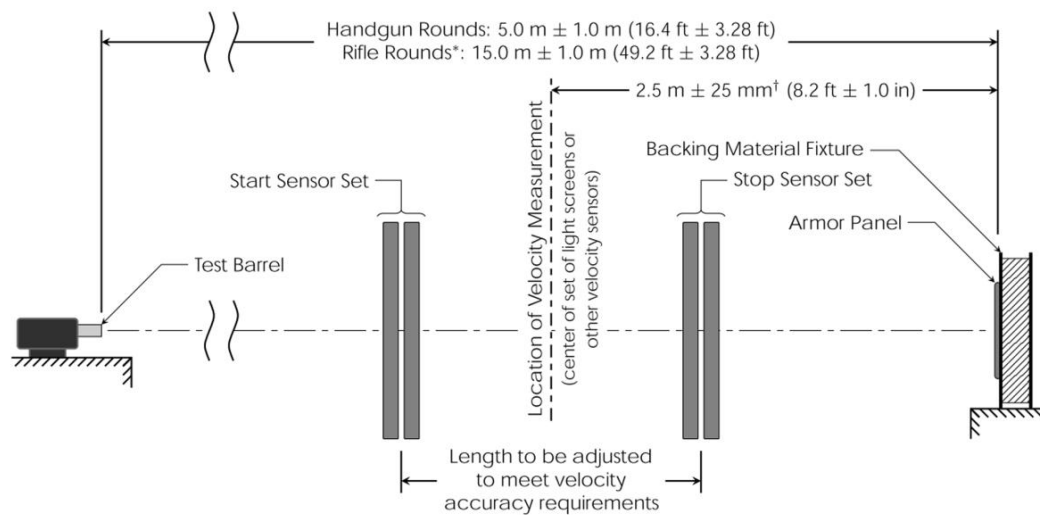


Figure 1: Ballistic test set up according to the US National Institute of Justice standard

(NIJ-0101.06) [26].

The distance of fire between test barrel and armor panel is set to be 5 m for test level I, II-A, II and III-A and 15 m for test level III and IV. The shot locations directly on the armor sample at test level I, II-A, II, III-A and III are depicted in Figure 2. The test level IV requires only one hit per armor.

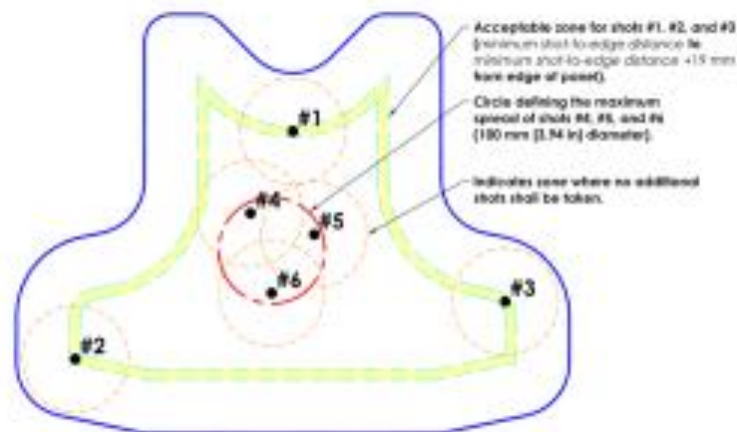


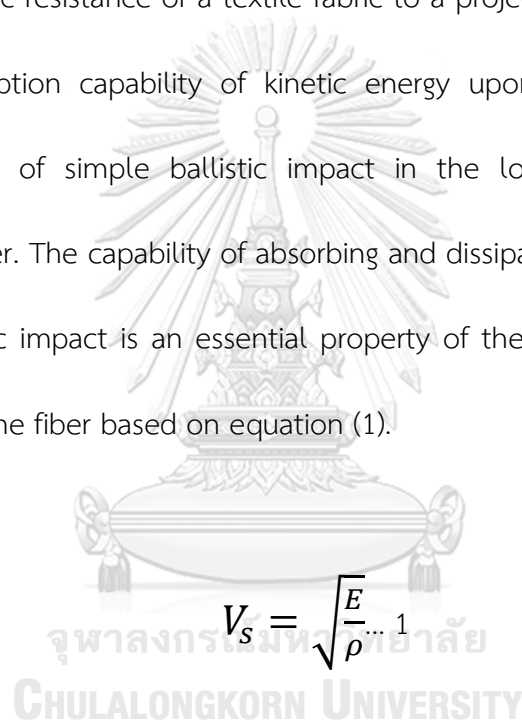
Figure 2: General armor panel impact locations according to NIJ standard [26].

2.2 SOFT BALLISTIC PROTECTIVE MATERIALS

As mentioned in Section 1, ballistic armor could be classified into soft and hard armors. Soft armor generally consists of several layers of high performance materials produced from ballistic fibers which have been increasingly developed in the past decade. Aramid based fibers such as KevlarTM, TwaronTM, TechnoraTM, and TerlonTM are most frequently used for this purpose due to their high protective impact strength. Besides aramid fibers, ultra-high molecular weight polyethylene fibers such as SpectraTM and DyneemaTM, are increasingly being used due to their low density, high strength, high toughness and high resistance to chemicals. These types

of fibers are typically more expensive than aramid fibers and are not without disadvantages, such as creep under load, low softening point and combustibility. VectranTM and PEFTM which are aromatic polyester based fibers may also be used due to their low rigidity, chemical resistance, high thermal stability and incombustibility. Properties of major high performance ballistic fibers are shown in Table 3 [28, 29].

The ballistic resistance of a textile fabric to a projectile is generally attributed to its high absorption capability of kinetic energy upon ballistic impact. This is analyzed by way of simple ballistic impact in the longitudinal and transverse directions of a fiber. The capability of absorbing and dissipating energy to surrounding area upon ballistic impact is an essential property of the fibers which is related to sonic velocity of the fiber based on equation (1).



$$V_s = \sqrt{\frac{E}{\rho}} \quad (1)$$

Where V_s is the sonic velocity of the longitudinal wave, E is fiber modulus and ρ is fiber density.

Table 3: Properties of high performance ballistic fibers [28, 29].

Property	Unit	E-glass	S-glass	Kevlar	Spectra	Carbon
Density	g/cm^3	2.54	2.49	1.45	0.97	1.85-1.96
Tensile strength	GPa	2.4	4.5	3.6	3.0	2.4
Elongation at break	%	3-4	5.4	2.8	3.5	0.38-0.5
Young's modulus	GPa	72.4	85	135	117	345-520
Specific tensile strength	GPa	9.6	18.5	25.3	31.5	12.2-13.3
Specific young's modulus	GPa	291	348	950	1231	1950-2868
Specific energy absorption	J/g	27-33	36-55	20-60	45-65	5-40

Thus, the velocity of wave propagation increases with the square root of fiber modulus and inversely with the square root of fiber density. The fiber with high sonic velocity could be able to spread out absorbed energy fast and efficiently. From equation (1), fiber modulus is proportional to sonic velocity thus such fiber that provides high modulus is referred to as high performance ballistic fiber [30]. The

higher the sonic velocity, the higher energy absorption is. Sonic velocity of some high performance fibers plotted against their specific energy absorption is exhibited in Figure 3.

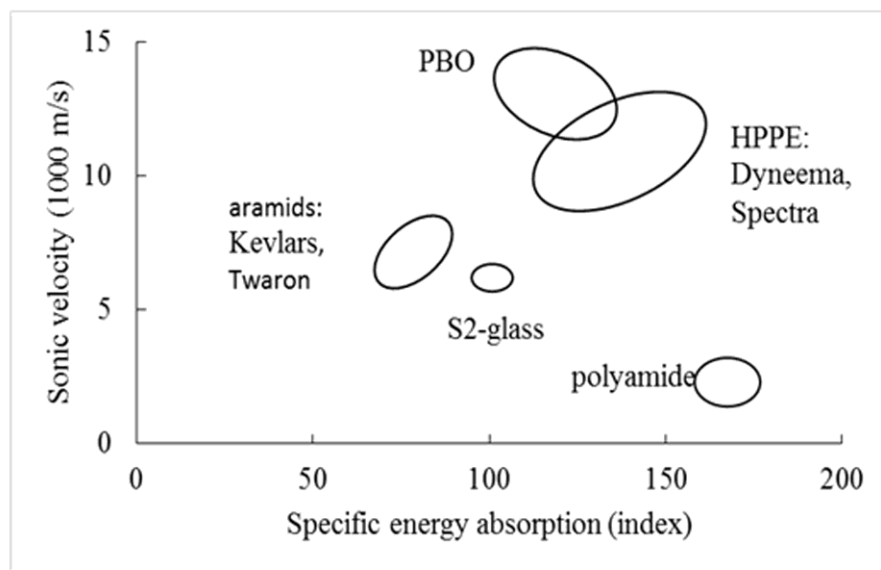


Figure 3: Performance of various types of ballistic fibers [30].

Figure 4 reveals schematically a fiber in a horizontal position which is impacted transversely by a projectile [31]. The ballistic impact causes the center portion of the fiber to deform before breaking. Two types of wave propagations are generated in the fiber upon impact. One is the longitudinal waves and the other is the transverse waves. The longitudinal waves propagate outward along the fiber from the point of impact while the transverse waves propagate outward in the thickness direction. The impact of a projectile results in a formation of a cone on the back-face

of the composite through the propagation of a transverse wave as seen in this figure. Upon impact, the primary yarns of the composite, which are the yarns directly impacted by the projectile, are strained to their tensile failure. Whereas the secondary yarns i.e. the yarns not directly impacted by the projectile will undergo deformation as a result of the cone formation. Besides the deformations of the primary and secondary yarns above which are the two major energy absorption mechanisms, the moving portion of the composite panels upon ballistic impact is also contributed to additional energy absorption through the kinetic energy of the moving cone [32].

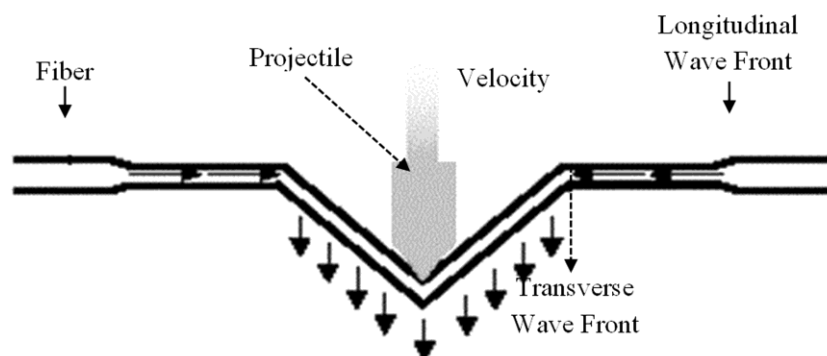


Figure 4: Wave propagation in a transversely impacted fiber [31].

Soft armor with adequate ballistic protection uses advanced woven or other fabrics of similar structures because of their flexibility, lightweight and comfort properties. Several researches on soft armor have investigated the behaviors of yarns

and fabrics during ballistic impacts. In addition to the fiber types, the degree of ballistic protection also depends on the yarn properties, fabric construction, and the number and types of layers used in the structure. These fabrics are used either with or without resin matrices to enhance the performance of a composites structure.

Aramid fibers, normally KevlarTM and TwaronTM, are highly attractive to both research and industrial applications to develop high performance ballistic armor due to its high modulus which relates to the ability to dissipate energy along the longitudinal direction as mentioned in the previous section. Aramid fiber embedded polybenzoxazine composite has recently been reported to provide high performance ballistic composite armors [18, 22]. There are numerous researches on various materials that show potential applications equivalent to soft ballistic armor as summarized in Table 4 [33-40].

Table 4: Systems of soft ballistic armor produced from varied high-performance fibers.

Materials	Projectile	Thickness (mm)	Areal density (g/cm ²)	Velocity (m/s)	Ref.
Alumina (Al ₂ O ₃)/Dyneema™/PU	7.49 mm	17.5	3.25	475	[34]
Woven Twaron™	9 mm	-	0.44-0.70	370	[35]
Graphite/epoxy laminate	12.7 mm	1.5-6	-	65-129	[36]
E-glass fiber/epoxy	6.33 mm	4.0-7.0	-	174	[33]
Glass fiber/resin	-	1.2-7.6	-	245	[37]
PE/PE composite	9 mm	5.1	0.44	V ₅₀ =390	[38]
PE/PE/aramid		5.4	0.52	V ₅₀ =450	
PE-PP/PP/PE-PP	1.1 g FPS	12	0.8	V ₅₀ =504	[39]
Carbon fiber/epoxy	5.46 mm FPS	6	0.84-0.87	257-276	[40]
PE fiber/epoxy			0.65	320	
PBO fiber/epoxy			0.79	447	
Carbon fiber/epoxy/PBO fiber/phenol PVB			-	464	
PBO fiber/phenol PVB			-	566-606	

2.3 HARD BALLISTIC PROTECTIVE MATERIALS

2.3.1 Ceramic and metallic ballistic materials

In recent decades, hard ceramic materials have been developed for certain ballistic armor applications. These ballistic ceramic materials mainly include Al_2O_3 , B_4C , and SiC [41, 42]. Figure 5 shows the relative ballistic efficiencies of several ceramics against impact from a 0.3-in. diameter projectile with a conical tip. The penetration of the projectile into the backup plate is measured [43]. Ceramics provide an advantage of being lighter in weight than steel and give ballistic stopping power comparable to steel. Ballistic ceramics are extraordinarily hard, strong and relatively light weight, making them efficient at eroding and shattering armor-piercing threats. Thus, in applications in which having armor with the lowest possible mass is important, such as human body armor and aircraft armor, ballistic ceramic materials are useful. The extra backing layer, usually a multi-layer of polymeric fabrics, polymer composite, or metal sheet is usually needed in ceramic armors. This backing layer serves to trap ceramic fragments as well as the residual deformed projectile or fragments resulting from its impact and penetration.

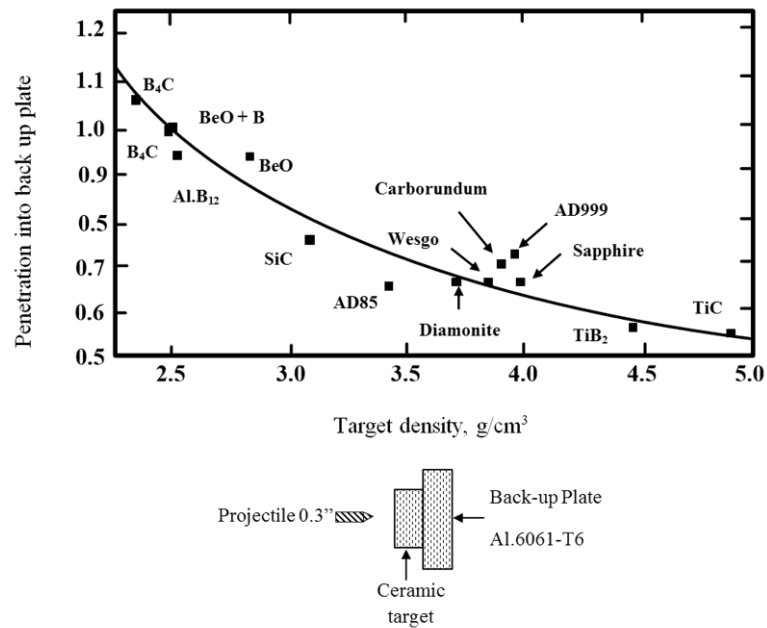


Figure 5: Relative ballistic efficiency of various ceramics as a function of their densities [43].

Ballistic armor that comprises of ceramic pellets are developed to accept high multi-hit capability by reducing propagation of shockwave through the armor upon impact by a projectile and lessening the effect of shattering pellets on their neighbors. The pellet was made from high-density ceramic including alumina, silicon carbide, silicon nitrile and boron carbide and typically regularly arranged and held in a matrix of thermosets or thermoplastics. Various shapes of ceramic material have been designed. For example, the 98% alumina pellets were designed to be cylindrical body with diameter of 19 mm and height of 19 mm with Al belt (thickness of 0.7 mm). The plate was covered by 10 mm of KevlarTM as backing layer weighing as 0.0014g/m^2 . The plate has areal weight density of 6.9 g/cm^2 [44]. Moreover, the

effects of size of the ceramic pellet on ballistic properties were investigated. The cylindrical pellets were composed of 98% of alumina, a total height of 8 mm and a diameter of 12.7 mm. The plate was covered with KevlarTM and fiberglass layers on both ends. The sample was tested with 10 rounds of 7.62 × 51 AP projectiles at a velocity of 840 m/s. This developed ballistic armor is comparable to the armor with 99.5% alumina and total height of 11.5 mm but less in areal weight density i.e. 2.7 g/cm² vs 3.65 g/cm² of the latter [45].

Normally, hard ballistic armor is designed to consist of two panels rearranged by an impact face as the first panel and a support portion as the second panel. One is designed to compose of auxiliary plate and main plate. Auxiliary armor plate with hole located at the front is made from steel with areal weight of 3.7 g/cm² and thickness of 8 mm which is used to destroy projectile before hitting the main plate. The spacing between the auxiliary and main plates allows the deflected projectile's path to further deviate from a normal impact on the main plate. The main plate is made of 98% alumina pellets with 16 mm height and backing with 3 mm fiberglass and wrapping with KevlarTM of 0.5 mm thick. The hard armor is weighed to be 9.4 g/cm² and it successfully stopped 14.5 mm API B 32 armor piercing projectile [46].

A common method of manufacturing structures made of ballistic ceramic materials is to sinter components of ceramic to form the structure using hot pressing. During a hot-pressing process, particles of ceramic material are first heated to elevated temperature and then subjected to increased isostatic gas pressure in an

autoclave. The increased temperature causes the ceramic material to undergo a process called sintering, whereby the particles adhere to each other. In the next step, the increased pressure and temperature encourage grain boundary diffusion to allow an increased densification of the structure. Reaction bonding has been used as an alternative in manufacturing ballistic ceramic structure over hot pressing because it uses less pressure and temperature. In reaction bonding, a composite is formed of ceramic particles bonded in a matrix of in-situ formed ceramic. The ceramic ballistic material manufactured from this method exhibits high strength, high modulus and attractive dynamic properties for use in ballistic armor applications [47].

In a report by Garcia and coworkers, a high-performance light weight composite armor system has been developed using boron carbide ceramics as the strike face, composite metal foam as a bullet kinetic energy absorber interlayer and aluminum 7075 or KevlarTM panels as backing plate with a total armor thickness of less than 25 mm. The ballistic composite was impacted by 7.62 × 51 mm M60 and 7.62 × 63 mm M2 AP according to the NIJ standard level III and IV, respectively. The results showed that the ceramic/metal foam/aluminum (or KevlarTM panel) could stop the complete penetration of both types of projectiles. They also found that the metal foam helps absorbed 50-60% of kinetic energy of projectile from total energy. Moreover, the depth of penetration of all projectiles in the composite was less than 44 mm as required by the NIJ standard [48]. Other ceramic and metallic composites for hard ballistic armor are summarized in Table 5 [49-52]. Commercial hard armor

for high ballistic protection is also illustrated in Figure 6 [53, 54]. These kinds of ceramic and metallic hard armors possess areal densities in the range of 6.1-15 g/cm² which is rather high for general body armor applications.

Table 5: Hard ballistic armors from ceramic and metallic composites.

Materials	Projectile	Thickness (mm)	Areal density (g/cm ²)	Velocity (m/s)	Ref.
Ceramic/metal	7.62 mm	22.3-26.3	-	835	[49]
Steel/Aluminium	7.62 mm APM	12-40	8.1-15.0	775-950	[50]
Ceramic/glass lamine/PC	7.62 mm AP	35.5	8.57	850	[51]
Alumina/toughened epoxy/aluminium	7.6 mm AP	18.3	6.1	940	[52]

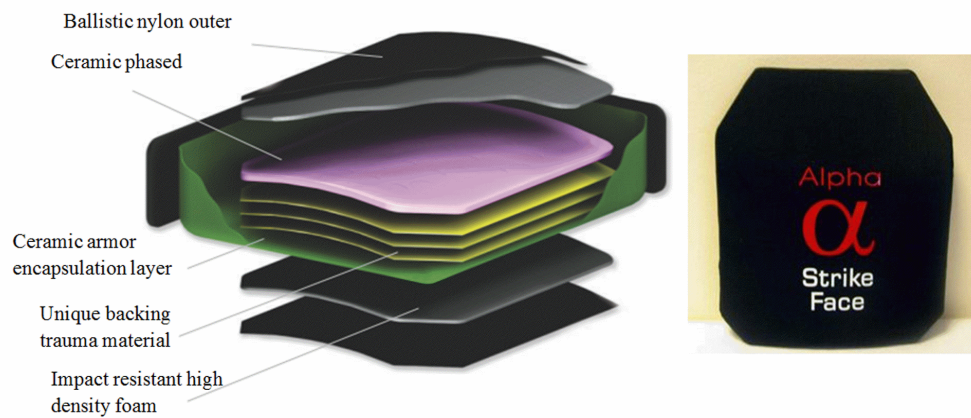


Figure 6: Commercial hard ballistic armor for high protection level a) VestGuard [53]
b) Alpha™ [54].

The effect of Al_2O_3 on ballistic behavior was investigated by Silva [55]. The results revealed that 92wt% and 99wt% Al_2O_3 showed higher Vickers hardness and bending strength than 96wt% Al_2O_3 . However, 92wt% Al_2O_3 provided the best ballistic performance. The projectile at velocity of 865 m/s (Level IV based on NIJ standard) could not penetrate or cause deformation in none on the backing metallic plates to alumina plates of 12 mm thickness.

2.3.1.1 Failure mechanism of ceramic ballistic materials

The failure mechanism of Al_2O_3 ceramic plate backing by steel armor was investigated after impacted by a tungsten projectile (diameter = 7.62 mm) with a velocity of $820 \pm 20\text{m/s}$ [56]. Its failure behavior is shown in Figure 7. A crater on the front surface of the ceramic plate is clearly seen. Moreover, three damage zones were observed at rear side of the plate, including intact edge zone, cracks and

fragments zone, and powders zone at center. Tensile stress caused by the deflection of the ceramic resulted in the radial crack formation on the rear surface of ceramic plate.

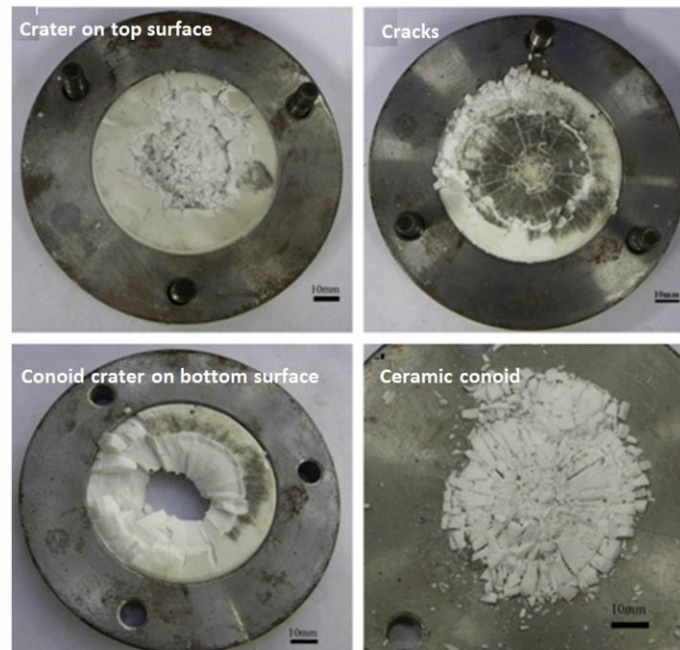


Figure 7: Failure modes of ceramic alumina; crater on top surface, cracks and conoid crater on bottom surface ceramic conoid [56].

CHULALONGKORN UNIVERSITY

2.4 POLYMER MATRIX COMPOSITE BALLISTIC MATERIALS

As ceramic is inherently brittle and its failure mode after an impact showed progressive crack propagation which seriously weakens the ballistic armor from another penetration of a projectile. Moreover, it is well documented that the most effective armors are not a single component system. This is due to the fact that the systems that combine multi layers of various types of materials serve well for multi-

functionality. Some hard armor can also consist of multilayers of steel in addition to the ceramic plates and stiff fiber-reinforced materials that also function to catch the slowed remnants of the projectile while keeping the integrity of the ballistic system. The main disadvantages of the steel containing hard armor remain heavyweight and inflexibility [57]. Polymer matrix composites fulfill those requirements and bond well with the ceramic and other layers to form an integral armor system.

In polymer matrix composites, resin plays an important role as a binder in a ballistic armor which provides an adhesive characteristic as well as increased ductility and energy absorption. Different polymers, especially thermosetting polymers such as epoxy [13, 14, 58], polyester [15], vinyl ester [16, 17] and phenolics [59-61], are generally used to apply as resin matrix for ballistic armor. Modern structural composites are frequently referred to as advanced composites. The term 'advanced' means the composites materials based on polymeric materials reinforced with high performance fiber such as aramid fiber (TwaronTM, KevlarTM, TerlonTM), ultra-high molecular weight polyethylene (SpectraTM, DyneemaTM), glass fiber (Type E and S), carbon fiber and polybenzoxazole (ZylonTM). Chemical structure of some high performance fibers for ballistic armor applications is shown in Figure 8.

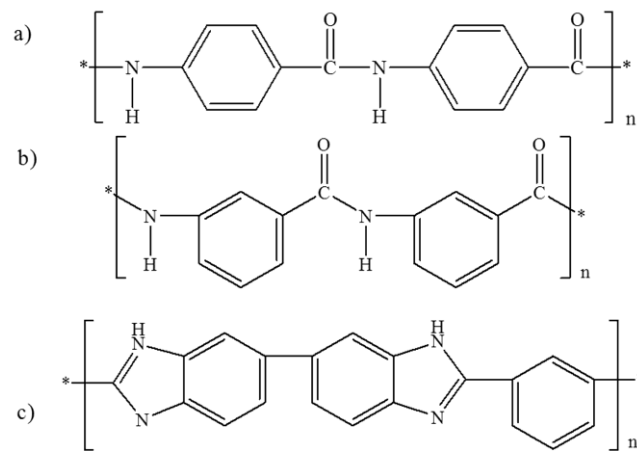


Figure 8: Chemical repeating units of a) para-aramid b) meta-aramid c) polybenzoxazole.

Composite materials are combination of two or more materials that are mixed on a microscopic scale to form a useful material. The study on type of fiber on ballistic performance was investigated by Sapozhnikov and coworkers [62]. They reported that laminates based on UHMWPE fibers (DyneemaTM) are better than aramid fibers (TwaronTM) with respect to the value of V_{50} (about 10%) and of the absorbed energy (about 25%) under high velocity impact conditions (900 m/s). However, UHMWPE fabric was higher in thickness than aramid in which thickness is one of an important parameter affected ballistic performance. Moreover, DyneemaTM composites are about twice as expensive as composites based on aramid fabrics. Therefore, the use of aramid fabric is more efficient when there are no increased requirements to protective structure weight.

Genihovich and coworkers [44] patented the use of polyethylene cloth with 30 plies (thickness of 8 mm) covered by carbon fiber reinforced epoxy composite as ballistic armor. The arrangement of fabric in this invention is shown in Figure 9. The plate with flexural strength of 50 kg has a ballistic efficiency required to protect the wearer from a 7.62 AP caliber. While Pilpel and coworkers [63] investigated the use of a ballistic composite to resist the penetration of a projectile. The structural composite armor is shown in Figure 10 which consists of striking plate made of E-glass fiber reinforced polypropylene or polyethylene. Support portion is made of S-glass fiber. The hybrid system of S-glass panel, hybrid E-glass and S-glass panels and HJ1(a phenol-typed thermosetting matrix) with areal weight density of 4.8 g/cm^2 could resist the penetration of 7.62 mm projectile with V_{50} of 889 m/s. The results of other material systems of this invention are displayed in Table 6.

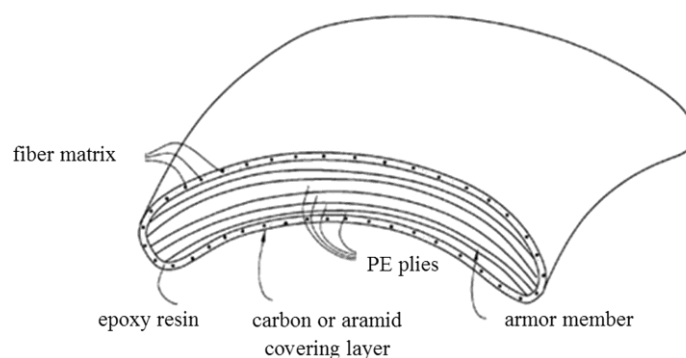


Figure 9: Arrangement of various fabrics in polymer composite armor disclosed in the US patent by Genihovich and coworkers [44].

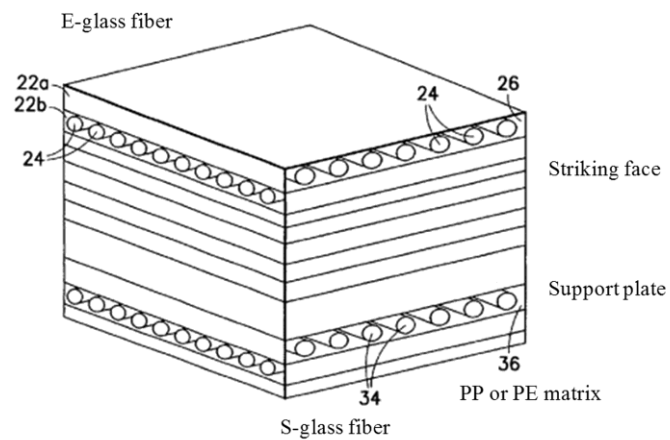


Figure 10: Composite armor and its arrangement as disclosed in the US patent by Pilpel and coworkers [63]

2.4.1 Failure mechanisms of polymer composites by energy absorbing mechanisms

During a ballistic impact, the following events could be possibly occurred depending on properties of composite materials and projectile parameters [64];

- the projectiles bounced or partially penetrated the target, indicating that the kinetic energy of projectile is less than the energy absorption capacity of the composite plate.
- the projectile perforated the composite plate completely with zero exit velocity or the projectile was captured by the composite plate, indicating that the entire kinetic energy of projectile is fully absorbed by the composite plate.
- the projectile penetrated the target and exited with certain velocity,

indicating that the maximum energy absorption of the plate is less than the energy possessed by the projectile.

Mohan and coworkers [65] discussed the failure mechanisms of the laminated composite after ballistic impact event by 6 mechanisms as follows:

Table 6: Various polymer composites and their achieved ballistic protection levels [63].

Material	Areal density (g/cm ²)	Test level	Velocity (m/s)
S-Glass fiber/ PP	0.73	III-A	457
E-Glass fiber/PP	0.85-1.09	II	373-419
S-Glass fiber/PP	1.09-1.70	III-A	442-479
(S-Glass + E-glass fibers at same weight)	0.97-1.70	III-A	450-543
S-Glass fiber/PP	2.99-4.88	III	655-875
(S-Glass + E-glass fibers at same weight)	2.99-4.88	III	577-843
S-Glass fiber/PP	1.22-2.44	IV	533-847
(S-Glass + E-glass fibers at same weight)	0.82-2.44	IV	408-810

2.4.1.1. Kinetic energy of the moving cone

During impact, an elliptical cone is formed on the back face of the composite plate. This conical deformation is on the basis of transverse wave propagation during the ballistic event. The longitudinal propagation of stress wave along the yarn takes place on the plane of the composite plate. Due to orthotropic nature of the composite plate, the shape of the wave front on the plane of the composite plate would be quasi-lemniscate/elliptical as can be seen in Figure 11. During the ballistic impact event, the distance travelled by the projectile and the depths of the cones formed are equal. Also, the velocity of the projectile and the moving cone would be equal. The yarns in each layer deform and cause some energy absorption.

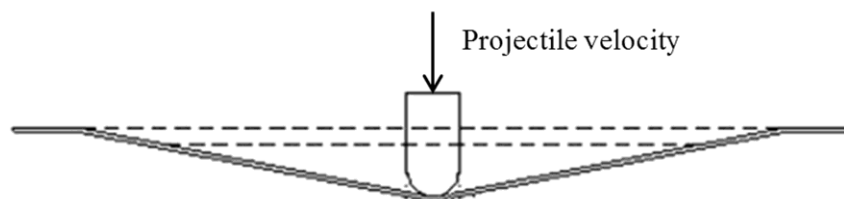


Figure 11: Cone formation by projectile during an impact event [65].

2.4.1.2. Tensile failure of the primary yarns

The primary yarns, the yarns directly impacted by the projectile, provide the force to resist the penetration of the projectile into the target. The strain is higher in primary yarns compared to that of secondary yarns. Tension in these yarns results in absorption of some energy. These yarns fail under tension when the strain of these

yarns exceeds the ultimate strain in the tension at high strain rate. All the primary yarns within one layer do not fail at one instant of time. When the projectile penetrates into the composite plate layers, there will be a sequential failure of yarns starting with the yarns in the top layer, and then proceeding towards the bottom layer. When the strain of a particular yarn reaches the dynamic failure strain in tension, the yarn fails. The length of yarns/fibers failing in tension is twice the distance covered by the longitudinal wave. A longer yarn absorbs more deformational energy prior to failure than a shorter yarn. Also, the complete length of a primary yarn is not strained to the same extent. The reason for this phenomenon is stress wave attenuation.

2.4.1.3. Deformation of the secondary yarns

All the yarns in each layer other than the primary yarns are called as secondary yarns. The energy absorbed by secondary yarns depends on the strain distribution within the secondary yarns. Based on their position, the secondary yarns experience different strain. The strain of the yarns, which are close to the point of impact experience strain, equals to the strain in the outermost primary yarn, whereas those yarns which are away from the impact point experience less strain. The strain in the secondary yarns induced by the growth of the cone and subsequent time-lag induces tension waves, and extends far beyond the boundary of the cone in a star shape. The star tips are the extent of the strains from the tension waves in the primary yarns. Though this phenomenon contributes some more amount of energy

absorption by second yarns, the strain at the cone boundary is assumed to be zero to reduce the complexity of the problem. Some principal energy absorption after ballistic impact event is illustrated in Figure 12.

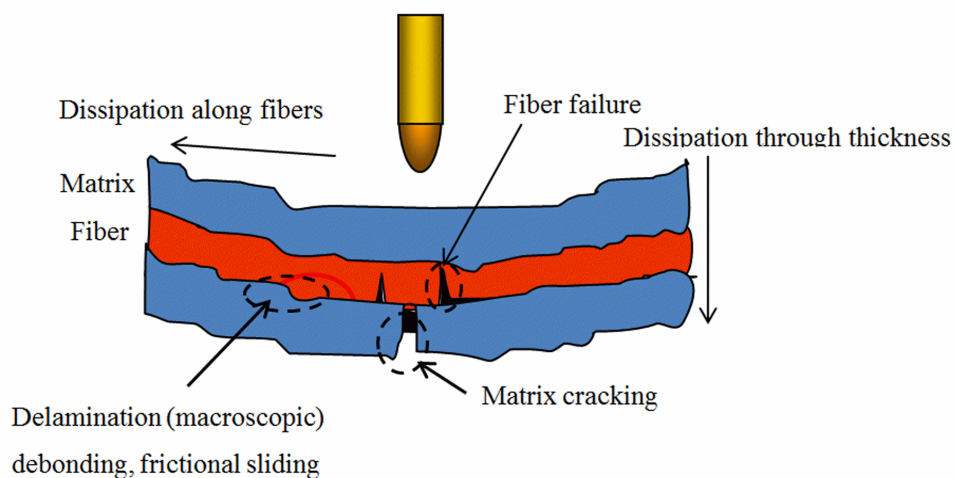


Figure 12: Principal energy absorption mechanisms in polymer composite [18].

2.4.1.4. Delamination and matrix cracking

A part of the kinetic energy possessed by the projectile is absorbed by the composite plate through failure mechanisms related to delamination and matrix cracking. Most of the conical area undergoes delamination and matrix cracking. Initially, the matrix of the composite plate cracks, leading to energy absorption. However, complete matrix cracking may not take place. This phenomenon can be seen by the matrix which is still attached to the fibers and does not separate from the reinforcement completely after ballistic impact. The interlaminar strength of the

composite plate decreases due to matrix cracking which causes delamination on further loading and deformation.

Zhang and coworkers [66] studied the failure mechanism of unidirectional UHMWPE laminates with different thickness. They found that the failure mechanisms are distinctly different from other fibers. Plugging and hole friction are the dominant failure modes for thin composites. However, delamination, fiber tension and bulge are the main failure modes for thick composites as illustrated in Figure 13.

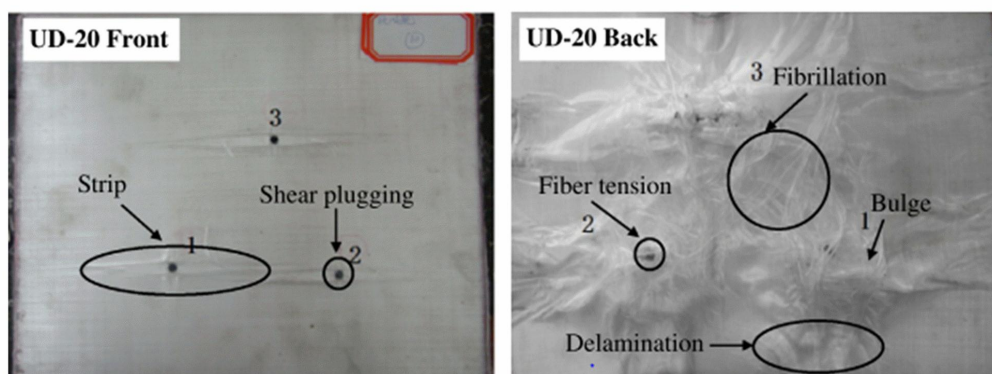


Figure 13: Ballistic failure modes of unidirectional UHMWPE composite [66].

2.5 POLYBENZOXAZINE/POLYURETHANE COMPOSITES

Epoxy, polyester, and vinyl ester are favorable to be used as a resin matrix for ballistic composites at present. Traditional phenolic resins have been widely used as matrices for composites in aircraft interiors because of its good heat resistance, flame retardant, dielectric properties, low smoke generation, and low cost. However, phenolic resins have serious shortcomings i.e. brittleness, release of water and ammonia during the curing process along with limited shelf life. Recently,

benzoxazine resin was chosen as a matrix in place of those traditionally used matrix resins due to its outstanding properties such as formation of no reaction by-product during polymerization, long shelf life, high thermal stability, good mechanical properties, and an ability to alloy with various types of resins for a wide range of applications [21, 67-72]. The properties of polybenzoxazine compared to those conventional ballistic resins are listed in Table 6 [73].

Various types of benzoxazine resins provide properties appropriate for an application as matrix resin for ballistic armor as disclosed by Rimdusit and coworkers [58], including monofunctional, bifunctional and multifunctional benzoxazine resins. Their chemical structures are depicted in Figures 14 and 15. Bisphenol-A and aniline based benzoxazine monomer or bis(3,4-dihydro-2H-3-phenyl-1,3-benzoxazinyl)isopropane, BA-a, was demonstrated to provide various favorable characteristics suitable of ballistic armor composite matrix such as ease of synthesis, substantial bonding with various ballistic fibers, and good mechanical properties [18, 21, 74]. Besides, BA-a resin possesses very low melt viscosity (<1000 cP at 120°C) compared to other bi-functional benzoxazine resins. This characteristic help facilitate fiber wetting during composite manufacturing [18]. The BA-a resin is synthesized from the reaction of bisphenol-A, paraformaldehyde and aniline without the use of any solvent as disclosed by Ishida in 1996 [75]. This method is a convenient method for preparation of various types of benzoxazine monomers. Chemical structure of BA-a is shown in Figure 16. Benzoxazine resin can be polymerized by the ring opening

polymerization of cyclic monomers by thermal cure without an additional of any catalyst or curing agent.

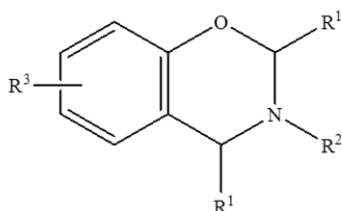


Figure 14: Monofunctional benzoxazine monomer.

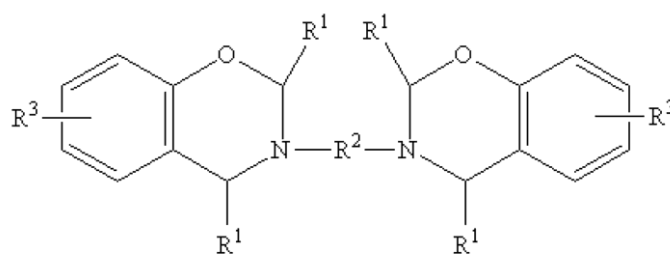


Figure 15: Bifunctional or multifunctional benzoxazine monomer where R^1 , R^2 and R^3 ,

are organic radicals.

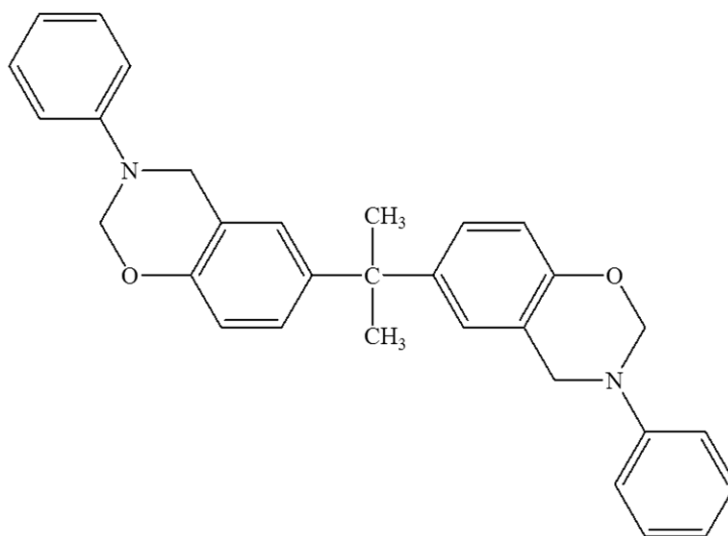


Figure 16: bisphenol-A, aniline based benzoxazine monomer (BA-a).

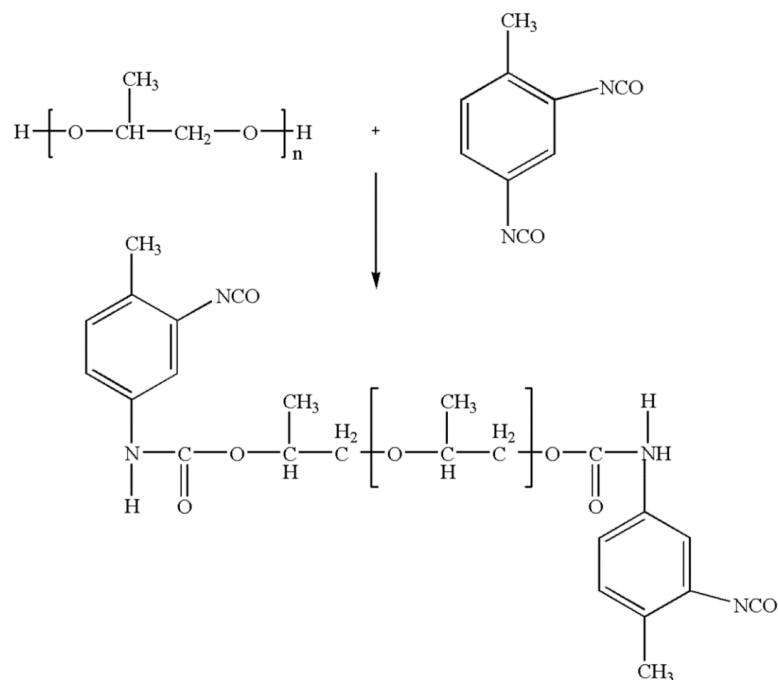
Urethane elastomer (PU) has been reported to form high performance alloys with the BA-a benzoxazine resin with substantial enhancement in toughness of the polybenzoxazine. The functionality of the hydroxyl-containing reactant as well as the isocyanate for urethane resin synthesis can be varied. The hydroxyl-containing components cover a wide range of molecular weights and types, including polyester, polycarbonate, and polyether polyols. This flexibility in the selection of urethane reactants leads to the wide range of the resulting properties. The outstanding properties of polyurethane account for the facts that their use is economically feasible and that their range of applications is steadily increasing. These properties are unique combination of a high elastic modulus, exceptional tear and abrasion resistance, resistance to UV radiation, and finally providing fairly easy and efficient

processing. PU used in this study was prepared from toluene diisocyanate and poly(propylene glycol) at a 2:1 molar ratio. The synthesis reaction of PU is shown in Scheme 1. The representative chemical structure of PU as illustrated in Scheme 1 is the structure with chain ends formed by the more reactive NCO in the para-position to the methyl group. This type of para structure is more abundant than the other structures as described by Pegoraro and coworkers [76].



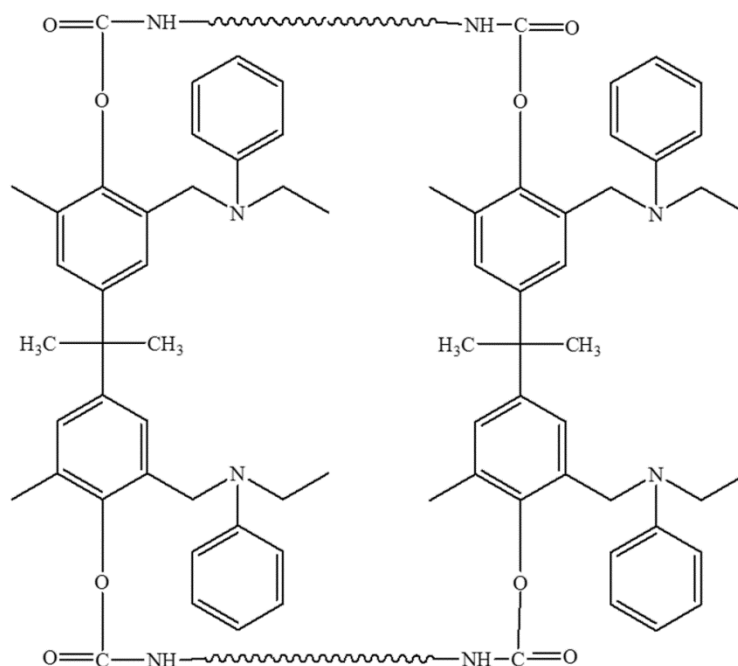
Table 7: Property comparison of major thermosetting resins used as ballistic composite matrices [73].

Property	Epoxy	Phenolics	Cyanate ester	Polybenzoxazine
Density (g/cc)	1.2-1.25	1.24-1.32	1.1-1.35	1.19
Max use temperature (C°)	180	~200	150-200	130-280
Tensile strength (MPa)	90-120	24-25	70-130	100-125
Elongation (%)	3-4.3	0.3	0.2-0.4	2.3-2.9
Dielectric constant (1MHz)	3.8-4.5	0.4-10	2.7-3.0	3-3.5
Cure temperature (°C)	RT-180	150-190	180-250	160-220
Cure shrinkage (%)	>3	0.002	~3	~0
TGA onset (°C)	260-340	300-360	400-420	380-400
T _g (°C)	150-220	170	250-270	170-340



Scheme 1: Chemical reaction of NCO-terminated PU prepared from toluene diisocyanate and poly(propylene glycol).

The polymerization between benzoxazine resin and urethane prepolymer occurred by thermal curing had been investigated by FTIR technique [77]. During thermal curing, the disappearance of tri-substituted benzene ring of benzoxazine resin and NCO group of urethane prepolymer were observed. Simultaneously, the phenolic group of polybenzoxazine reacted with NCO group of urethane prepolymer to form polybenzoxazine/PU copolymer network. The polymerization reaction between BA-a monomers and PU prepolymer is shown in Scheme 2.



Scheme 2: Polymerization reaction of PBA and PU.

Alloying BA-a resin with PU was found to substantially improve flexibility of the more rigid polybenzoxazine (PBA). Interestingly, the positive deviation on the glass transition temperature (T_g) of the PBA/PU alloys was also observed. T_g of the PBA/PU alloys ($T_g > 200^\circ\text{C}$) was found to be significantly greater than those of the parent polymers (i.e. T_g of the PBA is 165°C and that of PU is -71°C). Furthermore, the T_g of the PBA/PU alloy was observed to increase with an increase of the PU content. The formation of this polymer hybrid suggests the benefits of using polybenzoxazine as a matrix for ballistic armor composites due to its fine-tuned ability by alloying with other resins or polymers [20, 24, 25]. Fine-tuned mechanical properties can thus be obtained from the PBA/PU alloys to provide suitable structural integrity and energy

absorption for a ballistic composite application with synergistic behavior in their thermal stability as mentioned above.

The ballistic composite system of KevlarTM reinforced PBA/PU composite has been developed by our group. From the experiment, our KevlarTM reinforced 80/20 PBA/PU composite panel at 30 plies and 50 plies could resist the penetration from the ballistic impact of levels II-A and III-A based on NIJ standard, respectively [22]. This experiment suggests an importance of fine-tuned mechanical properties of the polymer matrix to suit the type of the fiber used. In this case, the addition of about 20 wt% of urethane elastomer is crucial to provide a composite with maximum penetration resistance. Moreover, the ballistic behaviors of the neat bisphenol A-based epoxy-KevlarTM composite (cured by an amine hardener) at the same fiber content has also investigated in comparison with the neat PBA-KevlarTM composite. Both composites showed complete penetration of the projectile. However, in this test, KevlarTM reinforced PBA composite was reported to show higher energy absorption characteristic than the epoxy composite as observed from a larger delaminated area due to a better fiber-matrix delamination process while very small delamination was observed in the epoxy composites [18, 22].

Kasemsiri observed the use of E-glass fiber reinforced PBA composite to destroy the tip of .44 Magnum projectile [78]. Even the composite was completely perforated by the projectile, it was found that E-glass composite could deform the projectile as seen in Figure 17 showing the potential use of the E-glass composite as

striking panel. Moreover, the failure pattern of the composite was obviously observed to be matrix cracking as noticed in Figure 18.



Figure 17: Deformation of .projectile after penetrated E-glass fiber reinforced PBA composite [78]

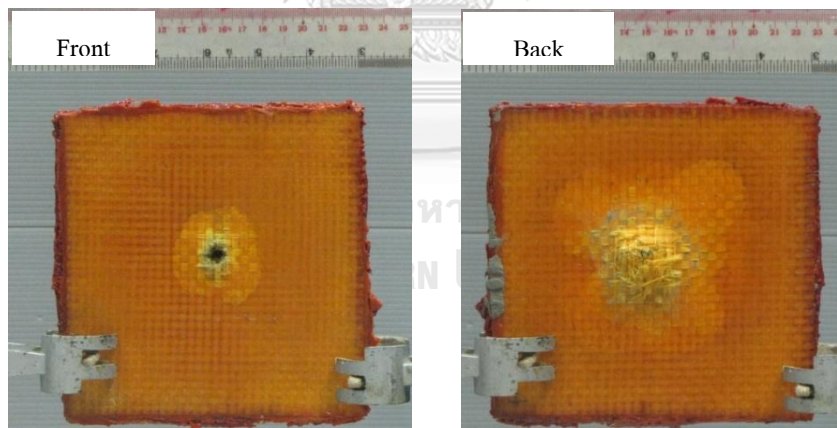


Figure 18: Failure mechanism of E-glass fiber reinforced PBA composite by matrix cracking [78].

2.6 REINFORCING FIBERS

2.6.1 Glass fiber

The basic component of glass fibers is silica blended with other types of oxides in which glass fiber is an amorphous solid nature make it differs from other ballistic fibers. it is known to have high strength, good temperature and corrosion resistance. They are manufactured by spinning into small filaments then pulled out through a nozzle from molten glass a a high production rate. Its main drawbacks are its relatively low fatigue resistance and high density, lower stiffness and strength compared to other ballistic fibers. However, its low price could make them an optimal solution for armors in which weight is not a primary concern. There are several types of glass fiber based on their applications. Type E and S glass fiber are two main types for ballistic fibers. type S glass fiber is high strength glass fiber which provides greater mechanical properties than E glass fiber so that it is more expensive than another one.

2.6.2 Aramid fibers

Aramid fiber can be divided into two types i.e. meta-aramid and para-aramid which the latter is ballistic fiber. Para-aramid fiber is long molecular chains of poly-para-phenylene terephthalamide. As known, aramid fiber has many outstanding characteristics which make its suitable to manufacture ballistic armor including low weight density and excellent mechanical but its sensitivity to ultraviolet radiation is

main drawback. Extended exposure to unprotected fibers can cause a loss of mechanical properties.

2.7. COMPUTER SIMULATION OF BALLISTIC IMPACT IN THE COMPOSITE MATERIALS

Typically, hard armor is designed by stacking varied sequence of different materials thus a large number of composite specimens are to be fabricated for an evaluation of their ballistic impact behaviors. Even if all materials are selected, geometrical parameters of the composite samples including size, curvature, and thickness as well as projectile parameters including shape, type of projectile material and projectile velocity are also needed to be optimized for a successful penetration resistant armor. Those parameters make ballistic armor evaluation process rather cumbersome, time-consuming and highly costly. This problem can be circumvented through a use of finite element method. With significant advancement in computer technology in the last few decades, this computing method has provided a large progress in ballistic armor research. Computer analysis yields much more information than that can be measured in a test and this makes it possible to understand the underlying physics better, which in turn makes the design process more accurate and faster. It is absolutely necessary to rely on some experimental results when the simulation methods are being developed. However, the accuracy of the simulation also depends on a chosen material model, some material data such as tensile

modulus, shear modulus or poisson ratio, and failure characteristic of the materials used. In the case of composites structures, delamination data, types of finite elements used, mesh density, types of contacts between different materials are necessary for the successful simulation of the ballistic impact behaviors of the specimen.

Numerous reports on computer simulations of ballistic behaviors of polymer composites via ABAQUS, LS-DYNA or ANSYS-AUTODYN software have been published [79-83]. For the simulation, material models, related to equation of state, which is used to define a relationship between pressure, density and internal energy, strength model and failure model are required. In principle, the behaviors of polymer composites can be presented through a set of orthotropic constitutive relations which based on a total stress formulation. A strength model is to define impact event failure at break point of material which can be categorized as isotropic and anisotropic types. A material stress/strain criterion is normally used in a failure mode for polymer composites. This model deals with predefined values of stress/strain at which the failure of material starts. Table 11 shows some useful results of various composite armor systems using AUTODYN simulation [16, 84-86]. Various simulation studies have been performed which can be divided into two major purposes 1) To predict types of materials or material designs and 2) To evaluate impact behaviors and their failures by varied projectile shapes and impact velocities of the projectiles.

Table 8: Parameters and simulation results of various composite armor systems using ANSYS AUTODYN program.

Composite systems	Parameters	Output results	Ref
Kevlar 29/epoxy/ Al_2O_3	-initial velocity -composite thickness	-stress/strain behavior -residual velocity	[84]
Kevlar/glass fiber/carbon fiber-epoxy	-stacking sequence -thickness -type of projectile	-energy of absorption -ballistic limit	[16]
Kevlar 29/PVB-Phenolic	-initial velocity	-tensile failure -back face deformation	[86]
Glass fiber/epoxy	-laminar orientation -thickness plate	-energy absorption	[85]

Material models are as follow: Orthotropic as equation of state, Elastic as strength, Material stress/strain as failure, Geometric strain as erosion model

Figure 19 shows an experimental result compared to a predicted damage of the composite by Lagrange model using ANSYS-AUTODYN program. The composites are sandwich structures based on Kevlar-29 fiber/epoxy resin with different stacking sequence of 6061-T6 aluminum plate. Impact test was performed using cylindrical shape of 7.62 mm diameter steel projectile at velocity of 180-400 m/s. The simulated results after ballistic tested were reported to be in good agreement with

the experimental results with an acceptable error of only 3.64% [84].

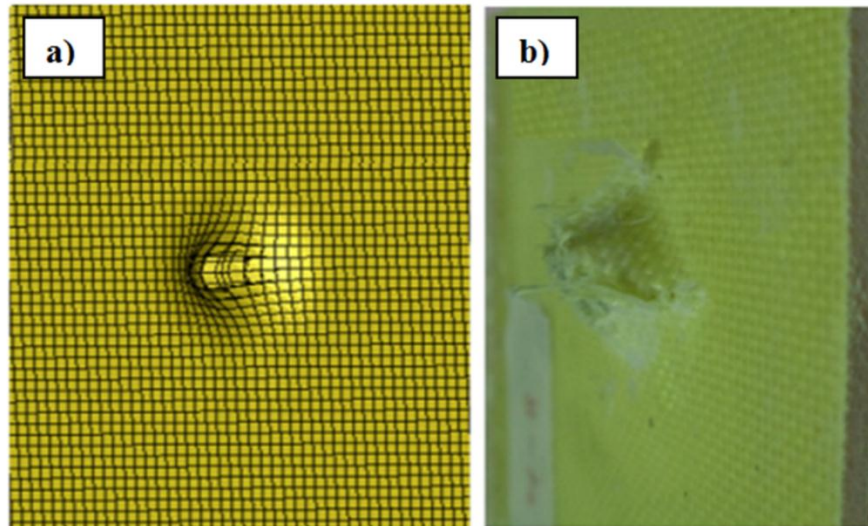


Figure 19: Comparison of the damage in the composite target a) simulated and b) observed [84].

In the reports by Ong and coworkers, by varying stacking sequence using computer simulation, a ceramic panel was found to be important as 1st layer to meet the incoming projectile followed by a wave spreading 2nd layer such as an advanced fiber composite (DyneemaTM) and porous foam as 3rd layer as a good shock attenuator by widening the shock rise time to delay the shock wave propagation [34]. Moreover, types of projectiles were also demonstrated by computer simulation to affect ballistic performance of composite armors with different stacking sequences. Comparison in the same thickness of target, the hierarchy of the ballistic limit velocity obtained for hybrid composite armors as reported by Bandaru and coworkers using ANSYS-AUTODYN program was as follows: for a blunt projectile: C/K > G/K > K/C > K/G and for a hemispherical projectile: G/K > C/K > K/G > K/C (C/K

represents carbon fiber layer in rich Kevlar layer and vice versa, G/K represents glass fiber layer in rich Kevlar layer and vice versa) [16].

For the simulation, material models, related to equation of state, strength model and failure model are required. In principle, the behaviors of polymer composites follow orthotropic constitutive relations based on a total stress formulation. A strength model is to define impact event failure at break point of material which can be categorized as isotropic and anisotropic types. A material stress/strain criterion is normally used in a failure mode for polymer composites. This model deals with predefined values of stress/strain at which the failure of material starts.

2.7.1 Materials modeling

The orthotropic EOS in ANSYS AUTODYN allows a non linear EOS to be used in conjunction with an orthotropic stiffness matrix. The stress tensor from these relations composed of hydrostatic and deviatoric components. The stress-strain relation for an orthotropic material follows equation (2) where the total stress, σ_{ij} can be related to the total strain, ϵ_{ij} through the constitutive coefficient matrix, C_{ij} .

$$\begin{bmatrix} \sigma_{11} \\ \sigma_{22} \\ \sigma_{33} \\ \tau_{23} \\ \tau_{31} \\ \tau_{12} \end{bmatrix} = \begin{bmatrix} C_{11} & C_{12} & C_{13} & 0 & 0 & 0 \\ C_{21} & C_{22} & C_{23} & 0 & 0 & 0 \\ C_{31} & C_{32} & C_{33} & 0 & 0 & 0 \\ 0 & 0 & 0 & C_{44} & 0 & 0 \\ 0 & 0 & 0 & 0 & C_{55} & 0 \\ 0 & 0 & 0 & 0 & 0 & C_{66} \end{bmatrix} \begin{bmatrix} \varepsilon_{11} \\ \varepsilon_{22} \\ \varepsilon_{33} \\ \gamma_{23} \\ \gamma_{31} \\ \gamma_{12} \end{bmatrix} \quad \dots 2$$

Where τ_{ij} and γ_{ij} are the shear stress and shear strains, respectively. To include non-linear shock effects in the above linear relations, it is first separated the volumetric (thermodynamic) response of the material from its ability to carry shear loads (strength). The strain components are split into their average ε_{ave} and ε_{ij}^d deviatoric components. The constitutive relation becomes as equation (3):

$$\begin{bmatrix} \sigma_{11} \\ \sigma_{22} \\ \sigma_{33} \\ \tau_{23} \\ \tau_{31} \\ \tau_{12} \end{bmatrix} = \begin{bmatrix} C_{11} & C_{12} & C_{13} & 0 & 0 & 0 \\ C_{21} & C_{22} & C_{23} & 0 & 0 & 0 \\ C_{31} & C_{32} & C_{33} & 0 & 0 & 0 \\ 0 & 0 & 0 & C_{44} & 0 & 0 \\ 0 & 0 & 0 & 0 & C_{55} & 0 \\ 0 & 0 & 0 & 0 & 0 & C_{66} \end{bmatrix} \begin{bmatrix} \varepsilon_{11}^d + \frac{1}{3}\varepsilon_{vol} \\ \varepsilon_{22}^d + \frac{1}{3}\varepsilon_{vol} \\ \varepsilon_{33}^d + \frac{1}{3}\varepsilon_{vol} \\ \gamma_{23} \\ \gamma_{31} \\ \gamma_{12} \end{bmatrix} \quad \dots 3$$

where $\varepsilon_{vol} = \varepsilon_{11} + \varepsilon_{22} + \varepsilon_{33}$ and $\varepsilon_{ave} = \frac{1}{3}(\varepsilon_{11} + \varepsilon_{22} + \varepsilon_{33})$

Pressure is defined as one-third of the trace of the stresses

$$P = -\frac{1}{3}(\sigma_{11} + \sigma_{22} + \sigma_{33}) \quad \dots 4$$

By expanding Eq (3), separating deviatoric and volumetric terms grouped separately, the expressions for the direct stresses are;

$$\sigma_{11} = \frac{1}{3}(C_{11} + C_{22} + C_{33})\varepsilon_{vol} + C_{11}\varepsilon_{11}^d + C_{12}\varepsilon_{22}^d + C_{13}\varepsilon_{33}^d \quad (4a)$$

$$\sigma_{22} = \frac{1}{3}(C_{21} + C_{22} + C_{23})\varepsilon_{vol} + C_{21}\varepsilon_{11}^d + C_{22}\varepsilon_{22}^d + C_{23}\varepsilon_{33}^d \quad (4b)$$

$$\sigma_{33} = \frac{1}{3}(C_{31} + C_{32} + C_{33})\varepsilon_{vol} + C_{31}\varepsilon_{11}^d + C_{32}\varepsilon_{22}^d + C_{33}\varepsilon_{33}^d \quad (4c)$$

Substituting Eq. (4a-c) into Eq (3), the following expression can be obtained for pressure:

$$P = -\frac{1}{9}[C_{11} + C_{22} + C_{33} + 2(C_{12} + C_{23} + C_{31})]\epsilon_{vol} - \frac{1}{3}[C_{11} + C_{12} + C_{13}]\epsilon_{11}^d - \frac{1}{3}[C_{21} + C_{22} + C_{12}]\epsilon_{22}^d - \frac{1}{3}[C_{31} + C_{32} + C_{33}]\epsilon_{33}^d \dots 5$$

On the right side, the first term represents the standard relationship between the pressure and volumetric strain which is Hooke's law at low compressions where the later terms are the coupling between the pressure and deviatoric strain. The first term of Eq (5) can be used to define the volumetric (thermodynamic) response of an orthotropic material in which the effective bulk modulus of the material K is defined as

$$K = \frac{1}{9}[C_{11} + C_{22} + C_{33} + 2(C_{12} + C_{23} + C_{31})] \dots 6$$

- Failure model of the samples

Composite panel after subjected to ballistic impact combine such many failure modes. Commonly, the failure from material stress and/or material strain are failure initiation. Once failures occur in composite material due to excessive tensile stress or strain or from shear stress or strain in through thickness, 11- direction, the delamination is formed and the stress in that direction is set to zero. However, if there are excessive of both two modes, the stress in the 11-direction is instantaneously set to zero, and the strain in the 11-direction of failure is stored.

Subsequently, if the material strains in the 11-direction exceeds the failure strain, the material stiffness matrix is modified as:

11-direction:

$$\begin{pmatrix} \sigma_{11} \\ \sigma_{22} \\ \sigma_{33} \\ \tau_{23} \\ \tau_{31} \\ \tau_{12} \end{pmatrix} = \begin{bmatrix} 0 & 0 & 0 & 0 & 0 & 0 \\ 0 & C_{22} & C_{23} & 0 & 0 & 0 \\ 0 & C_{32} & C_{33} & 0 & 0 & 0 \\ 0 & 0 & 0 & \alpha C_{44} & 0 & 0 \\ 0 & 0 & 0 & 0 & \alpha C_{55} & 0 \\ 0 & 0 & 0 & 0 & 0 & \alpha C_{66} \end{bmatrix} \begin{pmatrix} \varepsilon_{11}^d + \frac{1}{3} \varepsilon_{vol} \\ \varepsilon_{22}^d + \frac{1}{3} \varepsilon_{vol} \\ \varepsilon_{33}^d + \frac{1}{3} \varepsilon_{vol} \\ \gamma_{23} \\ \gamma_{31} \\ \gamma_{12} \end{pmatrix} \quad \dots 7$$

where α is the residual shear stiffness which is typically equal to 20% for composite. The 22- and 33-directions are assumed to be in the plane of the composite. Due to excessive stresses and/or strains in 22- and 33-directions, in-plane failure mode occurs. Once the failure is initiated, the stiffness matrix in fiber direction become as: equation (8) to (9)

22-direction:

$$\begin{pmatrix} \sigma_{11} \\ \sigma_{22} \\ \sigma_{33} \\ \tau_{23} \\ \tau_{31} \\ \tau_{12} \end{pmatrix} = \begin{bmatrix} C_{11} & 0 & C_{13} & 0 & 0 & 0 \\ 0 & 0 & 0 & 0 & 0 & 0 \\ C_{13} & 0 & C_{33} & 0 & 0 & 0 \\ 0 & 0 & 0 & \alpha C_{44} & 0 & 0 \\ 0 & 0 & 0 & 0 & \alpha C_{55} & 0 \\ 0 & 0 & 0 & 0 & 0 & \alpha C_{66} \end{bmatrix} \begin{pmatrix} \varepsilon_{11}^d + \frac{1}{3} \varepsilon_{vol} \\ \varepsilon_{22}^d + \frac{1}{3} \varepsilon_{vol} \\ \varepsilon_{33}^d + \frac{1}{3} \varepsilon_{vol} \\ \gamma_{23} \\ \gamma_{31} \\ \gamma_{12} \end{pmatrix} \quad \dots 8$$

33-direction:

$$\begin{pmatrix} \sigma_{11} \\ \sigma_{22} \\ \sigma_{33} \\ \tau_{23} \\ \tau_{31} \\ \tau_{12} \end{pmatrix} = \begin{pmatrix} C_{11} & C_{12} & 0 & 0 & 0 & 0 \\ C_{12} & C_{22} & 0 & 0 & 0 & 0 \\ 0 & 0 & 0 & 0 & 0 & 0 \\ 0 & 0 & 0 & \alpha C_{44} & 0 & 0 \\ 0 & 0 & 0 & 0 & \alpha C_{55} & 0 \\ 0 & 0 & 0 & 0 & 0 & \alpha C_{66} \end{pmatrix} \begin{pmatrix} \varepsilon_{11}^d + \frac{1}{3} \varepsilon_{vol} \\ \varepsilon_{22}^d + \frac{1}{3} \varepsilon_{vol} \\ \varepsilon_{33}^d + \frac{1}{3} \varepsilon_{vol} \\ \gamma_{23} \\ \gamma_{31} \\ \gamma_{12} \end{pmatrix} \dots 9$$

The combined effect of failure in all the three material directions results in a material that can only withstand hydrostatic pressure, by a change in the material stiffness and strength to isotropic with no stress deviators and no tensile material.

- Erosion criteria

An erosion algorithm that removes highly distorted elements when instantaneous geometric strain for erosion exceeds a definite value was implemented. The mass of removing cells is distributed equally to the remaining modes. By this distribution, the inertia and spatial continuity of inertia are conserved in the mesh. The specific value of erosion criteria is defined typically using a value of 0.5-2. However, the ballistic impact response is not sensitive to the variation of erosion strain. Principal strain components are used to calculate the geometric strain using the following equation:

$$\varepsilon_{eff} = \frac{2}{3} [|(\varepsilon_1^2 + \varepsilon_2^2 + \varepsilon_3^2) - (\varepsilon_1 \varepsilon_2 + \varepsilon_2 \varepsilon_3 + \varepsilon_3 \varepsilon_1) + 3(\varepsilon_{12}^2 + \varepsilon_{21}^2 + \varepsilon_{31}^2) |]^{1/2} \dots 10$$

In the present study, the geometric strain for erosion was considered as 1.5 for Kevlar composite targets.

2.7.2 Projectile modelling

A constitutive model for metals applicable at high-strain rates ($\approx 10^5 \text{ s}^{-1}$) was originally proposed by Steinberg and Guinan and latter enhanced by Steinberg, Cochran and Guinan. The yield stress increased with increasing strain rate but it is said that there must exist a limit. Experiments proved that at high pressure, higher than 5 GPa, the rate dependency becomes insignificant. Since the yield stress increases with increasing pressure and decreases with increasing temperature, this yield model is chosen as a function of effective plastic strain $\bar{\epsilon}_p$, pressure p and temperature T . The Steinberg-Guinan model for the flow stress is written as:

$$\sigma_y = [A + B(\bar{\epsilon}_p + \epsilon_0)]^n \left[1 + H_1 \frac{P}{J^{1/3}} - H_2(T - 300) \right] \quad \text{Equation 11}$$

Where $J = \frac{V}{V_0}$ is the volume ratio, A is the initial yield stress, B and n are work hardening parameters, ϵ_0 is the initial equivalent plastic strain, normally equal to zero and H_1 and H_2 are model parameters. This material models is used for lead.

CHAPTER III

LITERATURE REVIEWS

Bandaru AK. and co-workers [16] studied the effect of hybridization on the ballistic impact behavior of hybrid composite materials by simulation technique. They observed the position of Kevlar fiber/epoxy in glass fiber/epoxy to affect the ballistic limit value and energy absorption of the composite subjected by projectiles. It was found that the ballistic performance increased as the position of Kevlar fiber/epoxy layer changed from 1st position to 4th position as illustrated in Figure 20. The 4th position of Kevlar fiber/epoxy in glass fiber/epoxy exhibited the greatest energy absorption than the others. They also found that ballistic performance of the hybrid composite was sensitive to the geometry of the projectile. The hybrid composite absorbed more energy from blunt projectile than hemispherical one because the sharp nose of the hemispherical type projectile can easily penetrate the samples so that less impact energy was absorbed.

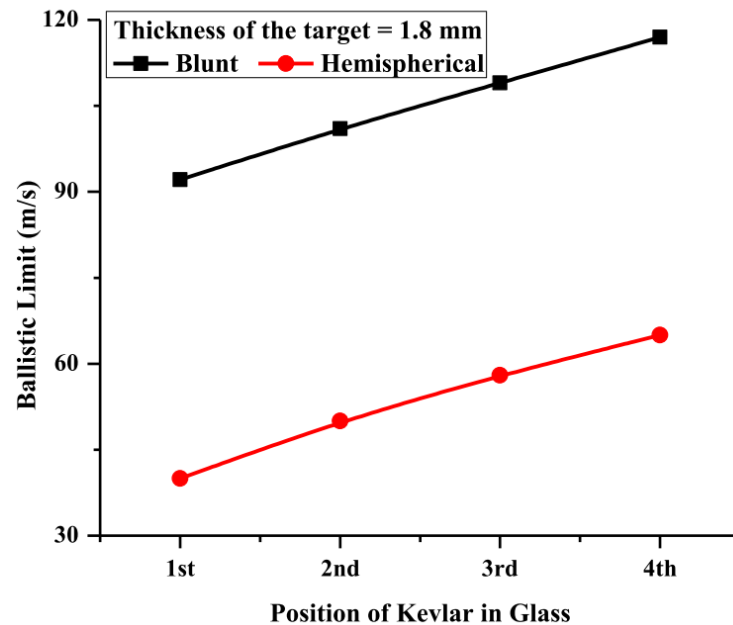


Figure 20: Ballistic limit for Kevlar fiber/epoxy in glass fiber/epoxy having thickness of 1.8 mm subjected to blunt and hemispherical projectiles.

Wielewski E and co-workers [58] fabricated fiber reinforced plastic materials into two panels and systematically investigated effect of number of plies in each panel on ballistic performance. They found that a single 12 plies plate of Kevlar reinforced epoxy had the highest kinetic energy absorption of all the arrangements as shown in Table 9. The results indicated that separating the number of plate significantly decreased the impact energy absorption so that the number of panel should be minimized.

Table 9: Initial and residual velocities of projectile for various plate arrangements.

Plate A	No. of piles	Plate B	No. of piles	V_i (m/s)	V_r (m/s)	ΔV (m/s)	ΔE_k (J)
Plate arrangements							
A ₁₂		–		332	206	126	88
B ₆		C ₆		326	269	57	44
D ₆		E ₆		325	257	68	51
F ₉		G ₃		328	244	84	62
H ₉		I ₃		327	249	78	58
J ₃		K ₉		324	246	78	58
L ₃		M ₉		326	239	87	64

Nayak N. and co-workers [13] investigated ballistic limit of Twaron/polypropylene and Twaron/epoxy composites. They found that Twaron/polypropylene had greater ballistic limit value than the other having the same thickness as shown in Figure 21. It was attributed to weak interaction between reinforcing fiber and polymer matrix facilitating flexible yarn movement so that ballistic limit increased. Strain at maximum stress of the sample was observed to be an effective value to identify ballistic performance of armor. Twaron/propylene composite also provided high deflection than too tight interaction between Twaron and epoxy. Furthermore, the ballistic limit value of the composite followed at linear relationship with composite thickness.

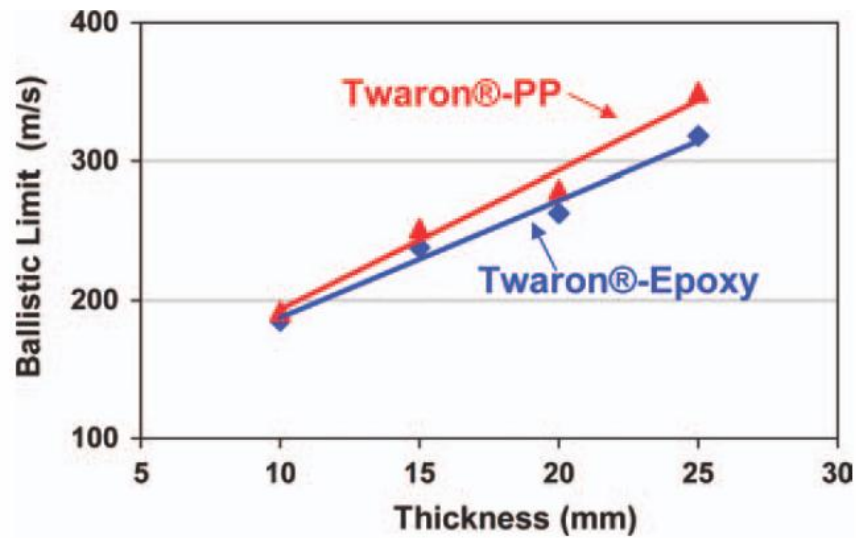


Figure 21: Ballistic limit as a function of composite laminate thickness.

The effect of interaction between fiber and matrix on ballistic performance was observed by Gopinath G. and co-workers [3] using finite element method. The composite laminates with and without matrix were designed. The two polymers including softer and stiffer matrix have been considered. It was found that the matrix decreased the maximum deflection of the sample and increased the size of the damage area. Moreover, the matrix attributed to enhance the reduction in the kinetic energy of projectile as seen in Figure 22.

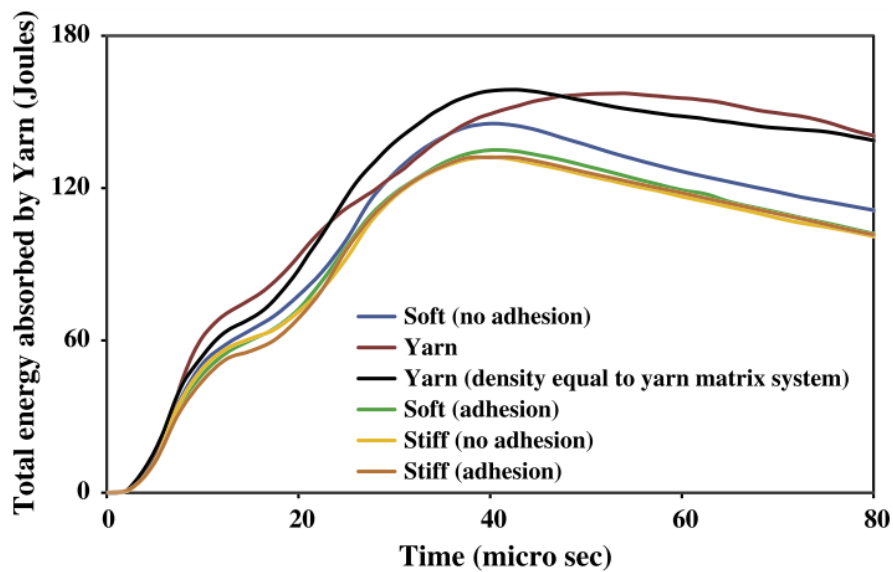


Figure 22: Time histories of energy absorption by the yarn.

Tham CY. and co-workers [86] monitored the back face deformation of fabric subjected to ballistic impact and recorded the formation of a pyramid which could be explained on the basis of transverse wave propagation. The yarns below the projectile area are stretched and the remaining material within the pyramid are also engaged in the process resulting in a larger volume being deformed and absorption of energy. During an impact, primary yarns are stretched and tensile waves travel down the primary yarns at the elastic wave speed, followed by a transverse displacement wave, engaging secondary yarns. Due to the crosswave of yarns, the elastic waves and transverse deformation doesn't travel radially away from the impact point, but along the orthogonal directions of the yarns. This gives rise to the observed pyramidal deformation. The base of the pyramid is longer towards the

clamped edges yarns; according to the model of Smith et al 1965 deflection propagates faster in this direction since stress in clamped yarns is higher.



CHAPTER IV

EXPERIMENTS

4.1 MATERIALS AND RESIN PREPARATION

Benzoxazine resin, urethane resin, glass fiber and aramid fiber were used to prepare specimens. Benzoxazine resin is based on bisphenol-A, aniline, and para-formaldehyde. Bisphenol A (polycarbonate grade) was supplied by PTT Phenol Co., Ltd. Para-formaldehyde and aniline were purchased from Merck Company and Panreac Quimica SA Company, respectively. Urethane prepolymer was prepared using toluene diisocyanate and polyether polyol with a molecular weight of 2000 which were obtained from IRPC Public Company Limited. The plain weave of E-glass fiber with area weight density of 600 g/m^2 and aramid fiber with 340 g/m^2 were used as reinforcing fiber which was purchased from Thai Polyadd Limited Partnership.

BA-a was synthesized using bisphenol A, aniline, and paraformaldehyde at a molar ratio of 1:2:4 based on solvent-less technology [75]. The three reactants were continuously mixed at about a temperature of 110°C for approximately 40 minutes. The obtained monomer was in clear yellowish color and solid at room temperature.

PU was prepared from toluene diisocyanate and polypropylene glycol (MW=2000). The two reactants were directly mixed in a four-necked round-bottomed flask under a nitrogen stream at about a temperature of 60°C for 40 minutes to yield a light yellow prepolymer. After cooling it to room temperature, the

urethane prepolymer was kept in a closed container with purged nitrogen and stored at cool temperature. The molecular structure of BA-a and PU are shown in Figures 23 and 24, respectively.

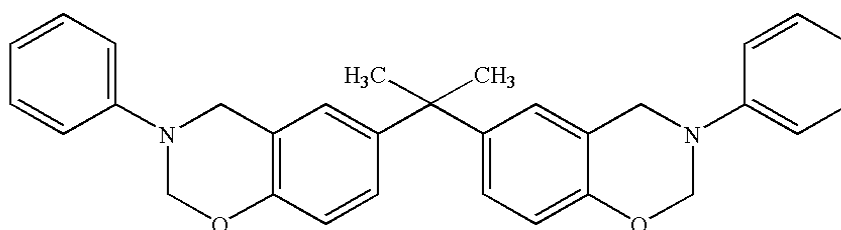


Figure 23: Bisphenol A – based benzoxazine monomer.

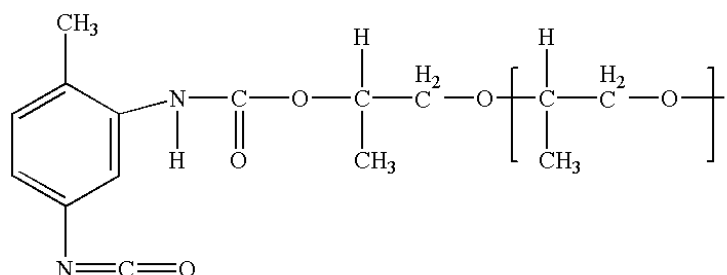


Figure 24: TDI and polypropylene glycol –based urethane prepolymer.

4.2 PREPARATION OF MATRIX AND SAMPLES

BA-a was mixed with PU to provide BA-a/PU alloy. The mixture was thoroughly stirred at an approximate temperature of 80°C until a homogeneous mixture was obtained. The BA-a and PU binary mixture at 0-40wt% of PU content were prepared and then evaluated as potential matrices for fiber-reinforced composites for a ballistic armor. Type E, S glass fibers and aramid fabrics were pre-impregnated with the binary mixture using hand-lay up procedure at a temperature

of 120°C. The weight fraction of the fiber was kept constant at approximately 65-70wt%. The pre-preges were then molded employing a compression molder at a temperature of 200°C using a pressure of 10 MPa for 2 hours. Properties of fabric used are shown in Table 10.

Table 10: Properties of fabric used in this study.

Fabric type	Weave pattern	Weight density (g/cm ²)	Warp	Weft	Modulus (GPa)	Elongation at break (%)
E glass	Plain	600	1900	1800	-	4.5-4.9
S glass	Plain	800	4500	3700	56	5.3
Aramid	Plain	360	3360 Dtex	3360 Dtex	67	N/A

4.3 CHARACTERIZATION OF THE SAMPLES

4.3.1 Interlaminar shear strength of aramid fiber reinforced PBA/PU composites

Interlaminar shear strength of aramid fiber reinforced PBA/PU composites with different PU content was determined according to ASTM 2344 [87]. The apparent interlaminar shear strength (ILSS) was calculated from the beam relationship based on equation (12). Test set up is shown in Figure 25.

$$\tau = \frac{3P}{4bh} \dots 12$$

where τ is the maximum interlaminar shear strength at failure (MPa), P is the maximum load (N), b is the specimen width (mm), and h is thickness of specimen (mm).

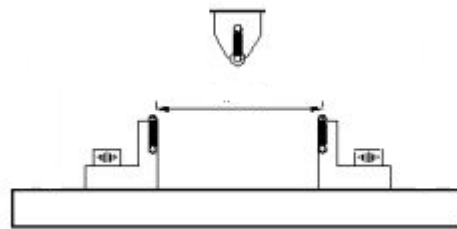


Figure 25 Set up for interlaminar shear strength test

4.3.2 Interfacial adhesion of aramid fiber reinforced PBA/PU composites

Interfacial adhesion between PBA/PU matrices and aramid fiber was evaluated by T-peel test method following ASTM D 1876 [88]. The specimens were fabricated having dimension of 305x25 mm². The test was performed using cross head speed of 254 mm/min. The test set up and specimen dimension are shown in

Figure 26.

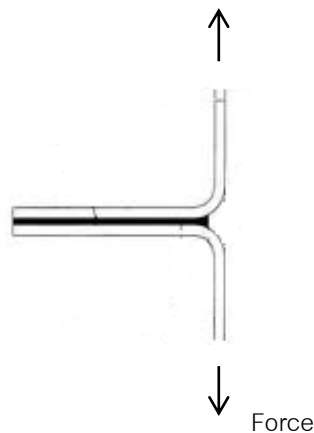


Figure 26: Interfacial adhesion test set up and specimen dimension.

4.3.3 Energy of absorption determination as soft ballistic armor

In order to determine the energy absorptions of aramid fiber reinforced PBA/PU specimens at PU mass concentrations of 0–40wt%, the composite panels with 8 plies having dimensions of $150 \times 150 \times 2.97 \text{ mm}^3$ were manufactured. The ballistic test was performed at Office of Logistics, Royal Thai Police, Bangkok, Thailand. The specimens were mounted on a metal frame. Four sides of the panels were clamped and placed 5 m in line to the gun barrel. The ballistic tests of the composite panels were performed at the center of the panels by impacting with 9 mm FMJ projectiles at a velocity of $367 \pm 9.1 \text{ m/s}$ and .44 Magnum SJHP bullets at a velocity of $436 \pm 9.1 \text{ m/s}$ according to NIJ Standard-0101.04 at protection levels II and IIIA, respectively 18. The ballistic test setup as suggested by NIJ is shown in Figure 27. The setup mainly consisted of a gun barrel, a specimen holder and two sets of chronographs which were used to determine the velocity of the bullet by measuring the time of bullet travelling through the distance of chronograph. The first

chronograph in front of the specimen was employed to measure the impact velocity of the bullet before impacting the specimen. The other chronograph was placed behind the specimen to measure the residual velocity of the bullet after penetrating the specimen. The energy of absorption by the composite specimen was determined by the difference of an initial kinetic energy and a final kinetic energy according to equation (13)

$$E_a = \frac{1}{2} m_j V_s^2 - \frac{1}{2} m_j V_r^2 \dots 13$$

It should be noted that nondeformable projectile and conservation of energy are assumed according to this equation. E_a is energy of absorption (J) whereas m_j is mass of projectile (g), V_s , V_r are striking and residual velocity (m/s), respectively.

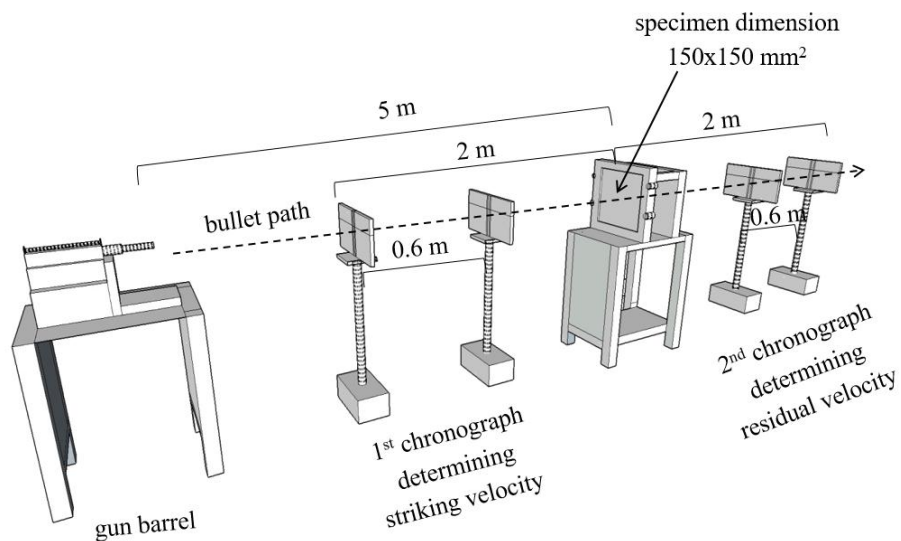


Figure 27: Ballistic test set up with two sets of chronograph to determine striking and residual velocity of projectile before the specimen is impacted and after it was penetrated.

The effect of composite thickness levels at 3, 4.5 and 6 mm having number of plies 8, 12 and 16 plies. on an energy absorption and ballistic limit (V_{50}) of the samples was also evaluated. V_{50} values of the samples were calculated based on equation (14) as follows.

$$V_{50} = \sqrt{(V_s^2 - V_r^2)} \dots 14$$

4.3.4 Ballistic impact test as hard ballistic armor

Type E and S glass fiber reinforced PBA composite was evaluated to be used as a striking panel of hard ballistic armor where aramid fiber reinforced PBA/PU composite was placed at the back as absorption panel. Each sample was separated by an air gap and tied together using adhesive tape. Ballistic test of the specimens was performed at Military Explosives Factory, Nakhon Sawan and Royal Thai Navy, Chonburi, Thailand. The performance of the specimens on penetration resistance was carried out based on NIJ standard at test level III. The specimen was placed on a steel frame 15 m in line with the gun barrel and subjected by 7.62x51 mm at a velocity of 847 ± 9.1 m/s at an angle of 90° to specimen for one shot at the center. The initial impact velocity is measured by placing optical sensors in the field which are connected to a data acquisition system. After the ballistic tests were carried out, each panel was secured by clamping the specimen horizontally and photographs of the front and back sides were taken. The failure pattern and damage areas on both surfaces of the sample were analyzed by using the SemAfore software. The damage

diameter of hole deformation along thickness direction of the specimen was also investigated. The equivalent diameters (D) of damage area of the specimen was calculated based on equation (15) and was presented instead of an approximate rectangle of the cone formation area.

$$D = 2 \sqrt{\frac{a \times b}{\pi}} \dots 15$$

where a and b are width and height of damage dimension, respectively.

For multi-hit performance evaluation, the curved human model specimen having $245 \times 290 \text{ mm}^2$ were manufactured and carried out ballistic test using the same projectile i.e. $7.62 \times 51 \text{ mm}$ with a velocity range of $847 \pm 9.1 \text{ m/s}$ based on level III of NIJ 0101.04 for body armor. The specimens were conditioned by spraying of water on both side for 15 min each and left for 10 min prior test. The panels were then attached to the backing material made of Roma Plastilina No.1 oil base modeling clay which is human body simulation and subjected ballistic test for six shots. The shot locations were marked as shown in Figure 28 where the location of each shot was not affected by previous impact damage. After each shot was performed, the penetration resistance of the panel was evaluated. In the case of the complete penetration on the specimen, the ballistic test was suddenly stopped. If only partial penetration occurred, the depth of penetration on the clay backing material was measured from the maximum momentary displacement of the rear surface of a ballistic panel.

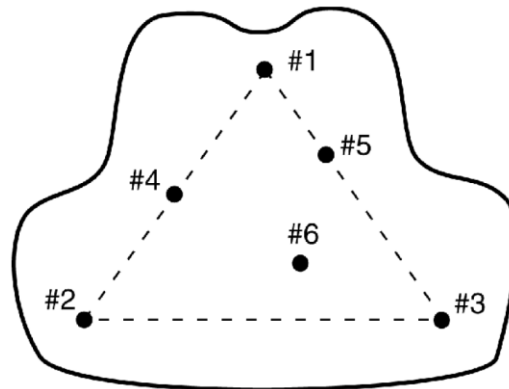


Figure 28: General armor panel impact locations for multi hits performance evaluation.

The optical micrograph on the impact and rear side of the damaged panels was taken using 5× magnification.

4.3.5 Computational studies on the ballistic behavior of the composites

The ballistic performance of aramid fiber reinforced PBA/PU ballistic panels were evaluated theoretically with a commercial hydrocode ANSYS AUTODYN. Aramid fiber reinforced PBA/PU composite were simulated as the orthotropic material in which the material properties differ along the three orthogonal planes. In ANSYS AUTODYN, the orthotropic equation of state (EOS) allows a nonlinear EOS to be used in coupled with an orthotropic stiffness matrix. The composite laminates reinforced with aramid fabrics having a plain weave pattern was assumed to have identical properties in the fiber directions but different properties from each other through the thickness direction. It was also assumed that materials were homogeneous. Four edges of the panels were constrained for the movement. An initiation of failure was resulted from the excessive tensile or shear stress and/or strain.

A 9 mm FMJ projectile made of a copper jacket with a lead core was modeled following the strength models of Steinberg-Guinan. The material properties of the projectile were obtained from the standard ANSYS AUTODYN material library as shown in Table [89]. The geometry of the projectile, the composite panel, and the mesh creation are shown in Figure 29. The simulation was performed under the same conditions as in the experimental work to have an accurate comparison. In order to validate the input properties of materials, energy absorptions of 8-ply 80/20 PBA/PU composite panels having a dimension of $150 \times 150 \times 2.97 \text{ mm}^3$ were theoretically predicted and compared with the values from ballistic impact experiments. The 8-ply of the specimens was employed to ensure the perforation so that the residual velocity of the projectile can be measured. The failure characteristics, deformation patterns, and energy dissipation mechanisms of the ballistic panel were deduced from the simulated ballistic impacts.

The ballistic limit of the composite system based on NIJ protection level IIIA was theoretically estimated from the 25-ply ballistic panel having dimension of $150 \times 150 \times 8.13 \text{ mm}^3$. The aramid fiber reinforced PBA/PU ballistic panel having the optimum ballistic performance was employed. The specimen dimensions resembled the ballistic panel utilized in the actual light weight body armor. The failure characteristics and deformation patterns of the ballistic panel were deduced from the simulated ballistic impacts. The ballistic limit were determined by varying impact velocities of the projectile until the sample were perforated. The reported value was

the maximum impact velocity of the projectile in which the ballistic panel was partially penetrated.

Table 11:Material properties for 9 mm FMJ and 7.62 mm projectiles [89].

Material: Lead core	Value	Property	Value
Density	11,340 Kg m ⁻¹	Equation of state	Shock EOS linear
Shear modulus	8,600 MPa	Gruneisen coefficient	2.74
Plasticity	Steinberg Guinan Strength	Parameter C1	2006 m/s
Initial yield stress	8 MPa	Parameter S1	1.429
Maximum yield stress	100 MPa	Parameter quadratic S2	0 s/m
Hardening constant	110	Failure	
Hardening exponent	0.052	Maximum equivalent plastic strain	2
Derivative dG/dP	1	Melting temperature	760 K
Derivative dG/dT	-9.976 MPa/°C		
Derivative dY/dP	0.0009304		
Material: Copper jacket	Value	Equation of state	Shock EOS linear
Density	8930 Kg m ⁻¹	Gruneisen coefficient	1.99
		Parameter C1	3940 m/s
		Parameter S1	1.48

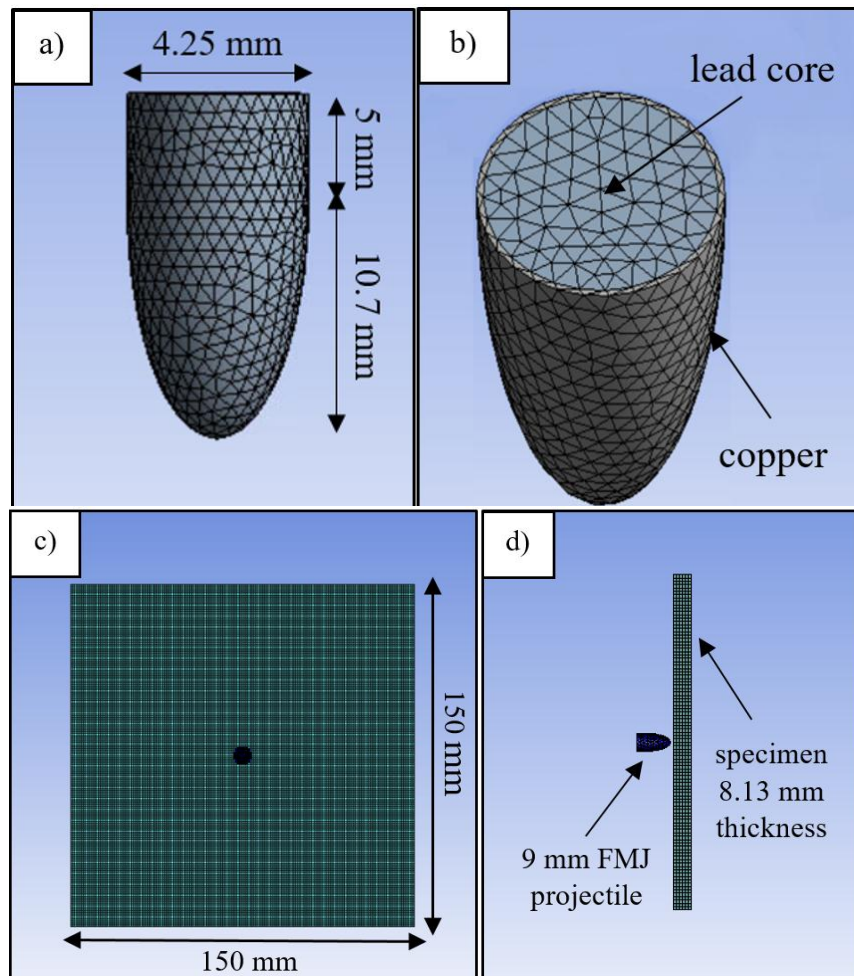


Figure 29: The mesh formation of a) copper jacket and b) a lead core of a 9 mm FMJ bullet c) Front view and d) side view of the aramid fiber reinforced 80/20 PBA/PU panel.

For hard armor, the simulation was done using the same conditions as in the experimental work to have an accurate comparison. The samples having dimension of $150 \times 150 \text{ mm}^2$ was set. S glass fiber reinforced PBA backed by that aramid composite subjected to $7.62 \times 51 \text{ mm}$ with velocity range from 838 to 856 m/s was also simulated. Figure 30 shows the 7.62 mm projectile and specimen used in this

investigation. Four edges of the panels were fixed. The comparison on the deformation of composite materials of experimental and simulation was carried out. The ballistic limit values of the specimens were determined by varying impact velocity of projectile until the sample failed to withstand the penetration of projectile. The coordination used in this research is that x and y-direction are in-plane directions or fiber direction and z-direction is through thickness.

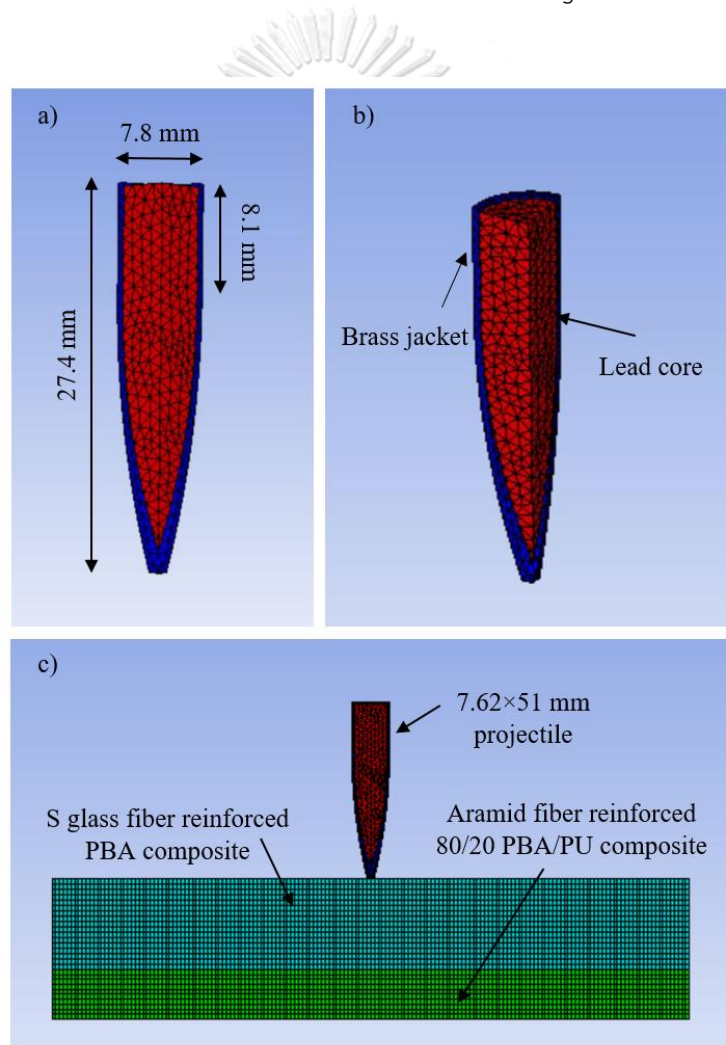


Figure 30: a) Dimension of 7.62x51 mm projectile b) Material of the projectile and c) Specimen geometry.

CHAPTER V

RESULTS AND DISCUSSION

5.1 INTERLAMINAR SHEAR STRENGTH OF ARAMID FIBER REINFORCED PBA/PU COMPOSITES

The interlaminar shear strength of aramid fiber reinforced PBA/PU composites is shown in Figure 31. Aramid fiber reinforced PBA composites exhibited the highest interlaminar shear strength of about 10.8 MPa while the composite with 40 wt% of PU exhibited the lowest ILSS value of 8.60 MPa. That is the interlaminar shear strength of the composites decreased with an increasing PU fraction in the matrix. The interlaminar shear strength of KevlarTM/epoxy composite was reported to be about 8.65-9.0 MPa [90] which was about the same as those of aramid fiber reinforced PBA/PU composites as discussed above. Interlaminar shear strength of sample depends primarily on the matrix properties and fiber-matrix interfacial strength rather than the fiber properties [91]. The higher interlaminar shear strength in the composite indicates the strong fiber-matrix interfacial strength.

5.2 INTERFACIAL ADHESION OF ARAMID FIBER REINFORCED PBA/PU COMPOSITES

Interfacial adhesion between PBA/PU matrices and aramid fiber was evaluated by T-peel test method following ASTM D 1876 [88]. The interlayer delamination strength, the maximum force per unit width of the sample to delaminate, of aramid fiber reinforced PBA/PU composites as a function of PU

contents is exhibited in Figure 31. From the figure, it was found that the neat PBA composite showed the highest value of peel resistance whereas the composite with an addition of PU in the benzoxazine matrix tended to provide lower peel resistant values. It might be because PBA could form stronger hydrogen bond with amide group in aramid fiber than urethane resin. The polar hydroxyl groups in polybenzoxazine network are more abundant than the polar urethane groups of the urethane elastomer due to a much longer hydrocarbon chain of the polyol used in the urethane synthesis (i.e. Mw of the polyol = 2000). In other words, the bonding strength of the PBA/PU matrices with aramid fiber can be tailored to give an appropriate value for fiber-matrix delamination process which is one crucial energy absorption in ballistic impact composites. KevlarTM/epoxy composite was reported to provide a rather high value of peel strength (i.e. 350 ± 25 N/cm [92]) thus lower energy absorption by fiber-matrix delamination and poorer ballistic resistance than our poly(BA-a/PU) matrices.

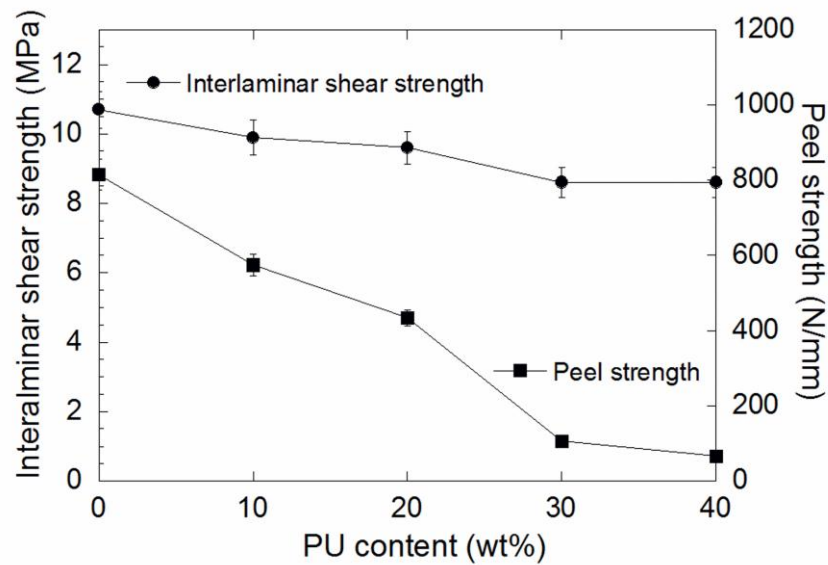


Figure 31: Interlaminar shear strength (ILSS) and peel resistance of aramid fiber reinforced PBA/PU composites.

In principle, weak fiber-matrix adhesion is advantageous for ballistic applications. Weak adhesion facilitates the easy debonding of fibers from the matrix and results in additional energy absorption mechanism through fiber pull out [93]. At the same time, composite laminates should also have good structural stiffness [3] [13], In our case, the PBA/PU matrix at 20wt% PU provides the best performance in terms of ballistic resistance suggesting this composition gives the balance between structural integrity and ballistic energy absorption. However, too weak matrix-fiber adhesion, i.e. in the composite with PU content of more than 20wt%, tended to provide less ballistic resistance. The specimens could be delaminated more readily and excessively as can be seen from the lower energy absorption of aramid fiber reinforced 70/30 and 60/40 PBA/PU composites. On the other hand, the composite with too strong matrix-fiber adhesion did not delaminate and fibers failed to detach

from the matrix thus less energy absorption was also observed. It could be concluded that a proper adhesion between matrix and fiber in the composite provided a high performance ballistic armor.

5.3 ENERGY ABSORPTION ABILITY OF ARAMID FIBER REINFORCED PBA/PU COMPOSITES

The energy absorptions of aramid fiber reinforced PBA/PU composites with various PU mass concentrations from 0–40wt% were evaluated. The composite panels were subjected to the complete penetration by 9 mm FMJ bullets at velocities of 367 ± 9.1 m/s according to NIJ Standard-0101.04 at the ballistic protection levels II. At the protection level II, the energy absorptions increased from 106.7 ± 24.8 J of poly (100BA-a-co-0PU) composite reinforced with aramid fibers to 130.7 ± 5.4 and 135.5 ± 8.3 J of the aramid fiber reinforced 90/10 PBA/PU and 80/20 PBA/PU composites, respectively (Table 12). The favorable effect of PU in aramid fiber reinforced PBA/PU composites was clearly evidenced. The enhancement in the energy absorption of the 80/20 PBA/PU composite specimen was ~127% greater than the energy absorption of the 100/0 PBA/PU specimen. For 70/30 PBA/PU and 60/40 PBA/PU composites reinforced with aramid fibers, the energy absorptions reduced to 116.6 ± 26.1 and 123.0 ± 13.6 J, respectively. The maximum synergistic effect in the energy absorption was observed at the composite specimen with the PU mass concentration of 20wt%. A considerably strong interfacial adhesion between the pure PBA and aramid fiber was formed as previously reported [19]. It was attributed to the

formation of the polar interaction between carboxyl and ether groups of aramid fibers and hydroxyl groups of the pure PBA [94]. Therefore, the projectiles could penetrate easily and the fiber failure was dominant. Aramid fiber reinforced 70/30 PBA/PU and 60/40 PBA/PU composite specimens delaminated more readily and excessively due to their weak adhesion interaction. Consequently, less energy absorptions by the composites were observed. In the latter case, the delamination of the composite laminates was a major failure mechanism.

Nayak *et al.* reported that the weak fiber-matrix adhesion is advantageous for ballistic applications. Weak adhesion facilitated the effortless debonding of fibers from the matrix and resulted in an additional energy absorption mechanism through the fiber pull-out [13]. The results from our ballistic test of the aramid fiber reinforced 80/20 PBA/PU composite revealed that an appropriate adhesion between the PBA/PU matrix and the reinforcing aramid fibers provided an enhancement in the ballistic performance as a result from the synergistic energy absorption. Noticeably, the percentage of the energy absorption by the aramid fiber reinforced 80/20 PBA/PU composite was less than that of the neat aramid fabrics in which 20 plies of the sample absorbed the impact energy about 500 J, corresponding to 90% absorption [35]. This could be related to higher energy absorption of multilayer panel in the non-perforation case than those of perforation case [95].

The ballistic performance of aramid fiber reinforced PBA/PU specimens at the PU mass concentrations of 0–40wt% were also evaluated at the NIJ ballistic

protection level IIIA as displayed in Table 13. The composite panels were impacted by .44 Magnum SJHP bullets with the velocities of 436 ± 9.1 m/s. The maximum synergy in the energy absorption of the aramid fiber reinforced 80/20 PBA/PU composite was also observed at this protection level. The energy absorption values of aramid fiber reinforced PBA/PU composites at the PU mass concentrations of 0, 10, 20, 30, and 40wt% were 355.7 ± 24.1 , 392.9 ± 14.2 , 399.2 ± 14.2 , 379.0 ± 17.5 , and 366.4 ± 19.5 J, respectively. In comparison to the fiber reinforced epoxy composite, the energy absorption by the 8-ply aramid fiber reinforced 80/20 PBA/PU composite was found to be greater than that of a 16-ply fiber reinforced epoxy composite (12 plies of aramid/epoxy plus 4 plies of glass fiber/epoxy). The energy absorption of the fiber reinforced epoxy composite was 369 J, whereas its thickness was 7.6 mm higher than the thickness of the 80/20 PBA/PU composite [16]. The results suggested that the copolymer of polybenzoxazine and polyurethane could be employed as the ballistic fiber-embedded polymer matrix that provided the better or comparable ballistic performance in terms of the energy absorption when compared to the conventional epoxy resin.

Currently, there has been limited reports on utilization of a copolymer as a binder for development of a ballistic armor. The enhancement on the ballistic protection capability has focused mainly on the development of the hybrid composites [16, 96], the particles with high energy absorption filled in the polymers composites [97, 98], and the honeycomb structures [99]. The energy dissipation of

the armor panel could be enhanced effectively by optimizing the adhesions between the polymer matrix and the reinforcing fibers. High energy absorbing ballistic panels could be potentially employed for a light-weight armor manufacturing since the number of plies and thickness of the panel could be reduced without compromising the ballistic performance. Although aramid fiber reinforced the pure PBA composite exhibited the lowest ballistic performance among other aramid fiber reinforced PBA/PU composites, KevlarTM reinforced PBA composites were reported to show a higher energy absorption than the neat bisphenol A-based epoxy composites reinforced with KevlarTM fibers at the same fiber content. At the complete penetration of the projectiles, the pure PBA composite showed a larger delaminated area due to a better fiber-matrix delamination process, while a very small delamination was observed in the epoxy composites [22].

Table 12: Energy absorption abilities of aramid fiber reinforced PBA/PU composites at various PU mass concentrations according to the NIJ protection level II.

Mass Ratio BA-a/PU	Sample number	Impact velocity (m/s)	Residual velocity (m/s)	Impact energy (J)	Residual energy (J)	Energy absorption (J)	Ave. energy absorption (J)	Ave. energy absorption/thickness (J)
100/0	1	358.08	327.30	789.20	659.36	129.85	106.68±24.77	37.17±8.86
	2	365.59	340.36	822.65	713.03	109.63		
	3	360.11	341.45	798.18	717.60	80.58		
90/10	1	375.75	345.21	869.01	733.49	135.52	130.69±5.35	45.43±0.91
	2	380.62	352.95	891.68	766.75	124.93		
	3	376.14	346.55	670.82	739.20	131.62		
80/20	1	364.76	333.15	818.92	683.14	135.79	135.5±8.26	48.39±2.95
	2	357.11	322.79	784.93	641.31	143.62		
	3	362.50	332.80	808.81	681.70	127.10		
70/30	1	356.32	332.11	781.46	682.40	99.06	116.16±18.05	40.20±5.86
	2	360.97	329.18	801.99	666.95	135.04		
	3	357.14	330.10	785.06	670.69	114.38		
60/40	1	355.88	330.18	779.53	671.01	108.52	122.95±13.56	42.54±5.26
	2	363.07	333.96	811.35	686.46	124.89		
	3	354.68	322.17	774.29	638.85	135.44		

Table 13: Energy absorption abilities of aramid fiber reinforced PBA/PU composites at various PU mass concentrations according to the NIJ protection level IIIA.

Mass Ratio BA-a/PU	Sample number	Impact velocity (m/s)	Residual velocity (m/s)	Impact energy (J)	Residual energy (J)	Energy absorption (J)	Ave. energy absorption (J)	Ave. energy absorption/thickness (J)
100/0	1	422.18	383.13	2160.22	1779.08	381.14		
	2	424.16	388.31	2180.53	1827.51	353.02	355.77±24.11	120.85±7.36
	3	419.98	385.87	2137.76	1804.62	333.15		
90/10	1	430.13	387.56	2242.34	1820.45	421.88		
	2	424.09	386.57	2179.81	1811.16	368.64	392.9±14.2	138.8±4.7
	3	420.01	380.09	2137.96	1750.95	387.01		
80/20	1	424.68	382.87	2185.88	1776.66	409.22		
	2	424.66	385.01	2185.67	1796.58	389.09	399.83±10.13	148.08±3.75
	3	425.10	384.20	2190.21	1789.03	401.18		
70/30	1	418.98	379.68	2127.60	1747.18	380.41		
	2	417.82	376.73	2115.83	1720.14	395.69	378.95±17.52	130.52±6.03
	3	416.01	378.55	2097.54	1736.80	360.74		
60/40	1	413.98	375.11	2073.69	1702.56	371.13		
	2	425.00	390.08	2189.18	1844.21	344.97	366.40±19.51	131.48±9.95
	3	423.48	384.35	2173.54	1790.43	383.12		

5.4 EFFECT OF THICKNESS ON BALLISTIC LIMIT AND ENERGY ABSORPTION OF ARAMID FIBER REINFORCED PBA/PU COMPOSITES

As the impacted kinetic energy of projectile is less than or equal to the energy absorption of the specimen, therefore the projectile can stuck in the target. On the other hand, complete penetration takes place as the impact kinetic energy of projectile is more than the energy absorption. When the projectile penetrates the target completely with zero residual velocity then initial velocity of the projectile is referred to as the ballistic limit of a specimen. In other word, ballistic limit of the sample is often defined as the minimum impact velocity that will result in complete perforation with zero exit velocity.

Ballistic limit at 50% (V_{50}) is generally referred to as a particular value of impact velocity at which at least 50% of the sample tested will be completely penetrated by the projectile. Unless large number of samples are tested to define the ballistic limit, it is very difficult to determine similarity of their ballistic limit value [100]. In other direction, V_{50} value can be determined regarding to as equation (17) [66]. It should be noted that by this method the projectile is hard enough and the specimens were totally penetrated during ballistic impact test.

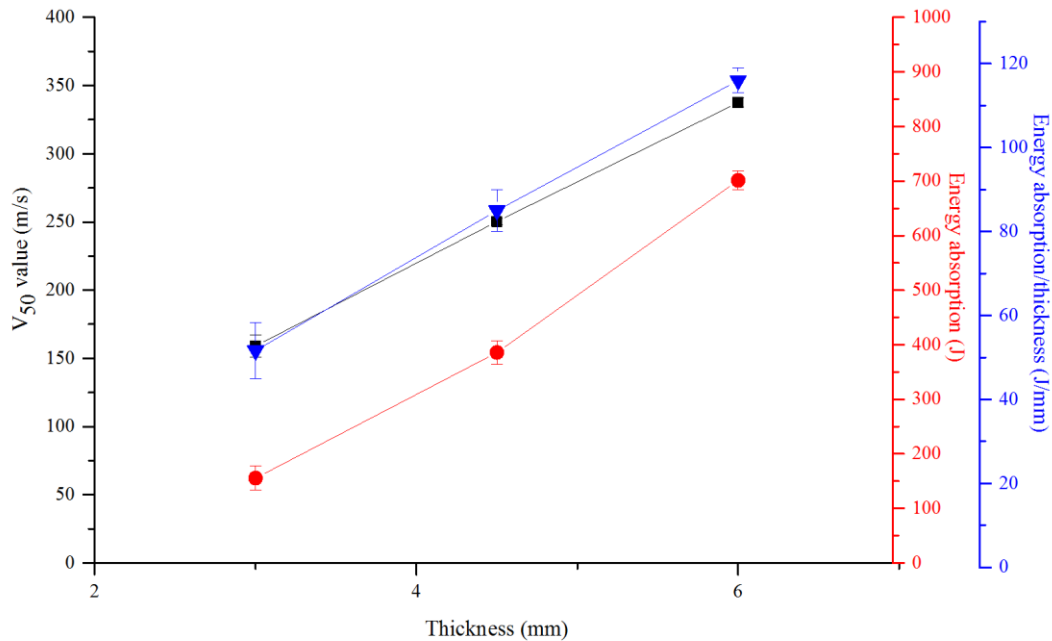


Figure 32: V_{50} value and energy absorption of aramid fiber reinforced 80/20 PBA/PU composites as a function of the sample thickness.

Samples having aramid fiber reinforced 80/20 PBA/PU with different thickness values of 3, 4.5, and 6 mm were subjected to ballistic test by 9 mm projectile at impact velocity 332 ± 12 m/s to determine the influence of thickness to V_{50} value and their energy absorption properties. As illustrated in Figure 32, V_{50} value and energy absorption increased linearly with increasing the composite thickness as expected. V_{50} values of the samples were calculated as 159.1 ± 8.3 , 250.3 ± 2.4 and 337.5 ± 3.4 m/s whereas energy absorption of the samples was 155.4 ± 22.1 , 385.7 ± 21.4 and 701.2 ± 17.3 J for thickness levels of 3, 4.5 and 6 mm, respectively. However, a sharp increase in energy absorption was observed if the thickness of the sample was

beyond the critical thickness significantly influencing overall performance of the panel [101].

A rapid increased in energy absorption/thickness of the specimen was also observed as can illustrated in Figure 32. Such values were calculated as 55.3 ± 6.7 , 89.7 ± 5.0 and 119.9 ± 3.0 with specimen thickness of 3, 4.5 and 6 mm, respectively. Gu *et al.* reported that energy absorbed by Twaron fabric increased linearly with the target thickness [102]. Iremonger *et al.* also found that the energy absorbed by fragment simulating projectile was proportional to the thickness of laminates [103]. The proportional constant depends upon the composite material and the projectile used. The occurrence of this trend denoted that for definitive projectile and striking velocity, energy of absorption per thickness has a critical value with thickness variation. The results implied that the performance of armor panel can be enhanced effectively by increased specimen thickness. However, the weight of specimen is also considerably affected by sample thickness which limits the movement of officer.

5.5 DEPTH OF DEFORMATION ON THE BACK FACE OF ARAMID FIBER REINFORCED PBA/PU COMPOSITES AND ARAMDI FABRIC AFTER BALLISTIC IMPACT

Aramid fabric with various numbers of plies is commercially used as energy absorption panel in a soft body armor to resist penetration of projectile based on NIJ standard at test level II-A to III-A. In this experiment, ballistic performances of the samples regarding to perforation resistance and depth of deformation on the back face of aramid fiber reinforced 80/20 PBA/PU composite and aramid fabric at number

of ply of 25, 30 and 35 plies were equally compared to each other. The center of specimens was subjected by .44 Magnum at a velocity of 427 ± 15 m/s. As can be seen in Figure 33, no perforation on both aramid fiber reinforced 80/20 PBA/PU composite and aramid fabric was noticed even at the minimum number of 25 plies. With a larger number of ply, depth of deformation on the back face of our composite and aramid fabric expectedly decreased. Those values of aramid composite were 20, 15 and 8 mm whereas the values of aramid fabric were 44, 35 and 21 mm at number of ply of 25, 30 and 35 plies, respectively. The results were in a good agreement with those observed in the system of aramid fabric where the increase in number of ply caused the decrease in damage depth and diameter [35]. Depth of deformation on the back side of our aramid composite was 45% less than aramid fabric compared at equal number of ply i.e. those values were 20 and 44 mm, respectively at 25 plies level. It was attributed to the projectile-yarn friction which investigated the inter-layer interaction and yarn-to-yarn friction. With the presence of PBA/PU binder, frictional contact between the projectile and aramid fiber reinforced PBA/PU composite was higher thus the mobility of the yarn upon impact would be reduced, resulting in higher energy absorption.

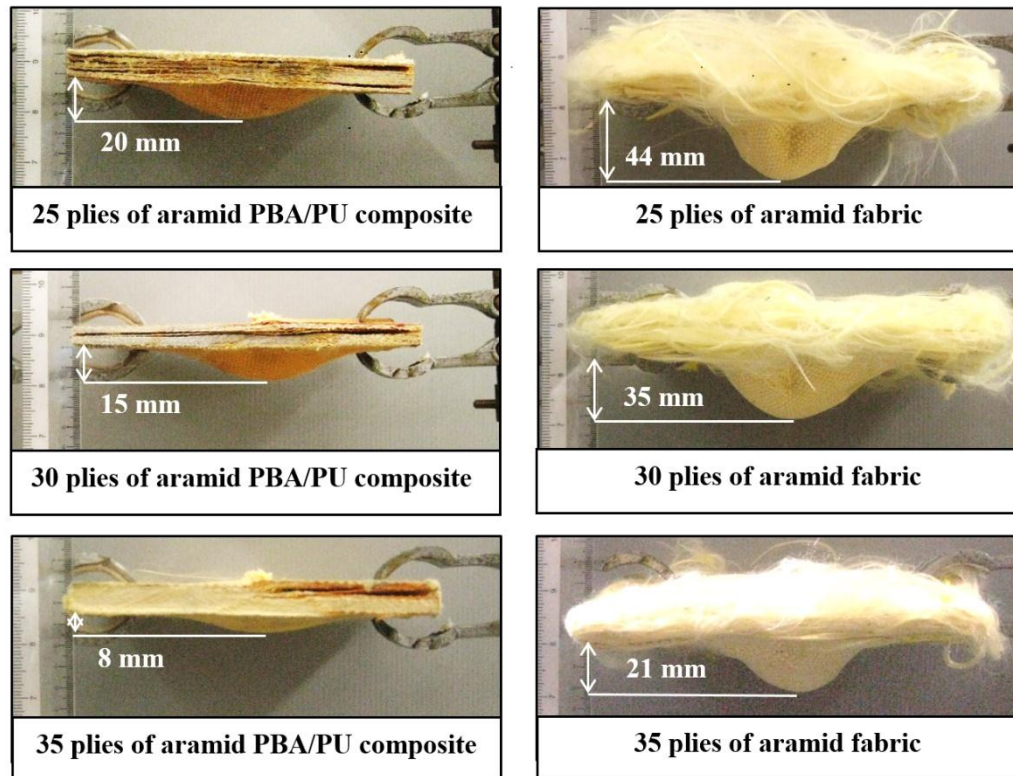


Figure 33: Depth of deformation on the back side of aramid fiber reinforced 80/20 PBA/PU composite compared to aramid fabric with vary thickness after subjected to .44 Magnum at a velocity of 427 m/s regarding to NIJ standard test level III-A.

Consequently, depth of penetration on back side of the composite sample was lower than aramid fabric with lower friction contact [104]. Karahan *et al.* studied the effect of three stitch types of aramid fabric using high twist para aramid sewing yarn in order to increase performance of aramid fabric by increasing fabric friction. The stitch types included 1) sewn inside from the edges 2) sewn inside from the edges and in diamond shape and 3) sewn inside from the edges and then with intervals in bias type. It was found that no significant difference in trauma depth and

trauma diameter was determined [35]. Therefore, it could be concluded that the performance of ballistic armor could be enhanced by 45% with the use of our aramid fiber reinforced 80/20 PBA/PU composite to substitute the use of aramid fabric regarding to trauma depth and diameter.

5.6 TENSILE PROPERTIES OF ARAMID FIBER REINFORCED PBA/PU COMPOSITES

The energy absorption by a ballistic panel during an impact of a projectile were attributed to several mechanisms including tensile failures, matrix cracking, delamination, and shear plugging. Tensile failures of primary yarns under an impact point and the surrounding secondary yarns were reported to be the main contributing mechanism for high energy absorptions [105]. Therefore, the tensile properties of the aramid fiber reinforced PBA/PU composites were primarily evaluated.

The effect of PU mass concentrations on the tensile properties of the aramid fiber reinforced PBA/PU specimen was investigated. The results are shown in Table 14. With an addition of PU in the aramid fiber reinforced PBA/PU composites, the modulus values significantly enhanced from 11.2 ± 0.8 GPa of the PBA composite to 17.3 ± 1.1 and 22.9 ± 0.5 GPa of the 90/10 PBA/PU and 80/20 PBA/PU composites, respectively. The modulus value then slightly decreased to 20.7 ± 2.2 and 16.7 ± 3.4 GPa when the PU mass concentrations in the composite specimens were 30 and 40wt%, respectively. The synergistic behavior in the tensile modulus of the aramid fiber reinforced 80/20 PBA/PU composite was two times higher than the tensile

modulus of the PBA composite reinforced with aramid fibers. The synergistic behavior in the flexural modulus of aramid fiber reinforced 80/20 PBA/PU was previously reported by Rimdusit *et al.* [22]. The tensile strength of aramid fiber reinforced 80/20 PBA/PU composite (446.6 ± 48.3 MPa) was 54 MPa higher than the tensile strength of the pure PBA reinforced with the aramid fibers (392.7 ± 34.0 MPa). The tensile strength of the Kevlar 29/epoxy composite [90] (170 MPa) was also lower than the tensile strength of our aramid fiber reinforced 80/20 PBA/PU composites. The aramid fiber reinforced 80/20 PBA/PU composites also exhibited better modulus and tensile properties than the Kevlar/epoxy composite having the tensile strength of 291.1 ± 12.5 MPa and the modulus value of 12.7 ± 1.1 GPa [106].

The measured tensile properties of aramid fiber reinforced PBA/PU composites was in agreement with the ballistic performance. The aramid fiber reinforced 80/20 PBA/PU composite provided the best ballistic performance and exhibited the synergistic behavior in the ballistic energy absorption, the tensile modulus, and the tensile strength. In addition, the aramid fiber reinforced 80/20 PBA/PU demonstrated the conformity between the structural integrity and the ballistic energy absorption. The measured modulus values of the ballistic panel were further employed for theoretical investigations.

Table 14: Tensile properties of the aramid fiber reinforced PBA/PU composites at various PU mass concentrations.

Mass ratio	Young's Modulus	Tensile strength	Strain at break
BA-a/PU	(GPa)	(MPa)	(%)
100/0	11.2±0.8	392.7±34.0	4.7±0.2
90/10	17.3±1.1	413.5±22.4	4.5±0.3
80/20	22.9±0.5	446.6±48.3	4.3±0.1
70/30	20.7±2.2	418.1±41.9	4.3±0.3
60/40	16.7±3.4	374.8±34.9	4.7±0.5

5.7 AND SIMULATION RESULTS COMPARISON ON EXPERIMENTAL MEASUREMENTS OF ARAMID FIBER REINFORCED PBA/PU COMPOSITES

An energy absorption of aramid fiber-reinforced 80/20 PBA/PU was also predicted by a hydrocode simulation and compared to the value determined from the experimental result. The simulation on ballistic test was conducted by impacting a 9 mm FMJ bullet at the velocity of 436 ± 9.1 m/s for one shot at the center of the 8-ply aramid fiber-reinforced 80/20 PBA/PU ballistic panel having dimensions of $150\times 150\times 2.97$ mm³. The conditions employed in the theoretical investigation were equivalent to the actual experimental setup. The properties of aramid fiber reinforced 80/20 PBA/PU composite are presented in Table 15. It was also assumed that materials were homogeneous. An initiation of failure was triggered from the excessive tensile stress and/or strain or shear stress and/or strain. The predicted

energy absorption of the aramid fiber reinforced 80/20 PBA/PU composite was 402 J. This value was quite similar to the measured energy absorption of 399 J. The difference was only 0.75%. Therefore, the theoretical modeling of the projectile and the ballistic panel and various material parameters utilized in the simulation were validated.

Table 15: Materials properties of the aramid fiber reinforced 80/20 PBA/PU composite.

Equation of state	Density, g/cm ³	Young modulus, kPa			Poisson's ratio		
	ρ	E_{11}	E_{22}	E_{33}	ν_{12}	ν_{23}	ν_{31}
Orthotropic	1.5	2.3×10^7	2.3×10^7	1.5×10^6	0.07	0.698	0.075
Strength	Shear modulus, kPa			Failure	Tensile failure strain		
	G_{12}	G_{23}	G_{31}		ϵ_{11}	ϵ_{22}	ϵ_{33}
Elastic	3×10^5	1.5×10^4	1.5×10^4	Material stress/strain	0.07	0.07	0.02

* Remark: Poisson's ratio and shear modulus of the composites were estimated by comparison of experimental and simulation results.

In the actual light weight body armor, the ballistic panel composed of the 25-ply aramid fiber-reinforced 80/20 PBA/PU composites. Hence, the ballistic impact on the 25-ply aramid fiber-reinforced 80/20 PBA/PU composites having a dimension of $150 \times 150 \times 8.13 \text{ mm}^3$ was simulated under the same conditions for the energy absorption prediction. The hole formation and fiber breakages under at the impact point and the deformation of primary yarn regions on the impact side of the composite were observed from both the theoretical results and the actual experimental measurements as illustrated in Figures 34. These results further

corroborated the validation of material parameters employed for the theoretical investigations. Therefore, the simulations were additionally exploited for predicting the failure mechanisms of the composite under the ballistic impact and the ballistic limit.

The time-dependent stress distribution and material deformations during the ballistic impact of the aramid fiber-reinforced 80/20 PBA/PU were illustrated in Figure 35. At the precise moment of the projectile impact, a much intense stress around the impact point was generated and the hole from fiber failures due to the excessive shear stress and/or strain was subsequently formed as observed in Figure 35a. The residual stress wave then propagated along the plane of the panel and through the transverse direction along the panel thickness, resulting in a stretching of the unbroken yarns and a conical deformation as noticed in Figures 35b and 36c. The stress was further propagated and hence the global deformation in the composite was observed (Figure 35d).

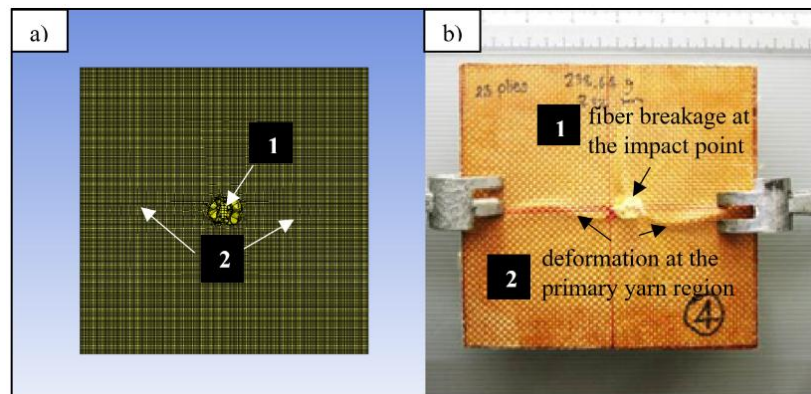


Figure 34: The comparison of the material deformations on the impact side of the 25-ply aramid fiber reinforced 80/20 PBA/PU composite panel from a) the theoretical simulation and b) the actual experimental measurement.

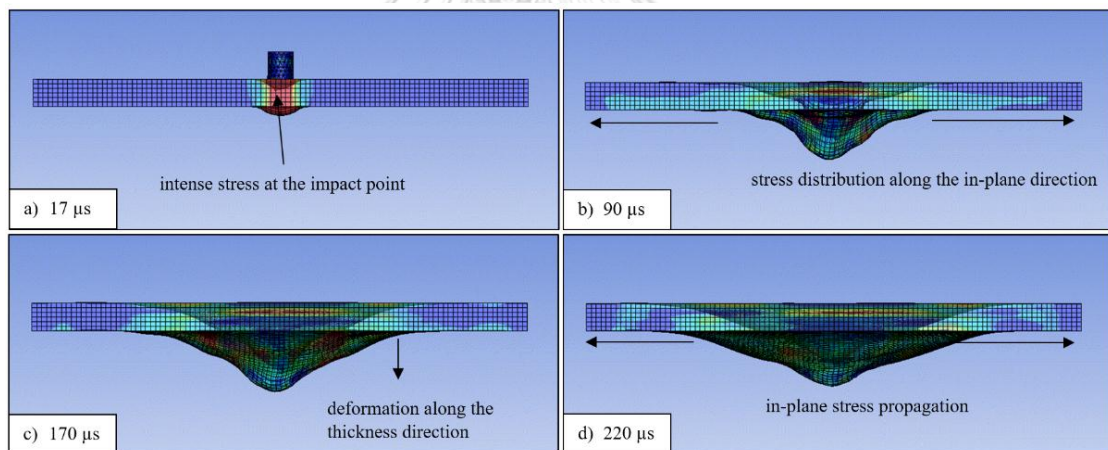


Figure 35: Time-dependent evolutions of the stress distribution and the panel deformations after impacting the 9 mm FMJ projectile onto the 25-ply aramid fiber reinforced 80/20 PBA/PU composite.

5.8 THE BALLISTIC LIMIT AND THE FAILURE MECHANISMS OF ARAMID FIBER REINFORCED 80/20 PBA/PU COMPOSITE PANEL

The ballistic limit of the 25-ply aramid fiber reinforced 80/20 PBA/PU composites with the dimension of $150 \times 150 \times 8.13 \text{ mm}^3$ was determined by varying an impact velocity of a 9 mm FMJ bullet until the perforation on the panel was achieved (Figure 36a). The theoretical ballistic limit of the aramid fiber reinforced 80/20 PBA/PU composite panel was determined to be 690 m/s. The ballistic limit of our ballistic panel was higher than the ballistic limits of the Kevlar/polypropylene composite [107], the Kevlar 29/epoxy laminate [86], and the hybrid laminates of PVB-kenaf fiber, PVB films, and Heracron[®] aramid fabric coated with PVB-phenolic film [108] in which the ballistic limits were reported to be 471 m/s, 680 m/s, and 665 m/s, respectively. The high ballistic limit of the aramid fiber reinforced 80/20 PBA/PU suggested that the poly(benzoxazine-co-urethane) polymer matrixes could be employed to enhance the ballistic performance of fiber reinforced polymer composites for soft body armor applications.

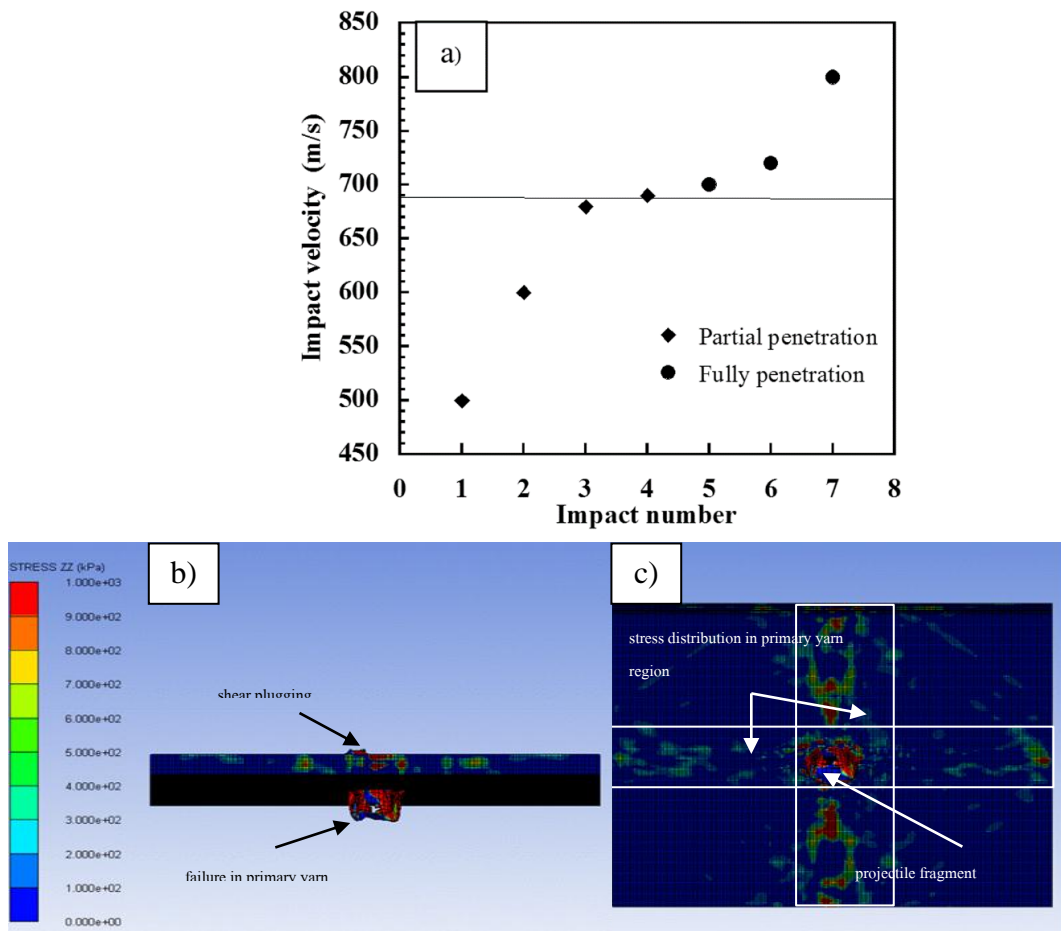


Figure 36: The theoretical ballistic limit determination (a), the failure mechanisms (b) and the stress distribution (c) of the 25-ply aramid fiber-reinforced 80/20 PBA/PU composite after subjected to an impact by a 9 mm FMJ projectile having an impact velocity of 800 m/s.

The failure modes of the 25-ply aramid fiber reinforced 80/20 PBA/PU panel impacted by a 9 mm FMJ projectile having an impact velocity of 800 m/s, which exceed the ballistic limit of the sample, is shown in Figure 36b. Shear plugging and failures in primary yarn were the main failure patterns as observed from the impact

face and the back side of the composite panel, respectively. The stretching and breakage of primary yarns were due to the excessive stress and strain values. Moreover, a much intense stress through thickness direction was also observed as illustrated in Figure 36c. The stress distribution in the primary yarn region was observed due to the plain weave design of the aramid fabric. This characteristic resulted in a pyramidal shape deformation on the back side of the composite.

5.9 MEASUREMENT OF E GLASS FIBER REINFORCED PBA COMPOSITE AS STRIKING PANEL FOR HARD BALLISTIC PANEL

At NIJ level III ballistic impact, the test was performed on the composites which were assembled from glass fiber reinforced PBA composite as striking panel and backed by aramid fiber reinforced 80/20 PBA/PU samples as energy absorption panel. The composite panels were subjected by 7.62x51 mm projectile at a velocity of 847 ± 9.1 m/s. It was found that even type E glass fiber reinforced PBA composite could deform the tip of projectile into fragmented but perforation on the composite panel of the first glass fiber composite panel and later aramid fiber composite panel was observed. This could be related to a high residual kinetic energy remained in the deformed projectile in a big mass. Consequently, two panels of type E glass composite were manufactured to further destroy the fragmented into small pieces with lower kinetic energy so that as aramid fiber composite samples would completely absorb the residual energy to prevent perforation on the specimen. The specimens of the first two panels of type E glass fiber reinforced PBA and later

aramid fiber reinforced 80/20 PBA/PU resisted the penetration of 7.62 mm projectile as can be seen on the back side of aramid composite panel as shown in Figure 37.

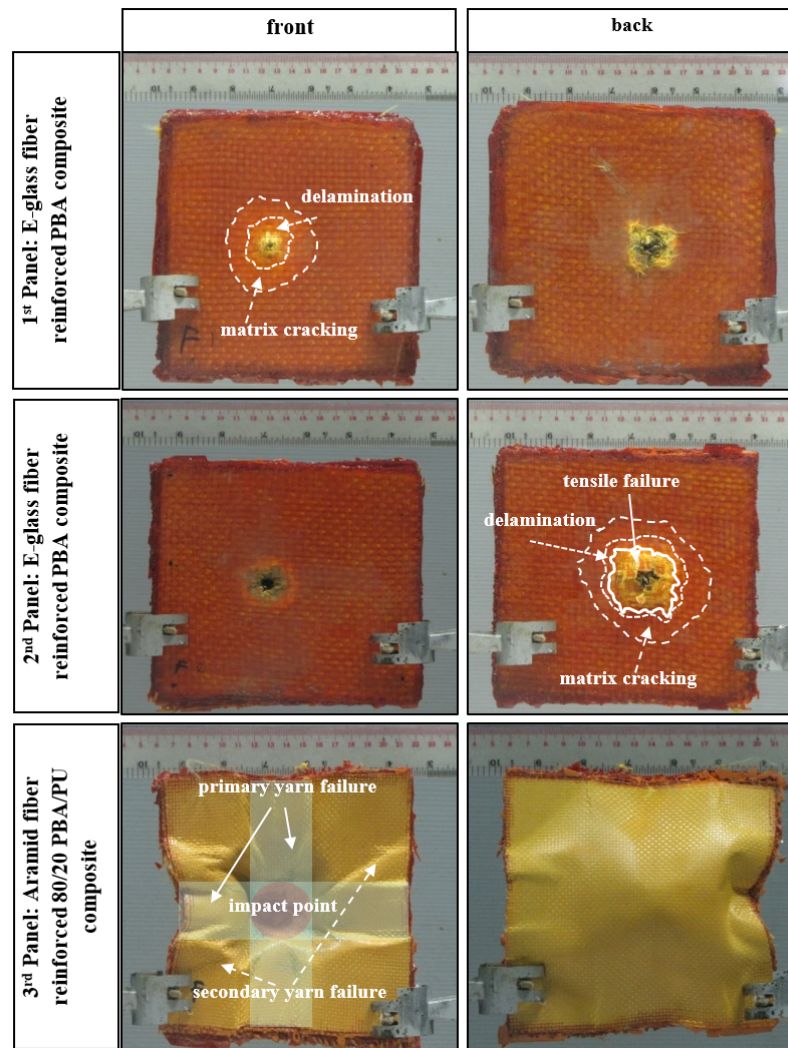


Figure 37: Ballistic impact behavior of the composite panels consisted of the first two panels of type E glass fiber reinforced PBA composites and aramid fiber reinforced 80/20 PBA/PU composite showing an ability of the composite to resist the penetration of 7.62x51 mm projectile at a velocity of 847 ± 9.1 m/s based on test level III of NIJ standard.

Damage pattern of type E glass fiber composite also with aramid fiber composite after having ballistic impacted was evaluated. The damage area on back side of the glass fiber sample was expectedly to be higher than that of front side as illustrated in Figure 37. This was due to the impact projectile behaved severe deviation from normal impact resulting in much extensive damage on back side of the specimen as also noticed from localized damage around perforation region [13] [109]. Major damage modes of glass fiber composite sample were clearly observed as fiber breakage at the impact point due to tensile failure as well as more intense delamination area and matrix cracking around perforated part. The damage pattern of our glass fiber reinforced PBA composite could be related to that of type E glass fiber/epoxy composites [96]. Damage configuration on the sample was nearly circular with higher intensity of damage in the inner region than the outer region. Such behaviors of the composite were also reported by Rahman *et al.* in system of glass fiber/epoxy/multiwall carbon nanotube [100]. The failure modes on the aramid composite were localized and the whole damage. Localized damage was related to the tensile failure in primary yarn that were in direct contact with the projectile where concentrated only at the specific target area around impact point. The whole damage involving secondary yarn breakage contributed to the high energy dissipation rate into the surrounding area. During the latter phenomena, more yarns are broken in which more energy has been absorbed for the composite panel [104].

Type E glass fiber reinforced PBA composite and aramid fiber reinforced 90/10 PBA/PU composite was also subjected to ballistic test at the same format to the ballistic armor with aramid fiber composite having 20wt% of PU content. As can be seen from side view of the last panel of aramid fiber composite, complete penetration was observed on the ballistic armor using aramid fiber composite with 10wt% of PU content as absorption panel as depicted in Figure 38. The results from this hard ballistic test was in a good agreement with those of the previous of energy absorption of sample which also confirmed that aramid fiber reinforced 80/20 PBA/PU specimen exhibited the highest energy absorption. Therefore, samples having such combination could have a real good potential to be used for ballistic armor manufacturer. The areal weight density of the composite system was 4.1 g/cm^2 .

The depth of cone formation of the non-perforated or partial penetrated aramid fiber reinforced 80/20 PBA/PU composite was lower than that of the perforated aramid fiber reinforced 90/10 PBA/PU specimen as can be observed in Figure 38. During the ballistic impact event, the composite panel absorbed some kinetic energy from the bullet and simultaneously transferred to surrounding area thus deformation was then occurred. Longitudinal/radial propagation of stress waves occurred on the plane of the target panel. Amount of residual energy which cannot be absorbed was transmitted to the back side of the sample resulting in a damage [110]. These findings were similar to those of results in that aramid fiber reinforced

80/20 PBA/PU composite absorbed and dissipate more impact energy thus less cone deformation on the back side occurred [111].

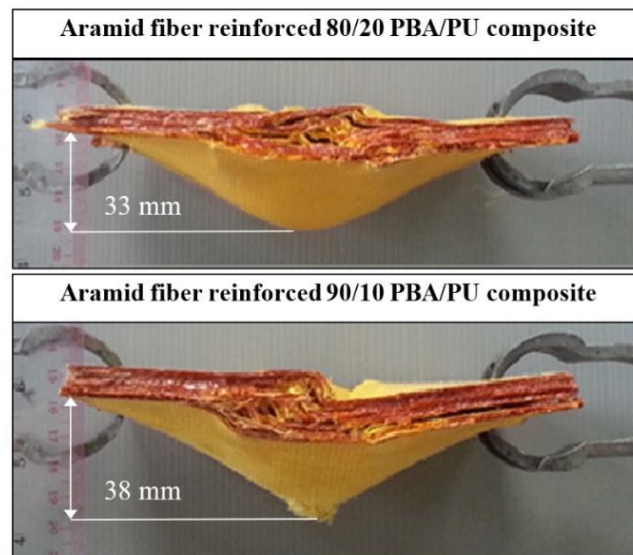


Figure 38: Comparison on depth of deformation on the back side of 3rd panel of aramid fiber reinforced PBA/PU composite with 20wt% and 10wt% of PU content after ballistic impacted by 7.62x51 mm based on test level III of NIJ standard.

The damage diameter of penetration hole along thickness direction of aramid fiber reinforced PBA/PU specimen after hard ballistic test was evaluated. The cone formation area was similar to rectangular shape thus equivalent damage diameter was calculated based on equation (15). Figure 39 shows the equivalent diameter of penetration hole at different depths along the thickness direction of aramid fiber reinforced PBA/PU sample having 10 and 20wt% of PU content. It appears that the equivalent diameter of damage hole of the composite increased along the depth. The damage holes were more dispersed with the depth in which more energy was

absorbed by each ply of the composite. At the depth of about 7.5 mm, complete penetration was observed on sample having 10wt% of PU content where the composite with 20wt% clearly had no perforation. The specimen could effectively absorbed impact energy and exhibited an ability to stop the movement of the projectile within 18 plies out of 25 plies of the sample. Some of residual energy of the sample was absorbed in elastic deformation of the composite while the remaining was created certain amount of damage in the sample.

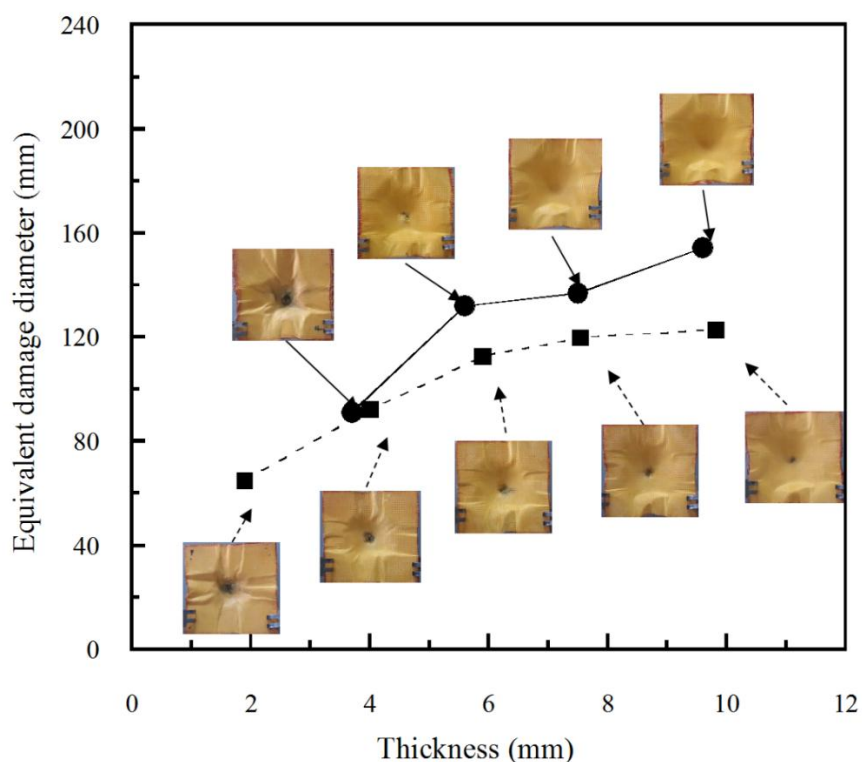


Figure 39: Equivalent damage diameter of hole at different depths along the thickness of aramid fiber reinforced PBA/PU composite:—●—80/20 PBA/PU and —■—90/10 PBA/PU composite.

In comparison, the equivalent diameter of damage region assessed from the specimen with 20wt% of PU content was more than that of the specimen having 10wt% of PU content. At about 9 mm thickness, the equivalent diameter of in plane damage of the specimen with 10 and 20wt% was measured to be 123 and 155 mm, respectively. On the other hand, when the projectile completely penetrated the sample, much more localized damage was dominant and was generally lower than the case where partial penetration of the sample was presented. Moreover, damage area or delamination area also related to energy absorption of the composite in such the way that the delamination areas increased with the increase of absorb energy during an impact event as reported by Hirai *et al.* [110].

5.10 Measurement of S Glass Fiber Reinforced PBA Composite as Striking Panel for Hard Ballistic Panel

Type S glass fiber reinforced PBA composite was also evaluated to be used as striking panel for hard ballistic armor and compared to those of type E glass composite. The S glass composite panels were prepared in the same format to as E glass composite panels and backed by aramid fiber reinforced 80/20 PBA/PU sample. Figure 40 illustrates the ballistic test results of the specimens after impacted by 7.62×51 mm projectile.

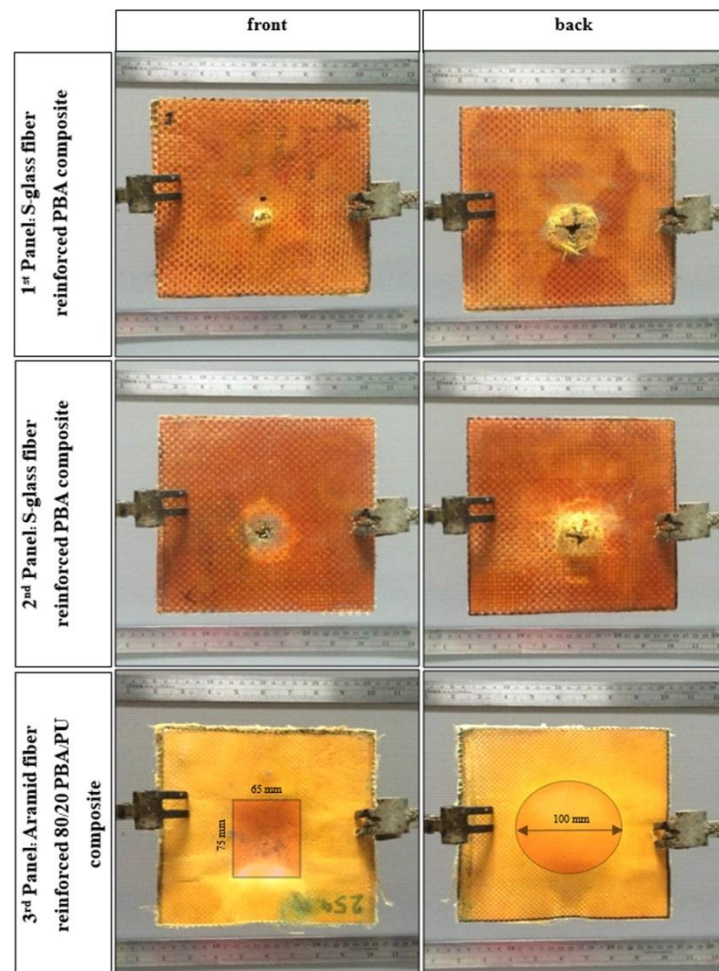


Figure 40: Ballistic impact response of the composite specimens made from two panels of 25 plies each of S-glass fiber reinforced PBA and 25 plies of aramid fiber reinforced 80/20 PBA/PU after impacted by 7.62x51 mm projectile.

It appeared that the specimens could potentially stop and catch the projectile by remaining complete perforation on the first two panels of S glass composites and partial penetration on the last panel of aramid composite. In comparison to the results of ballistic test using E glass composite, a much lower damage area and depth of penetration on aramid composite panel of these

composite system was clearly noticed. This could be related to that S glass fabric had tensile modulus of about 56 GPa which is greater than that of E glass fabric having the value of 38 GPa resulting in superior ballistic performance in terms of both reduction in back face deformation and depth of penetration on back side of the aramid composite. Moreover, it was attributed to higher sonic velocity of S glass composite in which the velocity of wave propagation increased with the square root of fiber modulus and inversely with the square root of fiber density [112]. The fiber with high sonic velocity could be able to spread out absorbed energy fast and efficiently [113]. Therefore, there was less amount of residual energy left to further penetrate the aramid composite panel and cause small deformation on the specimen. Furthermore, S-glass fiber composite was mainly made of silicon dioxide with high hardness providing an ability to destroy the projectile into fragment thus impact energy was also reduced and only fiber stretching with no failure was formed on the last panel. It could be observed that the shape of cone formation on the aramid panel closely rectangular. The center distances of damage area were measured and calculated into equivalent diameter which was about 78 mm. This result indicated a potential use of S glass fiber reinforced PBA composite as striking panel for hard ballistic armor. The areal weight density and total thickness of the laminate specimens were as high as 5.57 g/cm^2 and 32.6 mm, respectively. Although the specimens can resist the bullet their heavy weight and bulkiness limited further

their utilization as human body armor. The ballistic specimens having weight reduction was further developed.

The composite panels made of 35 plies of S glass fiber reinforced PBA backed by aramid fiber reinforced 80/20 PBA/PU composite were fabricated and subjected to projectile. As can be seen in Figure 41, S glass composite was completely penetrated by projectile as expected. Fiber breakage and matrix cracking on the panel where no perforation on the rear side of aramid composite was also observed indicating the penetration resistance of the specimens. The deformations on primary and secondary yarns were obviously noticed on impact side of the aramid composite whereas cone formation on the rear side of aramid fiber took place having damage diameter of about 140 mm. The fibril breakage was noticed on the impact side of both S glass fiber reinforced PBA composite and aramid fiber reinforced 80/20 PBA/PU composite as seen in Figure 42. Furthermore, the residual fragment of S glass composite after perforated was caught by the latter aramid panel

The failure modes occurred in this one panel of S-glass composite were likely the same to those of the armor panels having two panels of S glass composite backed by aramid composite panel. In comparison, the damage area on S glass composite were limit in specific area whereas the large area of panel made of ceramic such as alumina and silicon carbide was destroyed by crack propagation [55, 114, 115]. Therefore, the use of ceramic panel as strike face for multi-hit resistance

was obstructed. As can be seen in Figure 8, the damage diameter of the S glass panel was measured to be less than 7 mm.

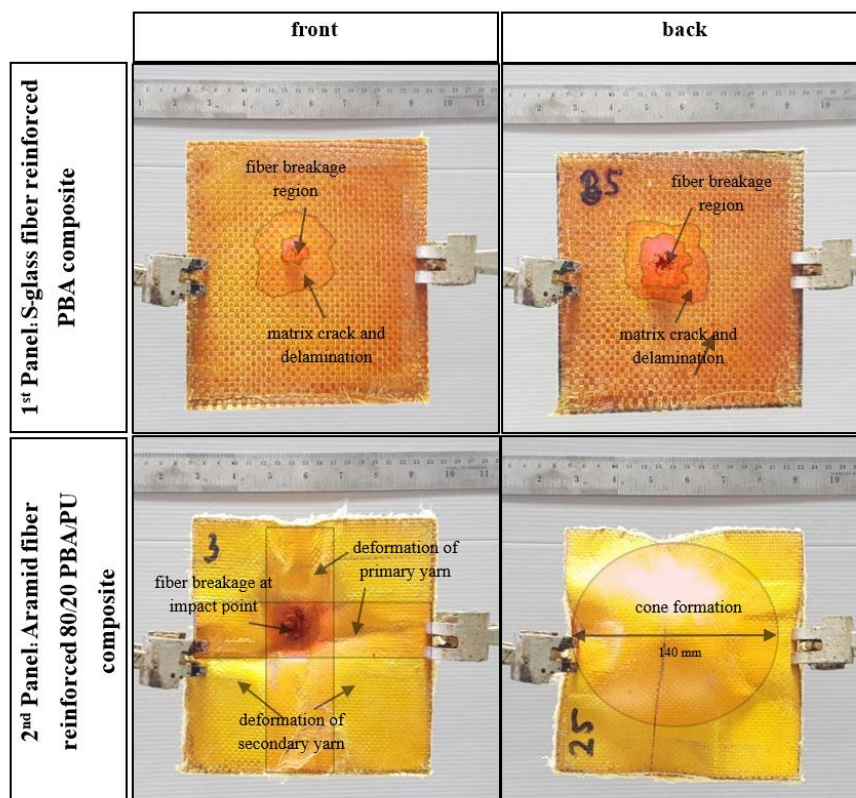


Figure 41: Ballistic impact response of composite specimens made from: 35 plies of S-glass fiber reinforced PBA composite and 25 plies of aramid fiber reinforced 80/20 PBA/PU composite after impacted by 7.62x51 mm projectile.

The areal weight density and total thickness of the armor panels were 4.5 g/cm² and 24.5 mm, respectively. These findings showed slightly higher in areal weight density than that of the samples manufactured from E glass composite but the thickness of the specimens was significantly reduced.

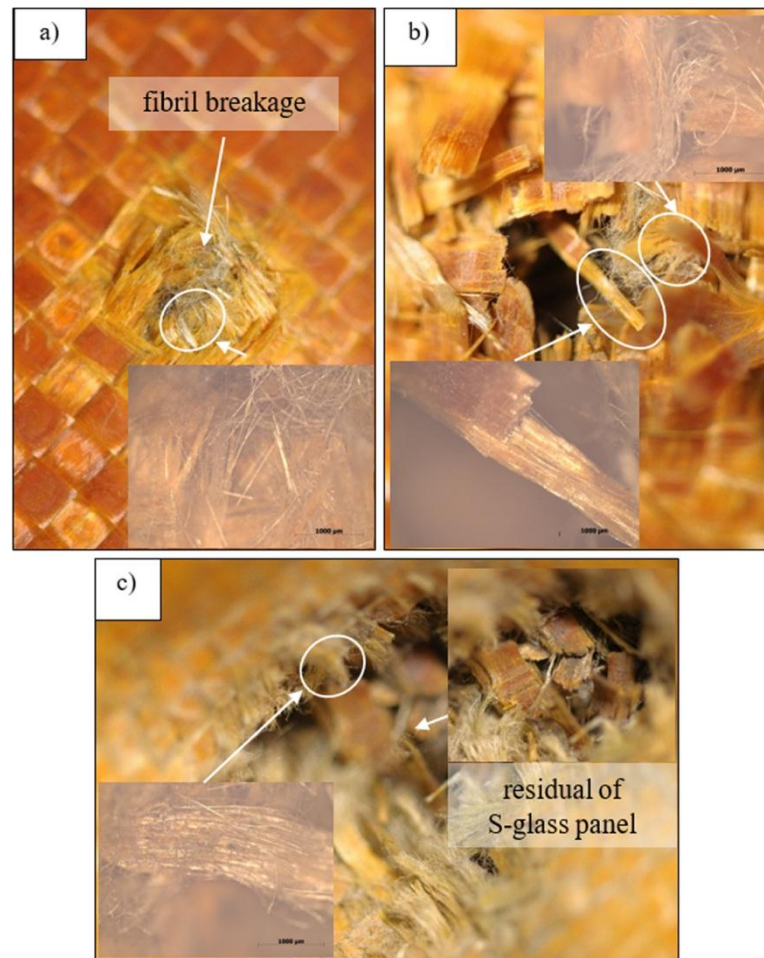


Figure 42: Macrograph of the composite specimens after impacted by 7.62x51 mm projectile a) impact side b) rear side of S glass fiber reinforced PBA composite c)

impact side of aramid fiber reinforced 80/20 PBA/PU composite

5.11 COMPARISON ON EXPERIMENTAL AND NUMERICAL RESULTS OF FIBER REINFORCED PBA/PU COMPOSITES

The properties of S glass fiber reinforced PBA used for simulation were shown in Table 16. The deformation on the rear side of the aramid composite from the predicted and experiment test was compared. From Figure 43, it appeared that the simulation results closely matched with the test result indicating an accuracy of the

estimated properties of those S glass and aramid composites to be further predict ballistic limit velocity of the specimen and its failure behavior.

Table 16: Materials properties of S glass fiber reinforced PBA composite used for simulation.

Equation of state	Density,	Young modulus, kPa			Poisson's ratio		
	g/cm^3	E_{11}	E_{22}	E_{33}	ν_{12}	ν_{23}	ν_{31}
Orthotropic	2.2	7×10^7	7×10^7	7×10^6	0.12	0.4	0.2
Strength	Shear modulus, kPa			Failure	Tensile stress, kPa		
	G_{12}	G_{23}	G_{31}		σ_{11}	σ_{22}	σ_{33}
Elastic	6×10^6	6×10^6	6×10^5	Material stress/strain	6×10^5	6×10^5	7×10^4

* Remark: Poisson's ratio and shear modulus of the composites were estimated by comparison of experimental and simulation results.

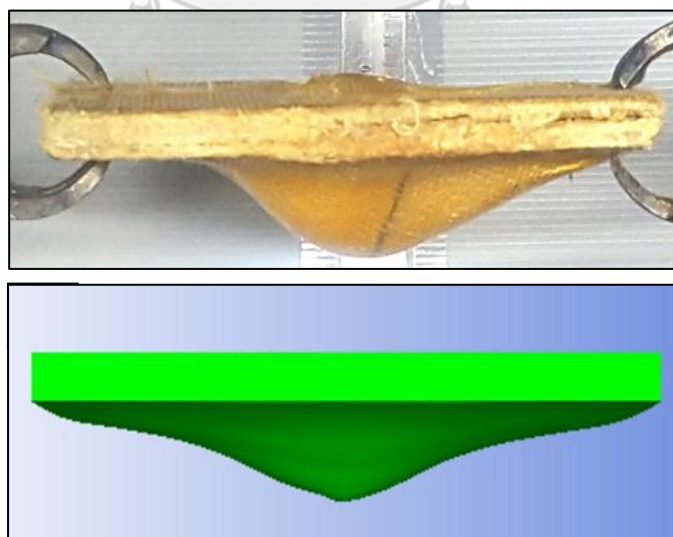


Figure 43: Back face deformation on the aramid composite after impacted by 7.62×51 mm showing the similar impact response of a) experimental and b) simulation.

5.12 BALLISTIC LIMIT VELOCITY EVALUATION OF FIBER REINFORCED PBA/PU COMPOSITE

The ballistic limit of the sample was measured by varying an impact velocity of 7.62x51 mm projectile until perforation was noticed. From Figure 44a), the value of the composite panel was determined to be at 930 m/s. Figure 44b) illustrates the failure of the sample on a resistance to the projectile having an impact velocity of 950 m/s which exceed ballistic limit of the sample.

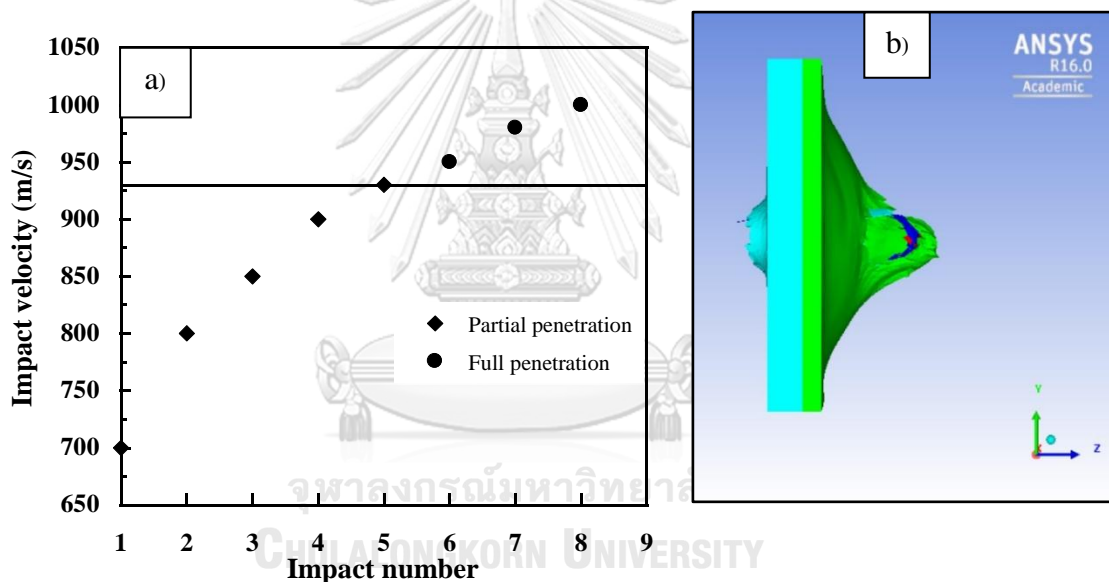


Figure 44: Ballistic characteristic a) Ballistic limit b) Failure in the composite panel by 7.62x51 mm having velocity of 950 m/s higher than its ballistic limit.

The failure of the specimens at each time interval is illustrated in Figure 45. The tip of projectile started to erode after penetrated into the S glass composite panel as shown in Figure 45a). An impact energy from the projectile transferred through the S glass panel to the aramid panel as evidenced from the cone formation

on the rear side of the last panel as presented in Figure 45b). An increase of deformation on the backing panel was observed because large amount of kinetic energy of the bullet was dissipated to destroy the sample. The tip of the bullet was flattened and mushroomed as can be seen from Figure 45c). After 44 μ s, the S glass panel was completely perforated and the bullet totally eroded left only portion of projectile to further penetrate the aramid composite as shown in Figure 45d).

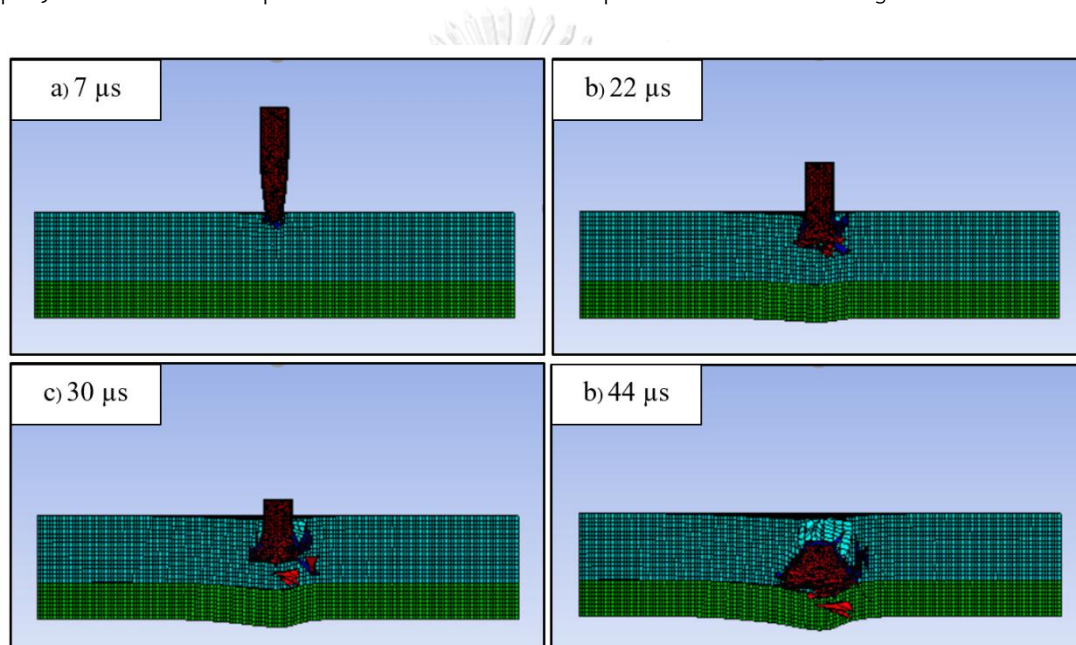


Figure 45: Impact response of the specimens impacted by 7.62x51 mm having velocity of 838 m/s at each time interval.

5.13 MULTI SHOTS PERFORMANCE OF FIBER REINFORCED PBA/PU COMPOSITE

PANEL

The specimens having dimension of 245x290 mm² was prepared into curved specimen to be evaluated as body armor. The ballistic tests were conducted by 7.62x51 mm within velocity range of 847±9.1 m/s for six projectile shots on the

specimens backed by clay witness. The projectiles were stopped and their kinetic energy was completely absorbed and dissipated inside the specimens leaving indentation in the clay witness as can be seen in Figure 46.

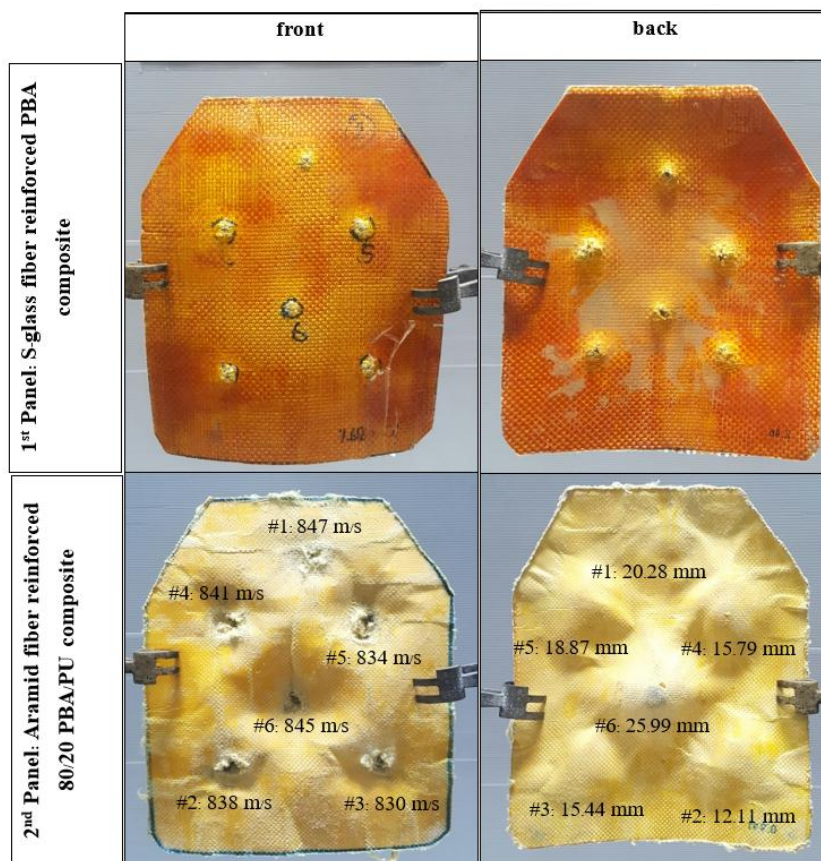


Figure 46: Multi-shot resistance of S-glass fiber reinforced PBA composite backed by aramid fiber reinforced 80/20 PBA/PU composite: showing impact velocity and depth of penetration measured from backing clay material for each impact shot.

Depth of penetration in the samples was measured from backing clay material and was recorded. The values were marked in Figure 46 in which the depth of penetration for all six impact shots were lower than 44 mm as limited based on NIJ standard for serious blunt trauma. The highest value of penetration on the

specimen was 25.99 mm located at the center of the specimen which was the last shot where all the damage area of the previous five shots were integrated resulting in the maximum deformation on the panel. Such findings indicated the high performance of armor system based on fiber reinforced PBA/PU composites to be used as human body armor.

Table 17: Comparison of areal weight density of our fiber reinforced PBA/PU composite and others hard ballistic armors.

Hard ballistic armors	Areal weight density (g/cm ²)	Ref.
E glass Fiber reinforced PBA/PU composite system	4.1	Present study
S glass Fiber reinforced PBA/PU composite system	4.5	Present study
Alumina ceramic/stainless/Kevlar TM reinforced benzoxazine alloy panels	7.1	[116]
S-glass and E-glass reinforced polypropylene	4.88	[63]
boron carbide ceramic/composite metal foam interlayer/ Kevlar	5.25	[48]

The ballistic performances of this developed armor were compared to those of other systems at the same threat level as summarized in Table 17. The armor based on S glass backed by aramid composite showed significant lower areal weight density and the similar thickness to the armor system manufactured from boron carbide ceramic/composite metal foam interlayer/ Kevlar panel having the value of 5.25 g/cm^2 and 24.5 mm, respectively. [48]. However, no multi-hit resistance as well as depth of penetration was reported.



REFERENCES

- [1] Yang, Y., and Chen, X. Investigation on energy absorption efficiency of each layer in ballistic armour panel for applications in hybrid design. Composite Structures 164 (2017): 1-9.
- [2] Nilakantan, G., and Nutt, S. Effects of fabric target shape and size on the V50 ballistic impact response of soft body armor. Composite Structures 116 (2014): 661-669.
- [3] Gopinath, G., Zheng, J.Q., and Batra, R.C. Effect of matrix on ballistic performance of soft body armor. Composite Structures 94 (2012): 2690-2696.
- [4] Liu, W., Chen, Z., Cheng, X., Wang, Y., Amankwa, A.R., and Xu, J. Design and ballistic penetration of the ceramic composite armor. Composites Part B: Engineering 84 (2016): 33-40.
- [5] Liu, W., et al. Influence of different back laminate layers on ballistic performance of ceramic composite armor. Material and Design 87 (2015): 421-427.
- [6] Sevket, E., Liaw, B., Delale, F., and Raju, R. A combined experimental and numerical approach to study ballistic impact response of S2 glass fiber/toughened epoxy composite beams. Composite Science and Technology 69 (2009): 965-982.

- [7] Grujicic, M., Pandurangan, B., Zecevic, U., Koudela, K.L., and Cheeseman, B.A. Ballistic performance of alumina/S-2 glass reinforced polymer matrix composite hybrid lightweight armor against armor piercing (AP) and non-AP projectiles. Multidiscipline modeling in materials and structures, 3 (2006): 287-312.
- [8] Haque, A., Abutalib, A., Rahul, K., Vaidya, U.K., Mahfuz, H., and Jeelani, S. Ballistic performance of monolithic ceramic backed by S2 glass vinyl ester composites, ICCM proceeding, 2001.
- [9] Tang, R.T., and Wen, H.M. Predicting the perforation of ceramic-faced light armors subjected to projectile impact. International Journal of Impact Engineering 102 (2017): 55-61.
- [10] Burger, D., Faria, A.R., Almeida, S.F.M., Melo, F.C.L., and Donadon, M.V. Ballistic impact simulation of an armour-piercing projectile on hybrid ceramic/fiber reinforced composite armours. International Journal of Impact Engineering 43 (2012): 63-77.
- [11] Cunniff, PM. Dimensionless parameters for optimization of textile based body armor systems. In: Proceedings of the 18th international symposium on ballistics, San Antonio, TX: Lancaster (Pennsylvania), 1999,. pp.1303-1310.
- [12] Lee, BL., Walsh, TF., Won, ST., and Patts, HM. Penetration failure mechanisms of armor-grade fiber composites under impact. Journal of Composite Materials 35 (2016): 1605-1633.

- [13] Nayak, N., et al. Effect of matrix on the ballistic impact of aramid fabric composite laminates by armor piercing projectiles. Polymer Composites 33 (2012): 443-450.
- [14] Wang, B., et al. Energy absorption efficiency of carbon fiber reinforced polymer laminates under high velocity impact. Material and Design 50 (2013): 140-148.
- [15] Çalioğlu, H., Sayer, M., and Demir, E. Impact behavior of particles filled-glass/polyester composite plates. Polymer Composite 32 (2011): 1125-1133.
- [16] Bandaru, A.K., Vetiyatil, L., and Ahmad, S. The effect of hybridization on the ballistic impact behavior of hybrid composite armors. Composite Part B.-Engineering 76 (2015): 300-319.
- [17] Grujicic, M., Pandurangan, B., Angstadt, D.C., Koudela, K.L., and Cheeseman, B.A. Ballistic-performance optimization of a hybrid carbon-nanotube/E-glass reinforced poly-vinyl-ester-epoxy-matrix composite armor. Journal of Material Science 42 (2007): 5347-5359.
- [18] Rimdusit, S., Jubsilp, C., and Tiptipakorn, S. *Alloys and Composites of Polybenzoxazines: Properties and Applications*, Springer, New York, 2013.
- [19] Okhawilai, M., and Rimdusit, S., Hard armor composites from ballistic fiber reinforced polybenzoxazine alloys. In: *Advanced and emerging*

polybenzoxazine science and technology, Ishida H. Froimowicz P. (ed). USA, ELSEVIER, 2017. pp 699-723.

- [20] Rimdusit, S., Bangsen, W., and Kasemsiri, P. Chemorhology and thermomechanical of benzoxazine-urethane copolymers. Journal of Applied Polymer Science 121 (2011): 3669-3678.
- [21] Ishida, H., and Agag T. (Eds.), Handbook of Benzoxazine Resin, Elsevier Press, Oxford, 2012.
- [22] Rimdusit, S., Pathomsap, S., Kasemsiri, P., Jubsilp, C., and Tiptipakorn, S. KevlarTM Fiber-Reinforced Polybenzoxazine Alloys for Ballistic Impact Application. Engineering Journal 54 (2011) 23-40.
- [23] Denchev, Z., and Dencheva, N., Manufacturing and properties of aramid reinforced composites, in *Synthetic polymer-polymer compsites*, Bhattacharyya SF (ed), Munich, Hanser Publishers, 2012. pp 251-280.
- [24] Rimdusit, S., Tanthapanichakoon, W., and Damrongsakkul, S. Toughening of polybenzoxazine by alloying with urethane prepolymer and flexible epoxy: A comparative study. Polymer Engineering and Science 45 (2005): 288-296.
- [25] Rimdusit, S., Mongkhonsi, T., Kamonchaivanich, P., Sujirote, K., and Tiptipakorn, S. Effects of poly molecular weight on properties of benzoxazine-urethane polymer alloys. Polymer Engineering and Science 48 (2008): 2238-2246.

- [26] Mukasey, M.B., Sedgwick, J.L., and Hagy, D.W. U.S. Department of Justice, National Institute of Justice, Ballistic resistance of body armor, NIJ standard 0101.06. 2008.
- [27] Holder, E.H., Mason, K.V., and Sabol, W.J. National institute of justice guide body armor, Selection & application guide 0101.06 to ballistic-resistance body armor, December 2014.
- [28] O'Masta, M.R., Deshpande, V.S., and Wadley, H.N.G. Mechanisms of projectile penetration in Dyneema® encapsulated aluminum structures. International Journal of Impact Engineering 74 (2014): 16-35.
- [29] Tam, D.K.Y., Ruan S., and Yu, T. High-performance ballistic protection using polymer nanocomposites. 2012: p. 213-237.
- [30] Jacobs, M.J.N., and Van Dingenen J.L.J. Ballistic protection mechanism in personal armour. Journal of Material Science 36 (2001): 3137-3142.
- [31] Cheeseman, B.A., and Bogetti, T.A. Ballistic impact into fabric and compliant composite laminates. Composite Structure 61 (2003): 161-173.
- [32] Morye, S.S., Hine, P.J., Duckett, R.A., Carr, D.J., and Ward, I.M. Modelling of the energy absorption by polymer composites upon ballistic impact. Composite Science and Technology 60 (2000): 2631-2642.
- [33] Naik, N.K., and Doshi, A.V. Ballistic impact behavior of thick composites: Parametric studies. Composite Structures 82 (2008): 447-464.

- [34] Ong, C.W., Boey, C.W., Hixson, R.S., and Sinibaldi, J.O. Advanced layered personnel armor. International Journal of Impact Engineering 38 (2011): 369-383.
- [35] Karahan, M., Kus, A., and Eren, R. An investigation into ballistic performance and energy absorption capabilities of woven aramid fabrics. International Journal of Impact Engineering. 35 (2008): 499-510.
- [36] Caprino, G., Lopresto, V., and Santoro, D. Ballistic impact behaviour of stitched graphite/epoxy laminates. Composite Science and Technology 67 (2007): 325-335.
- [37] Findik, F., and Tarim, N. Ballistic impact efficiency of polymer composites. Composite Structure 61 (2003): 187-192.
- [38] Harel, H., Marom, G., and Kenig, S. Delamination Controlled Ballistic Resistance of Polyethylene/Polyethylene Composite Materials. Applied Composite Materials 9 (2002): 33-42.
- [39] Alcock, B., Cabrera, N.O., Barkoula, N.M., Wang, Z., and Peijs, T. The effect of temperature and strain rate on the impact performance of recyclable all-polypropylene composites. Composites Part B- Engineering 39 (2008): 537-547.
- [40] Larsson, F., and Svensson, L. Carbon, polyethylene and PBO hybrid fibre composites for structural lightweight armour. Composites Part A-Applied Science and Manufacturing 33 (2002): 221-231.

- [41] Wang, S.F. et al. Transparent ceramics: Processing, materials and applications. Progress in Solid State University 41 (2013): 20-54.
- [42] Madhu, V., Ramanjaneyulu, K., Balakrishna, T., and Gupta, N.K. An experimental study of penetration resistance of ceramic armour subjected to projectile impact. International Journal of Impact Engineering 32 (2005): 337-350.
- [43] Meyers, M.A. Dynamic behavior of materials 1994: John Wiley Inc.
- [44] Ravid, M., Hasharon, H., Hirschberg, Y., and Hagalil, M. Ballistic armor, U.S. patent No. 2004/0020353 A1, 2004.
- [45] Ravid, M., and Hirschberg, Y. Ballistic armor, European patent No. EP1734332A, 2006.
- [46] Ravid, M., and Hirschberg, Y. Ballistic armor, U.S. patent No. US7513186B2, 2009.
- [47] Carberry, J., Norweed, J., Leighton, K.T., Hoff, K., and Cline, C. Ceramic ballistic armor product, U.S. patent No. US8101535B2, 2012.
- [48] Garcia-Avila, M., Portanova, M., and Rabiei, A. Ballistic performance of composite metal foams. Composite Structures 44 (2004): 307-316
- [49] Goncalves, D.P., Melo, F.C.L., Klein, A.N., and Al-Qureshi, H.A. Analysis and investigation of ballistic impact on ceramic/metal composite armour. International Journal of Machine Tools&Manufacture 44 (2004): 307-316.

- [50] Flores-Johnson, E.A., Saleh, M., and Edwards, L. Ballistic performance of multi-layered metallic plates impacted by a 7.62 mm APM2 projectile. International Journal of Impact Engineering 38 (2011): 1022-1032.
- [51] Straßburger, E. Ballistic testing of transparent armour ceramics. Journal of the European Ceramic Society 29 (2009): 267-273.
- [52] López-Puente, L., Arias, A., Zaera, R., and Navarro, C. The effect of the thickness of the adhesive layer on the ballistic limit of ceramic/metal armours. An experimental and numerical study. Journal of Impact Engineering 32 (2005): 321-336.
- [53] <http://www.vestguard.co.uk/>. [2015, July 28].
- [54] <http://www.bodyarmoroutlet.com>. [2015, July 28].
- [55] Silva, M.V., Stainer, D., Al-Qureshi, H.A., Montedo, O.R.K., and Hotza, D. Alumina-Based Ceramics for Armor Application: Mechanical Characterization and Ballistic Testing. Journal of Ceramics (2014): 1-6.
(<http://dx.doi.org/10.1155/2014/618154>).
- [56] Tan, Z.H., Han, X., Zhang, W., and Luo, S.H. An investigation on failure mechanisms of ceramic/metal armour subjected to the impact of tungsten projectile. International Journal of Impact Engineering 37 (2010): 1162-1169.
- [57] Übeyli, M. et al. The ballistic performance of SiC-AA7075 functionally graded composite produced by powder metallurgy. Material and Design 56 (2014): 31-36.

- [58] Wielewski, A., Birkbeck, R., and Thomson, A. Ballistic resistance of spaced multi-layer plate structures: Experiments on fibre reinforced plastic targets and an analytical framework for calculating the ballistic limit. Material and Design 50 (2013): 737-741.
- [59] Jordan, J.B., Naito, C.J., and Haque, B.Z. Progressive damage modeling of plain weave E glass/phenolic composites. Composite Part B-Engineering 61 (2014): 315-323.
- [60] Jordan, J.B., Naito, C.J., and Haque, B.Z. Quasi-static, low-velocity impact and ballistic impact behavior of plain weave E-glass/phenolic composites. Journal of Composite Materials 48 (2013): 2505-2516.
- [61] Jordan, J.B., and Naito, C.J. An experimental investigation of the effect of nose shape on fragments penetrating GFRP. Internal Journal of Impact Engineering 63 (2014): 63-71.
- [62] Sapozhnikov, S.B., Kudryavtsev, O.A., and Zhikharev, M.V. Fragment ballistic performance of homogenous and hybrid thermoplastic composites. International Journal of Impact Engineering 81 (2015): 8-16.
- [63] Pilpel, E.D., Holland, R.H., and Johnson, S. Composite ballistic panels and method of use, U.S. patent No. US7598185, 2009.
- [64] Naik, N.K., and Reddy, BCK. Ballistic impact behavior of woven fabric composites. International Journal of Impact Engineering 32 (2006): 1521-1552.

- [65] Mohan, S., and Velu, S. Ballistic impact behaviour of unidirectional fibre reinforced composites. International Journal of Impact Engineering 63 (2014): 164-176.
- [66] Zhang, D., Sun, Y., Chen, L., Zhang, S., and Pan, N. Influence of fabric structure and thickness on the ballistic impact behavior of Ultrahigh molecular weight polyethylene composite laminate. Material and Design 54 (2014): 315-322.
- [67] Dueramae, I., Rimdusit, S. Highly filled graphite polybenzoxazine composites for an application as bipolar plates in fuel cells. Journal of Applied Polymer Science 130 (2013): 3909-3918.
- [68] Plengudomkit, R., Okhawilai M., and Rimdusit, S. Highly filled graphene-benzoxazine composites for an application as bipolar plates in fuel cells. Polymer Composites (2015):.
- [69] Rimdusit, S. Hemvichian, K., Kasemsiri, P., and Dueramae, I. Shape memory polymers from benzoxazine-modified epoxy, Smart Material and Structures 22 (2013):.
- [70] Rimdusit, S., Kasemsiri, P., and Okhawilai, M. Ballistic armor from polymer composites, Thailand Patent pending issue number 1301004340, 2013.
- [71] Jubsilp, C., Ramsiri, B., and Rimdusit, S. Effects of aromatic carboxylic dianhydrides on thermomechanical properties of polybenzoxazine-dianhydride copolymers. Polymer Engineering and Sciences 52 (2012): 1640-1648.

- [72] Jubsilp, C., Takeichi, T., and Rimdusit, S. Property enhancement of polybenzoxazine modified with dianhydride Polymer Degradation and Stability 96 (2011): 1047-1053.
- [73] Reghunadhan Nair, CP. Advances in addition-cure phenolic resins. Progress in Polymer Sciences 29 (2004): 401-498.
- [74] Ishida, H., and Sanders, D.P. Improved thermal and mechanical properties of polybenzoxazines based on alkyl-substituted aromatic amines. Journal of Polymer Science Part B. Polymer Physics 38 (2000): 3289-3301.
- [75] Ishida, D. Process for preparation of benzoxazine compounds in solventless systems, U.S. Patent No. 5,543,516, 1996.
- [76] Pegoraro, M., Galbiati, A., and Ricca, G. ¹H nuclear magnetic resonance study of polyurethane prepolymers from toluene diisocyanate polypropylene glycol. Journal of Applied Polymer Science 87 (2003): 347-357.
- [77] Takeichi, T., Guo, Y., and Agag, T. Synthesis and characterization of poly(urethane-benzoxazine) films as novel type of polyurethane/phenolic resin composites. Journal of Polymer Science Part A: Polymer Chemistry 38 (2000): 4165-4176.
- [78] Kasemsiri, P. Development of Light Weight Ballistic Armor from Fiber-Reinforced with Benzoxazine Alloys, Dissertation, Degree of Doctoral, Department of Chemical Engineering, Faculty of Engineering, Chulalongkorn University, 2011.

- [80] Krishnan, K., Sockalingam, S., Bansal, S., and Rajan, S.D. Numerical simulation of ceramic composite armor subjected to ballistic impact. Composites Part B-Engineering 41 (2010): 583-593.
- [81] Nasr-Isfahani, M., Amani-Tehran, M., and Latifi, M. Simulation of ballistic impact on fabric armour using finite-element method. Journal of the Textile Institute 100 (2009): 314-318.
- [82] Gama, B.A., and Gillespie J.W., Finite element modeling of impact, damage evolution and penetration of thick-section composite. International Journal of Impact Engineering 38 (2011): 181-187.
- [83] Sockalingam, S., Gillespie, JW., and Keefe, M. On the transverse compression response of Kevlar KM2 using fiber-level finite element model. International Journal of Solids Structure 51 (2014): 2504-2517.
- [84] Ramadhan, A.A., Abu Talib, A.R., Mohd Rafie, A.S. and Zahari, R. High velocity impact response of Kevlar-29/epoxy and 6061-T6 aluminum laminated panels. Material and Design 43 (2013): 307-321.
- [85] Kavitha, S., Umadevi, R., and Sugandha, N. Experimental and numerical simulation of ballistic impact on glass fibre reinforced plastic composite panels. International Journal of Information Research and Review 2 (2015): 606-610.

- [86] Tham, C.Y., Tan, V.B.V. and Lee, H.P. Ballistic impact of a Kevlar helmet: experiment and simulations. International Journal of Impact Engineering 35 (2008): 304-318.
- [87] ASTM Standard D 2344, 2003, “Standard test method for short-beam strength of polymer matrix composite materials and their laminates” ASTM International, West Conshohocken, PA, 2003, DOI: 10.1520/D2344_D2344M.
- [88] ASTM Standard D 1876, 2003, “Peel resistance of adhesives (T-peel test)” ASTM International, West Conshohocken, PA, 2003, DOI: 10.1520/D1876-08R15E01
- [89] ANSYS AUTODYN Library Version 16 .
- [90] Chennakesava Reddy, A. Evaluation of curing process for Kevlar 49 epoxy composites by mechanical characterization designed for brake liners. International Journal of Science and Research 4 (2015): 2365-2371.
- [91] Ahmed, K.S., and Vijayarangan, S. Tensile, flexural and interlaminar shear properties of woven jute and jute-glass fabric reinforced polyester composites. Journal of Materials Processing Technology 207 (2008): 330-335.
- [92] Wu, S.R., Sheu, G.S., and Shyu, S.S. Kevlar fiber epoxy adhesion and its effect on composite mechanical and fracture properties by plasma and chemical treatment. Journal of Applied Polymer Science 62 (1996): 1347-1360.

- [93] Wang, L., Kanesalingam, S., Pil, R., Padhye, R. Recent Trends in Ballistic Protection. Textiles and Light Industrial Science and Technology 3 (2014): 37-47.
- [94] Liu, L., Huang, YD., Zhang, ZQ., Jiang, ZX., and Wu, LN. Ultrasonic treatment of aramid fiber surface and its effect on the interface of aramid/epoxy composites. Applied Surface Sciences 254 (2008): 2594-2509.
- [95] Joo, K., and Tae Jin, K. Numerical analysis of energy absorption mechanism in multi-ply fabric impacts. Textile Research Journal 78 (2008): .576-561
- [96] Pandya, KS., Pothnis, JR., Ravikumar, G., and Nail, N.K. Ballistic impact behavior of hybrid composites. Material and Design 44 (2013): .135-128
- [97] Manero, A., Gibson, J., Freihofe, G., Gou, J., and Raghavan, S. Evaluating the effect of nano-particle additives in Kevlar® 29 impact resistant composites. Composite Science and Technology 116 (2015): .49-41
- [98] Gibson, J., McKee, J., Freihofe, G., Raghavan, S., and Gou, J. Enhancement in ballistic performance of composite hard armor through carbon nanotubes. International Journal of Smart and Nanomaterial 4 (2013): .228-212
- [99] Liaghat, GH., Nia, AA., Daghyani, HR., and Sadighi, M. Ballistic limit evaluation for impact of cylindrical projectiles on honeycomb panels. Thin Wall Structure 48 (2010): .61-55

- [100] Rahman, M., et al. Effects of amino-functionalized MWCNTs on ballistic impact performance of E-glass/epoxy composites using a spherical projectile. International Journal of Impact Engineering 57 (2013): 108-118.
- [101] Gellert, E.P., Cimpoeru, S.J., and Woodward, R.L., A study of the effect of target thickness on the ballistic perforation of glass-fibre-reinforced plastic composites. International Journal of Impact Engineering 24 (2000): 445-456.
- [102] Gu, B. Ballistic Penetration of Conically Cylindrical Steel Projectile into Plain-woven Fabric Target - A Finite Element Simulation. Journal of Composite Materials 38 (2004): 2049-74.
- [103] Iremonger, M.J., and Went, A.C. Ballistic impact of fibre composite armours by fragment-simulating projectiles. Composites Part A: Applied Science and Manufacturing 27 (1996): 575-581.
- [104] Othman, A.R., and Hassan, M.H. Effect of different construction designs of aramid fabric on the ballistic performances. Material and Design 44 (2013): 407-413.
- [105] Naik, N.K., Shirao, P., and Reddy, B.C.K. Ballistic impact behaviour of woven fabric composites: Formulation. International Journal of Impact Engineering 32 (2006): 1521-1552.
- [106] Valenca, S.L., Griza, S., Oliveira, V.G., Sussuchi, E.M., and Cunha, F.G.C. Evaluation of the mechanical behavior of epoxy composite reinforced with kevlar plain

- fabric and glass-kevlar hybrid fabric. Composites Part B: Engineering 70 (2015): .8-1
- [107] Bandaru, AK., Chavan, VV., Ahmad, S., Algirusamy, R., Bhatnagar, N. Ballistic impact response of Kevlar® reinforced thermoplastic composite armors. International Journal of Impact Engineering 89 (2016): .13-1
- [108] Salman, SD., Leman, Z., Sultan, MTH., Ishak, MR., and Cardona, F. Effect of kenaf fibers on trauma penetration depth and ballistic impact resistance for laminated composites. Textile Research Journal 87 (2017): 2051-2065.
- [109] Sabet, A., Fagih, N., and Beheshty, M.H. Effect of reinforcement type on high velocity impact response of GRP plates using a sharp tip projectile. International Journal of Impact Engineering 38 (2011): 715-722.
- [110] Hirai, Y., Hamada, H., and Kim, JK. Impact response of woven glass fabric composite I. Effect of fiber surface treatment. Composite science technology 58 (1998): 91-104.
- [111] Okhawilai, M., Parnklang, T., Mora, P., Hiziroglu, S., Rimdusit, S. Development of high performance ballistic armor from fiber reinforced polybenzoxazine/polyurethane composites. International Journal of Impact Engineering, 2016. Under revision.
- [112] Cunniff, PM. An analysis of the system effects in woven fabrics under ballistic impact. Textile Research Journal 62 (1992): 495-509.

- [113] Abrate, S., Impact engineering of composite structures. Ballistic Impacts on Polymer Matrix Composites, Composite Armors, Personal Armor, R. Zaera, ed. F.G.R. Giulio Maier, Jean Salencon. 2011, New York: SpringerWienNewYork.
- [114] Medvedovski, E., Ballistic performance of armour ceramics: Influence of design and structure. Part 2. Ceramics International 36 (2010): 2117-2127.
- [115] Pawar, M.J., et al., Comparison of ballistic performances of Al₂O₃ and AlN ceramics. International Journal of Impact Engineering 98 (2016): 42-51.
- [116] Kamonchaivanich, P. Effects of diol molecular weight on properties of benzoxazine-urethane polymer alloys for ballistic armor applications, Master's Thesis, Department of Chemical Engineering, Faculty of Engineering, Chulalongkorn University, 2006



APPENDIX

จุฬาลงกรณ์มหาวิทยาลัย
CHULALONGKORN UNIVERSITY

VITA

Manunya Okhawilai was born on April 2nd, 1985 in Bangkok, Thailand. She finished high school from Saipanya School and received the bachelor's degree of Chemical Engineering from King Mongkut's University of Technology Thonburi in 2007. In 2009, she received the Degree of Master of Engineering in Chemical Engineering at the Department of Chemical Engineering, Chulalongkorn University. After the M.Eng graduation, she worked at Thai Film Industry for two years and then pursued her graduate study for a Doctoral Degree in Chemical Engineering at Chulalongkorn University.

